Non-Equilibrium Dynamics of Reaction-Diffusion Systems

Martin Howard

Somerville College

and

Department of Physics, Theoretical Physics

Oxford University.

Submitted for the degree of Doctor of Philosophy

at the University of Oxford

Trinity Term 1996.

Non-Equilibrium Dynamics of Reaction-Diffusion Systems

Martin Howard

Somerville College and Department of Physics,
Theoretical Physics, Oxford University.

Abstract

Fluctuations are known to radically alter the behaviour of reaction-diffusion systems. Below a certain upper critical dimension d_c, this effect results in the breakdown of traditional approaches, such as mean field rate equations. In this thesis we tackle this fluctuation problem by employing systematic field theoretic/renormalisation group methods, which enable perturbative calculations to be made below d_c.

We first consider a steady state reaction front formed in the two species irreversible reaction $A + B \to \emptyset$. In one dimension we demonstrate that there are two components to the front - one an intrinsic width, and one caused by the ability of the centre of the front to wander. We make theoretical predictions for the shapes of these components, which are found to be in good agreement with our one dimensional simulations. In higher dimensions, where the intrinsic component dominates, we also make calculations for its asymptotic profile. Furthermore, fluctuation effects lead to a prediction of asymptotic power law tails in the intrinsic front in all dimensions. This effect causes high enough order spatial moments of a time dependent reaction front to exhibit multiscaling.

The second system we consider is a time dependent multispecies reaction-diffusion system with three competing reactions $A+A \to \emptyset$, $B+B \to \emptyset$, and $A+B \to \emptyset$, starting with homogeneous initial conditions. Using our field theoretic formalism we calculate the asymptotic density decay rates for the two species for $d \leq d_c$. These calculations are compared with other approximate methods, such as the Smoluchowski approach, and also with previous simulations and exact results.

Submitted for the degree of Doctor of Philosophy
Trinity Term 1996.

To my family

"The petty done, the undone vast ..."

Robert Browning:
The Last Ride Together.

Acknowledgments

I would first like to thank my supervisor, Dr. John Cardy, for his constant encouragement, advice and support over the last two and a half years. Thanks are also due to my second collaborator, Dr. Gerard Barkema - especially for teaching me about simulations. I have also profited from discussions with other physicists in Oxford and elsewhere, particularly Ben Lee, Uwe Tauber and Klaus Oerding.

Financial support has been provided by the EPSRC (D. Phil. studentship), Merton College and the Department of Theoretical Physics (travel grants) and also Somerville College (award of a senior scholarship). I am very grateful to all these institutions for their generosity.

I must also thank my friends in Oxford, especially those in Merton, Somerville and in Rooms 6.2-6.3, for making the last few years such an enriching experience.

Finally I thank my family, for never telling me what to do.

Publications

The work appearing in chapters 2 and 3 has previously been published in:

M. Howard and J. Cardy: *J. Phys. A: Math. Gen.* **28** 3599 (1995)

G. Barkema, M. Howard, and J. Cardy: *Phys. Rev. E* **53** R2017 (1996),

and the work of chapters 2 and 4 in:

M. Howard: *J. Phys. A: Math. Gen. to appear* (1996).

Contents

Chapter 1

Introduction

The theory of reaction-diffusion systems is an old subject. Its quantitative origins lie in the work of Wilhelmy [1] in 1850, when he first wrote down a differential equation to describe the reaction kinetics of sucrose inversion. His theory was then built upon by the seminal researches of Harcourt and Esson [2] in the 1860s, who developed the rate equation approach still in common use today (see [3]). Further key contributions were made by Smoluchowski [4] in 1917, with the proposal of his theory of diffusion limited reactions. Nevertheless, the fact that reaction-diffusion systems remain an extremely active field of research after nearly 150 years is a timely reminder of the subject's complexity.

The reason for this longevity lies simply in the *non-equilibrium* nature of these systems. Most *equilibrium* problems in statistical physics are now well understood, thanks to powerful unifying machinery such as the Boltzmann distribution. However, the absence of such general techniques in non-equilibrium phenomena has made them very much harder to solve. Typically each new problem has required the development of an array of specialised techniques. In the past this has certainly

been true of reaction-diffusion systems. However, it is one of the aims of this thesis to present a more unified treatment, which can be used to describe all birth/death processes on an equal footing.

An understanding of reaction-diffusion systems is important, thanks to their wide ranging applications in the physical and biological sciences. The most obvious (and oldest) of these is to chemical reactions [5, 6]. Amongst the most intensively studied examples in this field are pattern forming systems, such as in the Belousov-Zhabotinsky reaction (for an introduction see [7, 8]). In this case an astonishing variety of temporal and spatial patterns can be observed in the distribution of reactants. Pattern formation also has considerable relevance to biological systems, and particularly to morphogenesis (the development of structure during the growth of an organism) . Turing [9] put forward the idea that reaction-diffusion patterns could be exploited by living organisms for the purpose of controlling cellular development. The key feature of these controlling Turing patterns is that their characteristic length scales are intrinsic to the reaction process, and are not determined by the geometry of the reaction vessel (as in, for example, convective Benard Cells). For many years this theory remained somewhat speculative as definitive observation of Turing patterns proved elusive. However, unambiguous evidence for the Turing mechanism has now been found - both in controlled reactors in the laboratory [10], and in nature (markings on marine angelfish) [11]. Hence, a proper analysis of reaction-diffusion systems seems important in understanding fundamental questions concerning the maintenance of life.

A somewhat more down to earth example of a reaction-diffusion system concerns the dynamics of excitons in polymer chains [12]. When certain polymer molecules (for example TMMC: $(CH_3)_4NMnCl_3$) are subject to a burst of laser light, this

can lead to the creation of excitons. Once formed, these excitons are essentially constrained to hop only along the chain molecule on which they were formed. In addition, when two excitons meet they coagulate to form a single exciton. Hence we can see that this is a genuine realisation of a simple one dimensional single species reaction-diffusion system. Indeed the exciton decay rates have been measured, and are found to be in excellent agreement with predictions based on the mapping to a reaction-diffusion process. Thus we can see that low dimensional reaction-diffusion systems have real physical applications.

A third, rather more exotic example concerns the dynamics of monopoles in the early universe [13]. It is believed that the only mechanism by which such a monopole can decay is by annihilation with its associated anti-particle: the anti-monopole. Hence the rate of particle decay can be calculated by analysing an irreversible two species reaction-diffusion process, beginning with random initial conditions. Although the original analysis was carried out with this astrophysical problem in mind, the results can, of course, be applied to *any* two species reaction-diffusion process with the same initial conditions.

In summary, we can see that reaction-diffusion systems have a diverse range of applications ranging from biology to astrophysics. However, one might well ask the question: what is wrong with using a rate equation approach to understand the kinetics of these processes? By employing a rate equation approach, we mean assuming that the rate of decay of a certain species due to a particular reaction is proportional to the product of densities of each particle involved in that reaction (an hypothesis originally developed by Harcourt and Esson [2]). If indeed this technique were adequate, then we would simply be left with a mathematical question of solving a (possibly very complex) set of partial differential equations.

However, as was pointed out by Ovchinnikov *et al.* [14] (see also [13, 15]), the rate equation method is fundamentally flawed due to its neglect of microscopic density fluctuations. In other words, correlations may be built up between particles as the system evolves - correlations which are ignored in this approach. Viewed from this perspective, the rate equations take on the role of a mean field approximation, which, under appropriate circumstances, will not provide an adequate description of the system. The obvious question of how to go beyond the rate equation method, and thus include fluctuation effects, will be the principal object of this thesis. As we shall see in the succeeding sections, surmounting this difficulty will require us to introduce many of the ideas of modern theoretical physics.

1.1 Methods of Analysis

One interesting feature of many reaction-diffusion systems is the presence of asymptotic power law density decays, such as those in the simple single species irreversible reactions $A + A \to \emptyset$ and $A + A \to A$. Such behaviour is somewhat reminiscent of equilibrium critical phenomena, where scale invariance (with a divergent correlation length) at the critical point leads to power law decays in the correlation functions. This suggests that it might be fruitful to apply the techniques of field theory and the renormalisation group, which have been so successful for equilibrium critical systems, to our non-equilibrium problem. Hence we would aim to use the machinery of diagrammatic perturbation theory and the ϵ expansion for the systematic calculation of fluctuation effects. Simultaneously, we might hope that these methods would, as in conventional applications, cast light on the existence of universality. Furthermore, these systematic techniques may also tell us something

about the nature of previous approximate methods (such as the Smoluchowski approach [4, 16]). As we shall see, these expectations will be fulfilled in subsequent chapters of this thesis.

In time dependent reaction-diffusion systems we note that power law decays (if they exist at all) are only present asymptotically - hence we see that a critical point may be approached only as $t \to \infty$. This differs fundamentally from equilibrium critical phenomena, where one must *tune* the temperature to a critical value to see the critical behaviour. Hence, in a limited way, we see that many reaction-diffusion processes can be viewed as being self-organised [17], as at late times they exhibit power law behaviour without any further fine tuning. However, in many time dependent processes the state into which the system organises is, of course, trivial - one with no particles remaining.

Before discussing in more detail the calculational techniques to be used in this thesis, we briefly mention some other exact methods that have been developed in the last few years. One approach consists of formally deriving mathematical bounds for quantities of interest. For example, Bramson and Lebowitz [18] have considered in detail the two species irreversible reaction $A+B \to \emptyset$, beginning with equal densities for the two species at $t = 0$. By rigorously deriving upper and lower bounds for the densities, they showed that these must decay as $t^{-d/4}$ for $d < 4$, and t^{-1} for $d \geq 4$. These results are in agreement with other techniques (for example those based on the renormalisation group [19]). A second methodology relies on the theory of integrable systems. Many one dimensional reaction-diffusion systems can be mapped onto integrable quantum spin chains, which are themselves related to two dimensional statistical mechanics models [20]. By using techniques such as the Bethe Ansatz these problems can often be solved exactly, yielding interesting

and highly non-trivial information concerning densities and correlation functions. Unfortunately, the problems considered in this thesis are currently too hard for the application of either of these techniques. However, we note that an exact solution using rather different methods does exist (in a certain limit) for the multispecies reaction-diffusion system to be considered in chapter 4.

On a more general level, the exact approaches outlined above together with perturbative methods turn out to be rather complementary. A common feature of all exact solutions on a lattice is that they assume an infinite reaction rate - in other words as soon as the appropriate particles meet on the same lattice site they instantaneously react with probability one. On the other hand, our field theoretic/renormalisation group methods lead to a finite *continuum* reaction rate, which allows one to examine the important question of *universality* in reaction-diffusion systems. Unfortunately this is at the expense of being restricted to perturbative calculations. Furthermore, work on separating these non-equilibrium systems into universality classes is still at an early stage. Nevertheless, it appears that there are far more categories than in equilibrium phenomena, where only a very few parameters (e.g. spatial dimension, nature of the order parameter) are known to determine the universality class.

1.2 Field Theoretic and Renormalisation Group Methods

The essence of the application of renormalisation group (RG) methods to critical phenomena lies in the concept of integrating out short wavelength degrees of freedom. If the system is at a critical point, where the correlation length diverges, this

process should not alter the physics in any way - and thus we are led to the concepts of renormalisation group flows and fixed points. Typically, above a critical dimension d_c, the running couplings will flow to Gaussian fixed points, indicating that mean field theory will be an adequate description. However, below d_c, the couplings may flow to different fixed points, entirely altering the critical behaviour of the system. In equilibrium critical phenomena, the archetypal example of this behaviour is in the Ising model, where for $d > 4$ mean field theory is sufficient, whereas for $d < 4$ the running coupling flows to a distinct (Ising) fixed point.

At first sight it is not quite obvious how these ideas might be applied to reaction-diffusion processes. The most systematic RG methods for conventional critical phenomena rely on a field theoretic formulation of the problem, using, for example, a Landau-Ginzburg action (see [21]). Ideally, we would like to develop a similar method in our problem - fortunately such a formalism does indeed exist. The idea is to begin with an exact description of the reaction-diffusion system in the form of a microscopic master equation. Using some standard techniques developed by Doi [22] and Peliti [23], this master equation can be transformed into a Schrödinger-like equation, and then into a path integral. These methods will be reviewed in more detail in chapter 2. In that chapter we will also discuss the possibility of writing Langevin-type equations for the evolution of the density fields. For the cases we discuss, the Gaussian form of the noise can be exactly derived from the field theoretic action. However, we will point out that the interpretation of these equations is not as straightforward as it might appear (a result of the equations involving fields, not simple densities). In addition, we will also discuss some subtleties concerning the nature of conserved noise.

Once an exact action for our system has been derived, field theoretic and RG

methods can be fruitfully applied to calculate the desired asymptotic properties. The first step in our analysis concerns the identification of divergences in the theory. In order to make physical sense of our calculations these divergences must be removed via a renormalisation procedure. The systems considered in this thesis are particularly simple in this respect in that the *only* renormalisation needed is reaction rate renormalisation, and this can be done to all orders in perturbation theory. This appealing feature is a consequence of the irreversible nature of the reactions, which restricts the vertices appearing in the field theoretic action. Expressing the bare reaction rates in terms of these renormalised couplings then leads to the cancellation of the divergences at the upper critical dimension d_c. The next step is to use an RG equation to show that, below d_c, the renormalised couplings flow to $O(\epsilon)$ fixed points at large times, where $\epsilon = d_c - d$. Hence, we have learnt that these systems are universal in the sense that for $d < d_c$ the asymptotic properties are independent of the reaction rates. A further consequence is that we will have transformed our perturbation expansion from being in powers of the renormalised couplings into an ϵ expansion. This feature is again closely related to the calculation of critical exponents in equilibrium critical phenomena. So, in summary, our basic methodology is to form a diagrammatic expansion for the densities, where the order of a particular diagram will be determined, as usual, by the number of loops embedded within it. In fact it will turn out that the zero loop diagrams are equivalent to the mean field rate equations. The next step is to evaluate these diagrams and replace the bare reaction rates with the renormalised couplings, and thus eliminate the divergences. Use of the RG equation then allows this perturbation series to be improved at late times, transforming it into an ϵ expansion.

The principal virtue of this approach with regard to the fluctuation problem is that it allows for a *systematic* calculation, whereby fluctuation effects may be evaluated order by order in a controlled fashion. This constitutes a great improvement over previous, rather *ad hoc* methods (such as the Smoluchowski approximation). In those cases it was unclear both how good the approximation actually was, and also how improvements might be made to it. The second of these defects is certainly remedied in the field theoretic approach.

1.3 Overview: The Reaction-Diffusion Front for $A + B \to \emptyset$

The first problem we will examine closely (in chapter 3, see also [24, 25]) concerns the effects of fluctuations on the reaction front formed in the two species irreversible reaction $A + B \to \emptyset$. The experimental arrangement is that A particles are fed in from the left hand edge of the system, and B particles are fed in from the right edge. The particles then diffuse towards the system centre where they annihilate in a steady state reaction front (see figure 1.1). In this thesis we will be interested in calculating the profile of both the reaction front and the particle densities. Historically, a time dependent version of this model (see pp. 13–14) was first introduced by Gálfi and Rácz [26], whereas the steady state front was first discussed by Ben-Naim and Redner [27].

Mean field analysis [27] predicts that the width w of the steady state reaction front scales as $w \sim (\lambda J/D^2)^{-1/3}$, where λ is the reaction rate, J are the (equal) rates of particle injection, and D are the (equal) diffusion constants. The asymptotic

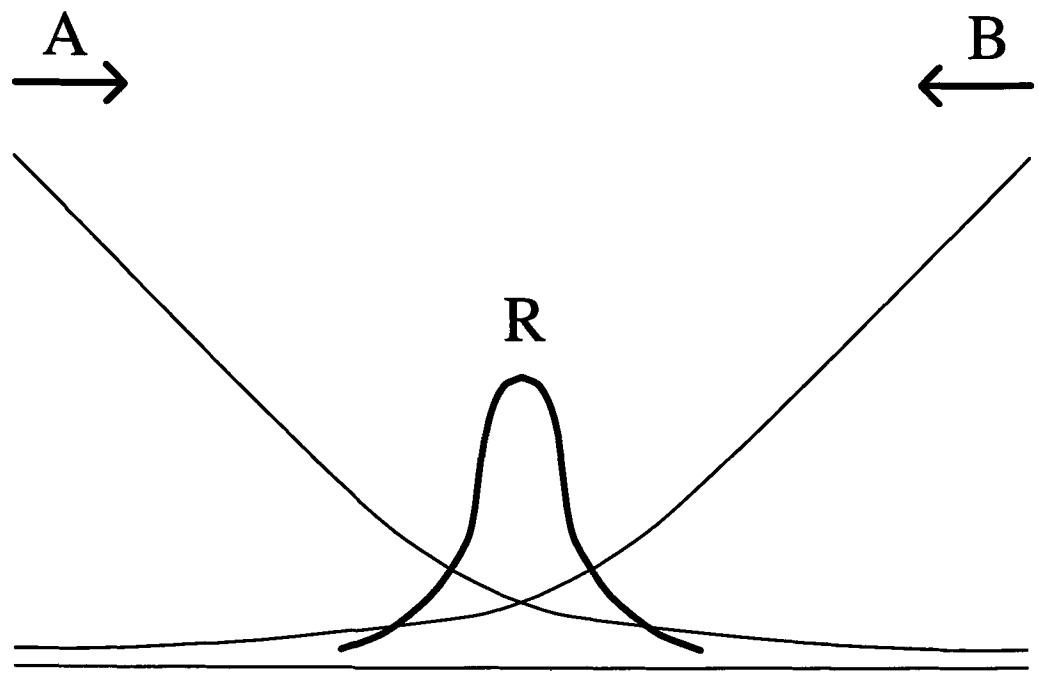

Figure 1.1: Schematic diagram of the front R and the density profiles in the reaction-diffusion front for $A + B \to \emptyset$.

form for the mean field reaction front is given by

$$R_{mf} \sim 0.3787\lambda \frac{(J/D)^{19/12}}{(\lambda/D)^{5/12}} |x|^{3/4} \exp\left[-\frac{2}{3}\left(\frac{\lambda J}{D^2}\right)^{1/2} |x|^{3/2}\right]. \tag{1.1}$$

However, below an upper critical dimension d_c where the fluctuations become relevant, we expect these mean field results to break down.

Our first result is to show that in dimensions $d = 2$ and higher, the reaction front is smooth, whereas in $d = 1$, the presence of noise causes the reaction front to wander around. In fact in an infinite system the centre of the front would perform a random walk and so would be completely delocalised. Nevertheless, in a finite system, with appropriate boundary conditions, the front is constrained to lie towards the centre of the reaction vessel, and we show that the wandering gives rise to a Gaussian profile in $d = 1$, with width:

$$w_g = \left[\frac{\ln(cL/w_g)}{\pi(J/D)}\right]^{\frac{1}{2}}, \tag{1.2}$$

where c is a constant and L is the system size. Thus we find a basic $w_g \sim (J/D)^{-1/2}$ scaling for the wandering reaction front. Hence in the fluctuation regime $\lambda J^{-1/2} D^{-1/2} \gg 1$, where the fluctuation width is much greater than the mean field width, we expect to find a Gaussian reaction front profile. However, in the opposite regime $\lambda J^{-1/2} D^{-1/2} \ll 1$, we expect the mean field predictions to work well. Clearly, one important feature of our theoretical predictions is that they apply to the case of a finite reaction rate. This is in contrast to previous, mainly numerical work, which assumed an infinite reaction rate [28, 29]. In $d = 1$ this is an important distinction, as with an infinite reaction rate it would be impossible for, say, the rightmost A particle to penetrate past the leftmost B particle. Hence, our simulations have also employed a finite reaction rate, and this allows us to observe the two different regimes predicted above, where we find good agreement with our theoretical analysis.

We next consider the form of the *intrinsic* front profile - i.e. the shape of the reaction front averaged over some suitably short period of time. In the $d = 1$ fluctuation regime, the intrinsic front is obscured by the dominance of the wandering front profile - however, in higher dimensions it is the intrinsic profile which is most significant. This intrinsic profile (in the $d = 1$ fluctuation regime) is nevertheless accessible numerically by measuring the relative reaction rate, i.e. plotting the reaction rate as a function of the displacement between successive reaction events. Assuming that the front wanders little between these successive events, we will then effectively be measuring the convolution of the intrinsic reaction front with itself.

From a theoretical angle, we can calculate the asymptotic properties of the intrinsic front by using field theoretic/RG methods, which predict a critical dimen-

sion $d_c = 2$ for this system. One essential difference between this problem and those previously discussed is that we now wish to understand the *steady-state* properties of the front. It will turn out that considering large x (where x is the distance from the reaction front centre) will play an analogous role to considering large times t in time dependent problems. Only in this asymptotic large x limit will the reaction rate flow to an $O(\epsilon)$ fixed point, allowing us to calculate the universal properties of the front in that region. The result of this calculation for the reaction front gives (for $d < 2$):

$$R = AD(J/D)^{\frac{19}{12}}|x|^{(9-7\epsilon)/12}\exp\left(-B(J/D)^{\frac{1}{2}}|x|^{(3-\epsilon)/2}\right) + CD^2J^{-1}|x|^{-7+2\epsilon} + \ldots \tag{1.3}$$

valid for $|x|(J/D)^{1/2} \gg 1$, where A, B, C are universal, dimension dependent constants. We also find expressions for the asymptotic density profiles of the two species. In $d = 2$ we find logarithmic corrections entering the expansion, consistent with the reaction rates being marginal parameters at the upper critical dimension. The results of equation (1.3) compare favourably with $1d$ numerical simulations, where we find evidence for the above stretched exponential term. However, our simulations were not quite sensitive enough to detect the power laws.

Comparison of these results with the mean field expression (1.1), shows that the fluctuations have acted to widen the front. Physically, this is a result of the anticorrelations built up between particles in low dimensions. The power laws arise as a consequence of a conservation law in the system: namely the reaction process conserves the difference between the number of A particles and the number of B particles. Hence the density difference field simply obeys a noisy diffusion equation, and this allows fluctuations to propagate far from the reaction front centre, leading

to power law tails.

We round off our discussion of this problem by considering a closely related situation, where the shape of the reaction front changes with time. In this set up, we begin with completely segregated species and then allow the system to evolve [26] (see figure 1.2). It turns out that by making the correspondence $J \sim t^{-1/2}$, we can, at late times, relate this problem to the above steady state formulation. However, the existence of the power law tails predicted above, and the fact that the reaction process will only have been running for a finite time in this time dependent model, leads to a prediction of multiscaling for high enough order spatial moments of the time dependent reaction front. We relate this result to a recent controversy in the literature [28, 29].

1.4 Overview: A Multispecies Reaction-Diffusion System

The second problem to be considered at length in this thesis (see also [30]) concerns the role of fluctuations in a multispecies reaction-diffusion system, with three irreversible reactions:

$$A + A \rightarrow \emptyset \qquad A + B \rightarrow \emptyset \qquad B + B \rightarrow \emptyset.$$

We choose initial conditions where the A and B particles are positioned randomly according to a Poisson distribution, such that on large enough scales the system is homogeneous. We first review previous work on this problem, including application of the Smoluchowski approximation [31]. This uncontrolled approach leads to asymptotic density decay exponents which depend on the ratio of diffusion constants, results which are in fairly good agreement with $1d$ simulations [31]. We

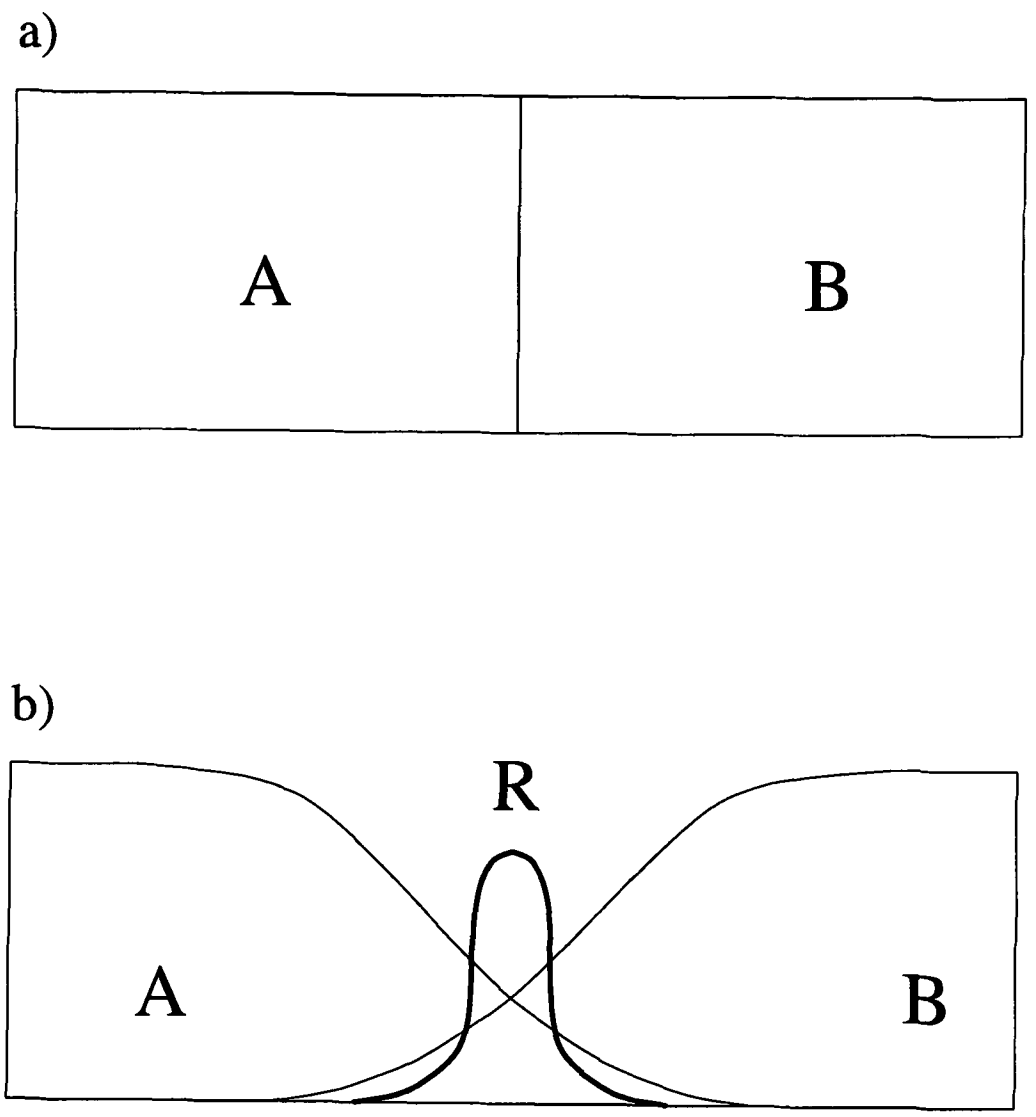

Figure 1.2: Schematic diagrams for the evolution of the time dependent system with the reaction $A + B \rightarrow \emptyset$: a) complete species segregation at $t = 0$, b) profile at late times.

then briefly discuss an exact $1d$ solution due to Derrida *et al.* [32, 33, 34], valid for the case where one of the species is greatly in the majority and where the minority species is immobile. This solution relies on solving an exactly equivalent problem - namely the probability that a given spin never flips in the zero temperature Glauber dynamics of the Ising Model. In this case, it was shown that this probability decays away exactly as $t^{-3/8}$.

Our main analysis then involves the development of the field theory approach, though we also restrict our analysis to the case where one of the two species greatly outnumbers the other. This condition leads to a great simplification in the calculation and allows analytic progress to be made. However, we note that for the case where the *majority* species is immobile, the entire rate equation approach fails and the behaviour of the densities is not accessible by perturbative methods [35]. Leaving this special case aside, we find that, below the upper critical dimension $d_c = 2$, the three reaction rates all flow asymptotically to $O(\epsilon)$ fixed points, which are themselves dependent on the ratio of diffusion constants. We then use the RG to improve the lowest (tree) level of the field theory, and find exponents that are identical to those of the Smoluchowski approach. For example, if the initial density of the A particles greatly outnumbers that of the B particles (i.e. $n_A \gg n_B$), then we find an early time regime where (for $d < 2$)

$$\langle a \rangle = O(t^{-d/2}) \tag{1.4}$$

$$\langle b \rangle = O\left(t^{-\frac{d}{2}\left(\frac{1+\delta}{2}\right)^{d/2}}\right), \tag{1.5}$$

where δ is the ratio of diffusion constants: $\delta = D_B/D_A \leq 1$. In $d = 2$, we again find logarithmic corrections to the mean field (rate equation) results, a consequence of the reaction rates being marginal in $d = d_c = 2$.

The advantage of the field theory approach is that it is again (at least conceptually) simple to go beyond this lowest order calculation and include additional fluctuation effects. To do this we perform a one loop calculation and evaluate the density decay exponents using an ϵ expansion. The technical details on how to carry out this procedure are addressed at length in chapter 4. For the case of the minority B species in the early time regime discussed above, we now have $\langle b \rangle = O(t^{-\beta})$, where

$$\beta = \left(\frac{1+\delta}{2}\right)\left(1 - \frac{\epsilon}{2}\left[\frac{3}{2} + \ln\left(\frac{1+\delta}{2}\right) - \frac{\delta(1+\delta)}{4}\left[1 + 2\ln\left(\frac{1+\delta}{2}\right)\right]\right.\right.$$
$$\left.\left. -\frac{1}{4}(\delta^2-1)\left(1 + (1+\delta)\left[f\left\{\frac{2}{1+\delta}\right\} - \frac{\pi^2}{6}\right]\right)\right]\right) + O(\epsilon^2), \qquad (1.6)$$

and

$$f\{x\} = -\int_1^x \frac{\ln u}{u-1} du \qquad (1.7)$$

is the dilogarithmic function [36]. Hence, we have succeeded in our desired aims of both understanding the nature of previous approximations, and also showing how they might be systematically improved. We conclude by suggesting one or two other systems to which these RG techniques could successfully be applied.

Chapter 2

Formalism

In this chapter we will set up the required formalism for the use of field theoretic/RG methods. We will begin by giving exact descriptions of our reaction-diffusion systems in terms of master equations, which will then be mapped onto Schrödinger-like equations, and then finally onto path integrals. This process will be carried out for the reaction $A + B \to \emptyset$, and we will then indicate how the techniques can easily be generalised to other similar systems. Previous reviews of these methods can be found in references [23, 37].

First of all we will make some very brief general remarks about our overall approach. Although the end result of the mapping is a quantum field theory, the systems we are considering are purely classical, with no quantum effects. The fact that our methods resemble a quantum theory is a consequence of the stochastic nature of the underlying classical dynamics. We will, however, identify the various salient differences between our formalism and those of ordinary quantum field theories (as in, for example, the calculation of averages). In addition, we will be developing a bosonic field theory - in other words multiple occupancy of a given

lattice site will be permitted. This is in contrast to a fermionic field theory, where occupancy of each site for a given species of particle would be restricted to 0 or 1.

2.1 The Model for $A + B \rightarrow \emptyset$

We consider a model where A and B particles are moving diffusively on a hypercubic lattice, with lattice constant l. There is some probability of mutual annihilation whenever an A and a B particle meet on the same lattice site. In addition, particles of type A are added at a constant rate to lattice sites on the hypersurface $x = -L$, and particles of type B are similarly added to sites at $x = L$. In other words, opposing currents of A and B particles are maintained at opposite edges of the system (see figure 1.1). The two hypersurfaces $x = \pm L$ mark the boundaries of the system beyond which the particles are not permitted to move. The model is defined by a master equation for $P(\{n,m\},t)$, the probability of particle configuration $\{n,m\}$ occurring at time t. Here $\{n,m\} = (n_1, n_2, \ldots, n_N, m_1, m_2, \ldots, m_N)$, where n_i is the occupation number of the A particles, and m_i the occupation number of the B particles, at the ith lattice site. The appropriate master equation is

$$
\begin{aligned}
&\frac{\partial}{\partial t}P(\{n,m\},t) = \\
&\frac{D}{l^2}\sum_{i,e}\{(n_e+1)P(\ldots n_i-1, n_e+1, \ldots, \{m\},t) - n_i P(\{n,m\},t)\} \\
&+\frac{D}{l^2}\sum_{i,e}\{(m_e+1)P(\{n\}, \ldots m_i-1, m_e+1, \ldots, t) - m_i P(\{n,m\},t)\} \\
&+\lambda\sum_{i}[(n_i+1)(m_i+1)P(\ldots n_i+1, m_i+1\ldots,t) - n_i m_i P(\ldots n_i, m_i \ldots, t)] \\
&+K\{P(\ldots, n_{-L}-1, \{m\},t) - P(\ldots, n_{-L}, \{m\},t)\} \\
&+K\{P(\{n\}, m_L-1\ldots,t) - P(\{n\}, m_L\ldots,t)\},
\end{aligned}
\tag{2.1}
$$

where i is summed over lattice sites, and e is summed over the nearest neighbours of i. The first, second, and third lines of the equation describe diffusion of the A and B particles respectively (with equal diffusion constants D), whilst the fourth line describes their annihilation within the system (with rate constant λ). The final four terms are due to the addition of A and B particles at the edges of the system at a rate K, corresponding to the maintenance of steady particle currents.

The master equation can be mapped to a second quantised form following a standard procedure developed by Doi [22] and Peliti [23]. The first step is to introduce bosonic creation and annihilation operators at each lattice site, with commutation relations:

$$[a_i, a_j^\dagger] = \delta_{ij} \qquad [b_i, b_j^\dagger] = \delta_{ij}, \tag{2.2}$$

and where all other commutators vanish. The vacuum ket is defined by $a_i|0\rangle = b_i|0\rangle = 0$ for all i. For the state defined by $|n_i, m_i\rangle = (a_i^\dagger)^{n_i}(b_i^\dagger)^{m_i}|0\rangle$, we have

$$a_i|n_i, m_i\rangle = n_i|n_i - 1, m_i\rangle \qquad a_i^\dagger|n_i, m_i\rangle = |n_i + 1, m_i\rangle \tag{2.3}$$

$$b_i|n_i, m_i\rangle = m_i|n_i, m_i - 1\rangle \qquad b_i^\dagger|n_i, m_i\rangle = |n_i, m_i + 1\rangle. \tag{2.4}$$

Hence the state of the system at time t is given by

$$|\Upsilon(t)\rangle = \sum_{\{n,m\}} P(\{n, m\}, t) \prod_i (a_i^\dagger)^{n_i}(b_i^\dagger)^{m_i}|0\rangle, \tag{2.5}$$

and we find that the master equation acquires the Schrödinger-like form

$$\frac{\partial}{\partial t}|\Upsilon(t)\rangle = -\hat{H}|\Upsilon(t)\rangle, \tag{2.6}$$

where

$$\hat{H} = -\frac{D}{l^2}\sum_{i,e}\{a_i^\dagger(a_e - a_i) + b_i^\dagger(b_e - b_i)\} - \lambda\sum_i(1 - a_i^\dagger b_i^\dagger)a_i b_i - K\{a_{-L}^\dagger - 1 + b_L^\dagger - 1\}. \tag{2.7}$$

We can formally solve equation (2.6) to give:

$$|\Upsilon(t)\rangle = e^{-\hat{H}t}|\Upsilon(0)\rangle. \tag{2.8}$$

One can immediately notice some differences between this formalism and ordinary quantum mechanics. Firstly, this theory does not involve imaginary numbers explicitly in its equation of motion. Secondly, one calculates the average of a quantity $F(t)$ in the following way:

$$\langle F(t)\rangle = \sum_{\{n,m\}} F(\{n,m\},t)P(\{n,m\},t), \tag{2.9}$$

where $F(\{n,m\},t)$ is the value of the quantity $F(t)$ in the state with occupation numbers $\{n,m\}$ at a time t. Note that this expression is *linear* in the probability P. This has the consequence that in the second quantised formalism the average becomes

$$\langle F(t)\rangle = \langle|\hat{F}|\Upsilon(t)\rangle, \tag{2.10}$$

where $\langle| \equiv \langle 0|\prod_i e^{a_i}e^{b_i}$ is called the projection state. One obvious property of this state is that $\langle|a_i^\dagger = \langle|b_i^\dagger = \langle|$, hence any operator represented in normal ordered form, with all its creation operators commuted to the left of its annihilation operators, can be written entirely in terms of a_i and b_i.

We are now in a position to perform the mapping to a path integral. This is a very standard procedure and we shall only briefly sketch its progress. The starting point is to associate with each state a generating function:

$$|\Upsilon(t)\rangle = \sum_{\{n,m\}} P(\{n,m\},t)|\{n,m\}\rangle \rightarrow \Upsilon(\{z,\xi\},t) = \sum_{\{n,m\}}\prod_i P(\{n,m\},t)z_i^{n_i}\xi_i^{m_i}. \tag{2.11}$$

In a similar way, given the matrix elements of an operator, a kernel can be associated with that operator. Using these correspondences the scalar product of arbitrary states, and also the action of an operator on a ket can both be expressed in an

integral form. Next we aim to express the time evolution operator $U_t = \exp(-\hat{H}t)$ as a path integral. The strategy here is to divide the evolution of the system into a very large number of time slices N, where $N = (t/\delta t)$. Consequently we can employ the Trotter formula:

$$U_t = \exp(-\hat{H}t) = \lim_{\delta t \to 0}(1 - \hat{H}\delta t)^{t/\delta t}. \tag{2.12}$$

We can then use the above correspondences to rewrite these products of time evolution operators acting on the initial ket as a multiple integral. Taking the limit $N \to \infty$ then transforms the expression for U_t into a path integral. For the purpose of calculating averages we must also include terms due to the projection state from (2.10). Putting all of this together, we end up with the following action for the steady state reaction front system:

$$S = \sum_i \left(\int_{-\infty}^{t} dt' \left\{ \hat{a}_i \dot{a}_i + \hat{b}_i \dot{b}_i - \frac{D}{l^2} \left[\hat{a}_i \sum_e (a_e - a_i) + \hat{b}_i \sum_e (b_e - b_i) \right] \right.\right.$$
$$\left.\left. -\lambda(1 - \hat{a}_i \hat{b}_i) a_i b_i \right\} - a_i(t) - b_i(t) \right). \tag{2.13}$$

Here the first four terms represent the diffusion of the A and B particles, the next two terms are due to the reaction step, and the final two terms result from the projection state. In addition to the above action, we also have the conditions

$$K = \frac{J}{l} = \frac{D}{l^2}(a_o - a_{-L}) \qquad 0 = \frac{D}{l^2}(b_o - b_{-L}) \tag{2.14}$$

at $-L$, and

$$K = \frac{J}{l} = \frac{D}{l^2}(b_o - b_L) \qquad 0 = \frac{D}{l^2}(a_o - a_L) \tag{2.15}$$

at $+L$. Here the sites $-L$, L are at the edges of the system, with site o being immediately outside L or $-L$. Taking the continuum limit of this action, we arrive

at

$$S[\hat{a},a,\hat{b},b,t] = \int \Big(dx d^{d-1}y \int_{-\infty}^{t} dt' \Big\{ \hat{a}(\partial_t - D\nabla^2)a + \hat{b}(\partial_t - D\nabla^2)b \\ -\lambda_0(1-\hat{a}\hat{b})ab \Big\} - a(t) - b(t) \Big), \quad (2.16)$$

subject to the conditions

$$-J = -D\partial_x b \qquad 0 = -D\partial_x a \quad (2.17)$$

at $+L$, and

$$J = -D\partial_x a \qquad 0 = -D\partial_x b \quad (2.18)$$

at $-L$. Here y are the coordinates for directions perpendicular to the applied currents. These conditions may be made explicit in the action by including a pair of delta functions (see below):

$$S = \int \Big(dx d^{d-1}y \int_{-\infty}^{t} dt' \Big\{ \hat{a}(\partial_t - D\nabla^2)a + \hat{b}(\partial_t - D\nabla^2)b \quad (2.19) \\ -\lambda_0(1-\hat{a}\hat{b})ab - \hat{a}J\delta(x+L) - \hat{b}J\delta(x-L) \Big\} - a(t) - b(t) \Big).$$

It is now convenient to make the substitutions $\hat{a} = 1 + \bar{a}$ and $\hat{b} = 1 + \bar{b}$. The integrals of $\partial_t a$ and $\partial_t b$ over time then generate the surface terms $a(t)$ and $b(t)$, which remove the final two projection state terms. This cancellation simplifies the perturbative calculations, as it removes the need to sum over an expansion of the end state densities $a(t)$ and $b(t)$. Hence our action becomes

$$S = \int dx d^{d-1}y dt' \Big[\bar{a}(\partial_t - D\nabla^2)a + \bar{b}(\partial_t - D\nabla^2)b + \lambda_0 \bar{a}ab + \lambda_0 \bar{b}ab \\ +\lambda_0 \bar{a}\bar{b}ab - \bar{a}J\delta(x+L) - \bar{b}J\delta(x-L) \Big]. \quad (2.20)$$

If we integrate over the $\bar{a}$ and $\bar{b}$ fields in the path integral, and neglect the $\bar{a}\bar{b}ab$ term, we obtain the classical (mean field) equations (see chapter 3 and [27])

$$(\partial_t - D\nabla^2)a + \lambda_0 ab - J\delta(x+L) = 0 \quad (2.21)$$

$$(\partial_t - D\nabla^2)b + \lambda_0 ab - J\delta(x-L) = 0. \tag{2.22}$$

On the further conditions that no particle annihilation occurs at the edges of the system, and that $\nabla a = 0$ and $\nabla b = 0$ outside, integrating the first equation from $-L-\epsilon$ to $-L+\epsilon$, and the second from $L-\epsilon$ to $L+\epsilon$, in the limit $\epsilon \to 0$, gives the required boundary conditions.

In the next chapter we will demonstrate that the diffusion constant does not exhibit singular behaviour in the renormalisation of the theory. Hence it is convenient to absorb it into a rescaling of time, as in [38]. Defining $\bar{t} = Dt'$, $\bar{\lambda} = \lambda_0 D^{-1}$, and $\bar{J} = JD^{-1}$, and introducing the fields $\phi = \frac{1}{2}(a+b)$ and $\psi = \frac{1}{2}(a-b)$, we have

$$S = \int dx d^{d-1}y d\bar{t} \left[2\bar{\phi}(\partial_{\bar{t}} - \nabla^2)\phi + 2\bar{\psi}(\partial_{\bar{t}} - \nabla^2)\psi + 2\bar{\lambda}\bar{\phi}(\phi^2 - \psi^2) + \right. \tag{2.23}$$
$$\left. \bar{\lambda}(\bar{\phi}^2 - \bar{\psi}^2)(\phi^2 - \psi^2) - \bar{J}\bar{\phi}[\delta(x+L) + \delta(x-L)] - \bar{J}\bar{\psi}[\delta(x+L) - \delta(x-L)] \right].$$

Consequently the new classical (mean field) equations are

$$\partial_{\bar{t}}\psi_c = \partial_x^2\psi_c + \frac{1}{2}\bar{J}[\delta(x+L) - \delta(x-L)] \tag{2.24}$$
$$\partial_{\bar{t}}\phi_c = \partial_x^2\phi_c - \bar{\lambda}(\phi_c^2 - \psi_c^2) + \frac{1}{2}\bar{J}[\delta(x+L) + \delta(x-L)]. \tag{2.25}$$

2.2 Noise

So far the quartic term in the action has been neglected with the result that the classical (mean field) results have been recovered. However, we can take into account the non-classical term by including Gaussian noise in the equations for ϕ and ψ, leading to equations which are exact. This modification can be derived by replacing the quartic piece in the action by a noise variable, integrating over the noise distribution, and demonstrating that this recovers the original term. Observ-

ing that

$$\int_{-\infty}^{\infty} d\eta_\phi e^{i\bar{\phi}\eta_\phi} e^{-\eta_\phi^2/[4\bar{\lambda}(\phi^2-\psi^2)]} \sim e^{-\bar{\lambda}\bar{\phi}^2(\phi^2-\psi^2)}, \tag{2.26}$$

and

$$\int_{-\infty}^{\infty} d\eta_\psi e^{\bar{\psi}\eta_\psi} e^{-\eta_\psi^2/[4\bar{\lambda}(\phi^2-\psi^2)]} \sim e^{\bar{\lambda}\bar{\psi}^2(\phi^2-\psi^2)}, \tag{2.27}$$

where η_ϕ and η_ψ are Gaussian noise variables, we see that the system is described exactly by the equations:

$$\partial_{\bar{t}}\psi = \partial_x^2\psi + \frac{1}{2}\bar{J}[\delta(x+L) - \delta(x-L)] + \eta_\psi \tag{2.28}$$

$$\partial_{\bar{t}}\phi = \partial_x^2\phi - \bar{\lambda}(\phi^2 - \psi^2) + \frac{1}{2}\bar{J}[\delta(x+L) + \delta(x-L)] + i\eta_\phi, \tag{2.29}$$

where

$$\langle \eta_\psi(x,\bar{t})\eta_\psi(x',\bar{t}')\rangle = \langle \eta_\phi(x,\bar{t})\eta_\phi(x',\bar{t}')\rangle = 2\bar{\lambda}(\phi^2-\psi^2)\delta(x-x')\delta(\bar{t}-\bar{t}'). \tag{2.30}$$

Clearly we have lost the simple interpretation of the a and b fields as being the local densities of A and B particles, as now the above equations include complex noise. Nevertheless, we can still interpret $\langle\psi\rangle$ and $\langle\phi\rangle$ as being averaged densities, which also satisfy

$$\partial_{\bar{t}}\langle\psi\rangle = \partial_x^2\langle\psi\rangle + \frac{1}{2}\bar{J}[\delta(x+L) - \delta(x-L)] \tag{2.31}$$

$$\partial_{\bar{t}}\langle\phi\rangle = \partial_x^2\langle\phi\rangle - \bar{\lambda}\langle\phi^2 - \psi^2\rangle + \frac{1}{2}\bar{J}[\delta(x+L) + \delta(x-L)]. \tag{2.32}$$

However, caution must be exercised in the interpretation of the Langevin-type equations (2.28) and (2.29). The reason for this stems from the commutation properties of the bosonic operators introduced in the second quantised formalism (see equation (2.2)). When one calculates, for example, the occupation number of the A particles at a site i, one is actually calculating the quantity $\langle a_i^\dagger a_i\rangle$. As we have shown before, the method by which averages are calculated in this theory

leads one to "sandwich" operators between the projection state on the left, and the state of the system on the right. Since we have $\langle|a_i^\dagger = \langle|$, we are effectively just calculating $\langle a_i\rangle$. However, consider now the calculation of the average square occupation number $\langle a_i^\dagger a_i a_i^\dagger a_i\rangle$. In order to compute this quantity we must first rewrite it in a normal ordered form, with all the creation operators moved to the left of the annihilation operators. Hence we can see that the average square occupation number is *not* given by $\langle a_i^2\rangle$, but by $\langle a_i^2 + a_i\rangle$. This important fact must be borne in mind if these Langevin equations are to be used correctly. For most of this thesis we will not pursue this approach - however an important exception concerns the analysis of the wandering reaction front for $A + B \to \emptyset$ in one dimension. In this case the Langevin equation (2.28) will form the starting point for our analysis.

A further important issue concerns the origin of the noise in the action (2.20). Tracing back the causes of the quartic terms, we see that they arise as a result of the stochastic nature of the reaction step. However, we note that there is no explicit contribution to the action from conserved diffusive noise. In this respect our formalism differs from various others introduced in the literature, for example that by Janssen [39], where this aspect of the noise is explicitly included. Nevertheless, our formulation of the problem is exact and we thus conclude that the effects of the conserved noise are taken into account in the commutation relations of our bosonic operators. A further indication that our theory is complete is given in work by Droz and McKane [40], where it was shown that an action derived using our methods is in a one to one correspondence with those of a different formalism, called the Poisson representation (see [41]). In this framework the state of the system is treated as being in a superposition of multivariate uncorrelated Poissons. However, also in [41], it is shown that this formalism is exactly equivalent to the original master

equation. Hence, by this somewhat circuitous route, we again reach the conclusion that our methods are exact and that the absence of conserved diffusive noise in our action is not a cause for concern. Indeed our methods are, in some respects, superior to those including the extra conserved noise, as the interaction vertices in our field theory are simpler, meaning that performing perturbative calculations is easier.

The problem of conserved noise is particularly important for the $1d$ wandering front calculation mentioned above. In that case we note that the noise for ψ in equation (2.28) is *not* conservative. As the reaction step does conserve the difference between the number of particles of each species, this appears to be a problem. However, a resolution of this difficulty again lies in the commutation relations of the bosonic operators, which have the consequence that the fluctuations in the ψ field are not the same as the (conserved) fluctuations in the density difference.

An alternative way to generate conserved noise more explicitly within our formalism has been suggested by Janssen [42] [1]. Instead of making the shifts $\hat{a} = 1 + \bar{a}$ and $\hat{b} = 1 + \bar{b}$, he suggested the transformations

$$\hat{a} = e^{\bar{a}} \qquad a = e^{-\bar{a}}\tilde{a} \tag{2.33}$$

$$\hat{b} = e^{\bar{b}} \qquad b = e^{-\bar{b}}\tilde{b}. \tag{2.34}$$

In this case conserved diffusive noise now appears in the action coupled to the $\tilde{a}$ and $\tilde{b}$ fields. Furthermore, one can demonstrate that the noise for $\tilde{\psi} = \tilde{a} - \tilde{b}$ is now conserved. Unfortunately the overall structure of this field theory is much more complicated, and thus using it for actual calculations appears difficult.

We round off this discussion of noise in reaction-diffusion systems by considering

[1] I thank Klaus Oerding for bringing this to my attention.

the nature of shot noise in the steady state front problem. Cornell [43] has analysed the effects of *Poissonian* boundary noise on the stability of the reaction front. He has concluded that in all dimensions such noise can be neglected for large enough systems. However, as was first pointed out by Cornell and Droz [44], the simple imposition of the steady *non-Poissonian* particle injection included in the action (2.20), is an unstable configuration. This is a result of fluctuations in the boundary particle currents (so called shot noise), which would cause the system to almost entirely fill up with particles of just one species. There are various methods of stabilising the front from this form of noise. One possibility is to consider a time dependent system (as in figure 1.2), where the presence of a constant density reservoir at large enough x will act to pin the reaction front. Alternatively, in a steady state formulation, one might choose to insert particles at the boundaries only when they are annihilated in the front. This procedure does, however, introduce rather unphysical correlations between particle annihilation and particle injection. In order to get around this problem we introduce the idea of reservoirs used in the simulations of chapter 3. In any case, our later analytic RG calculations will only consider the effects of noise emanating from the reaction front, and not from the boundaries. As we shall see, this approach will be successful in calculating the properties of the reaction front.

2.3 The Model for a Multispecies Reaction - Diffusion System

The derivation of the field theoretic action for the time dependent multispecies reaction-diffusion system is very similar to before. We shall simply restrict ourselves

to a consideration of the differences between this case and that discussed earlier. The principal modification lies in the replacement of boundary conditions with initial conditions.

At $t = 0$ the A and B particles are distributed at random according to a Poisson distribution, where the average initial density of each species is n_A and n_B respectively. Hence, if the average occupancy of B particles at a given site is μ, then the probability of having a number m of B particles at that site is given by

$$P(\text{No. of } B \text{ particles at a site } = m) = \frac{\mu^m e^{-\mu}}{m!}. \tag{2.35}$$

More generally, if the average occupancy of the A particles at a given site is ν, then for the initial distribution we have

$$P(\{n,m\}, t=0) = C \prod_i \frac{\nu^{n_i}\mu^{m_i}}{n_i! m_i!}, \tag{2.36}$$

where C is a normalising constant, independent of the $\{n,m\}$. The task now is to incorporate this probability distribution into our field theory. We first notice that

$$|\Upsilon(t=0)\rangle = C \sum_{\{n,m\}} \prod_i \frac{\nu^{n_i}\mu^{m_i}}{n_i! m_i!} (a_i^\dagger)^{n_i} (b_i^\dagger)^{m_i} |0\rangle \tag{2.37}$$

$$= C \prod_i \sum_{\{n,m\}} \frac{\nu^{n_i}\mu^{m_i}}{n_i! m_i!} (a_i^\dagger)^{n_i} (b_i^\dagger)^{m_i} |0\rangle \tag{2.38}$$

$$= C \prod_i e^{\nu a_i^\dagger + \mu b_i^\dagger} |0\rangle. \tag{2.39}$$

Hence, when the expectation value of an operator $\hat{F}$

$$\langle |\hat{F} \exp(-\hat{H}t)| \Upsilon(t=0)\rangle \tag{2.40}$$

is turned into a path integral, we can see that the initial conditions will lead to extra pieces within the action. These will have the form of the terms inside the product in equation (2.39).

Therefore, after making the mapping to a path integral, taking the continuum limit, and performing the shifts $\hat{a} = 1 + \bar{a}$ and $\hat{b} = 1 + \bar{b}$, we end up with:

$$S = \int d^d x \left(\int dt \left[\bar{a}(\partial_t - \nabla^2)a + \bar{b}(\partial_t - \delta\nabla^2)b + 2\lambda_{AA}\bar{a}a^2 + \lambda_{AA}\bar{a}^2a^2 \right. \right. \quad (2.41)$$
$$\left. \left. +2\lambda_{BB}\bar{b}b^2 + \lambda_{BB}\bar{b}^2b^2 + \lambda_{AB}\bar{a}ab + \lambda_{AB}\bar{b}ab + \lambda_{AB}\bar{a}\bar{b}ab \right] - \bar{a}n_A - \bar{b}n_B \right).$$

In this action the diffusion constant D_A has been absorbed into a rescaling of time and of the reaction rates. We also define $\delta = D_B/D_A$. Note that the final two terms are due to the initial conditions, though their form has changed a little from equation (2.39) due to the taking of the continuum limit (i.e. ν (μ) has become n_A (n_B), the initial A (B) species density).

Note that if we integrate over the $\bar{a}$ and $\bar{b}$ fields in the path integral, we again recover the mean field equations [31] (see also chapter 4):

$$\frac{da}{dt} = -2\lambda_{AA}a^2 - \lambda_{AB}ab \quad (2.42)$$
$$\frac{db}{dt} = -2\lambda_{BB}b^2 - \lambda_{AB}ab. \quad (2.43)$$

These equations, together with the action (2.41), will form the starting point for our analysis of chapter 4.

Chapter 3

The Reaction-Diffusion Front for

$A + B \rightarrow \emptyset$

3.1 Previous Work

The reaction front formed by the two species annihilation $A + B \rightarrow \emptyset$ has been the subject of great attention since the initial work of Gálfi and Rácz [26]. They introduced a time dependent model where a reaction front evolves from initial conditions where the A and B particles are completely segregated (see figure 1.2). Their starting point was the mean field rate equations for the particle densities a and b:

$$\frac{\partial a}{\partial t} = D\nabla^2 a - \lambda ab \tag{3.1}$$

$$\frac{\partial b}{\partial t} = D\nabla^2 b - \lambda ab, \tag{3.2}$$

where a mean field approximation of the form $\langle ab \rangle \propto \langle a \rangle \langle b \rangle$ has been made. At late times, Gálfi and Rácz showed that the mean field reaction front has the scaling

form

$$R(x,t) = \lambda a(x,t)b(x,t) \sim t^{-\beta} S\left(\frac{x}{t^{\alpha}}\right), \tag{3.3}$$

for the case where the densities of the two species are equal in their initial segregated zones. Note that the position $x = 0$ marks the centre of the front. In addition, it was demonstrated that in the mean field approximation the exponents take the values $\alpha = \frac{1}{6}$ and $\beta = \frac{2}{3}$. Their derivation included the assumption that the width of the reaction front is very much narrower than the width of the depletion zone of A and B particles. This assumption was shown to be justified *a posteriori* since the depletion zone grows diffusively as $t^{1/2}$, whereas the width w of the front was found to grow only as $w \sim t^{1/6}$. These results are now well backed up by the results of simulations (see for example [26, 45, 46, 47, 48, 49, 50, 51]), and also real chemical experiments [52, 53].

Ben-Naim and Redner [27] were the first to study the case of a steady state reaction interface, maintained by fixed particle currents imposed at opposite edges of the system. Their equations for the particle densities were identical to those of Gálfi and Rácz, except for the presence of the boundary conditions:

$$J = -D\partial_x a|_{x=-L} \quad 0 = -D\partial_x b|_{x=-L} \quad 0 = -D\partial_x a|_{x=L} \quad -J = -D\partial_x b|_{x=L}. \tag{3.4}$$

The mean field equations (see (2.24) and (2.25)) are soluble analytically for large $|x|$ (as they are in the large $|x|$, large t limit of the time dependent front - see [45]). The appropriate solutions are $\psi_c = -(\bar{J}/2)x$ (for $|x| \leq L$), whilst substituting $\phi_c = (\bar{J}/2)|x| + u$ into the mean field equation for ϕ_c, gives asymptotically the Airy equation for u, as was first noted in [27]. Asymptotically we have

$$\phi_c = \frac{J}{2D}|x| + C\left(\frac{J^2}{D\lambda}\right)^{1/3}\left(\frac{\lambda J}{D^2}\right)^{-1/12}|x|^{-1/4}e^{-(2/3)(\lambda J D^{-2})^{1/2}|x|^{3/2}} + \ldots, \tag{3.5}$$

where we have determined the constant $C \approx 0.3787$ numerically. From an analysis of the steady state mean field equations, Ben-Naim and Redner also demonstrated the relations $w \sim (\lambda J/D^2)^{-1/3}$, and $\rho \sim (J^2\lambda^{-1}/D)^{1/3}$, where ρ is the particle concentration in the reaction zone.

A further important development in [27] concerns the introduction of the quasi-static approximation. For the time dependent problem, in the region $w \ll x \ll t^{1/2}$, the majority species density profile is of the form $b \sim b_0 x/t^{1/2}$. Hence the flux of particles arriving at the origin is given by $J = D\partial_x b \sim t^{-1/2}$. The characteristic timescale on which this current varies is $(d \log J/dt)^{-1} \sim t$. This should be compared with the equilibration time for the front, which is of order $(w^2/D) \sim t^{1/3} \ll t$. As a result, we see that the front is formed quasistatically, and hence, in this simple mean field approach, we may obtain the results of the time dependent model from the steady state case by writing $J \sim t^{-1/2}$.

All the above considerations have been based on the mean field rate equations (3.1) and (3.2). However, as we have previously mentioned, we expect this approximation to break down below some critical spatial dimensionality, due to the presence of fluctuations. Cornell and Droz [54] have used dimensional analysis to propose the value $d_c = 2$ for this upper critical dimension. They have also put forward scaling forms for a,b and the reaction front R, which are postulated to be valid both above and below the critical dimension in the scaling limit $w \to \infty$ (or $J \to 0$):

$$R = \frac{J}{w} S\left(\frac{x}{w}\right) \qquad a = \frac{wJ}{D} A\left(\frac{x}{w}\right) \qquad b = \frac{wJ}{D} B\left(\frac{x}{w}\right) \tag{3.6}$$

In other words, the profiles are characterised by a single length scale w, which is suggested in [54] to vary as $w \sim (J/D)^{-1/2}$ in $d = 1$, and $w \sim (\lambda J/D^2)^{-1/3}$ for $d \geq 2$, in the scaling limit. Cardy and Lee [55] have given RG arguments which

support this conclusion. Hence, application of the quasistatic approximation leads to the conclusion $w \sim t^{1/4}$ for the time dependent problem in one dimension. These results have, for the most part, been confirmed by simulations [29, 54], but there has been an ongoing controversy concerning the existence of multiscaling in the higher order spatial moments of the time dependent reaction front (see [28, 29]). Simulations have also indicated that the reaction front profile in one dimension is very well described by a Gaussian [29]. This result has hitherto not been explained. We will discuss these matters further after we have presented some further analysis.

3.2 Interface Fluctuations

The first problem we consider is that of the centre of mass fluctuations of the reaction front. This is similar to the question of the fluctuations of an interface in the dynamical Ising Model, as described by the time dependent Landau-Ginzburg (TDLG) equation with noise (for example in model A - see [56]). This equation may be mapped to a path integral for the order parameter field Φ (the local magnetisation), with the introduction of response fields $\tilde{\Phi}$, using the Martin-Siggia-Rose formalism:

$$\int \mathcal{D}\Phi\mathcal{D}\tilde{\Phi}e^{-\int dx d^{d-1}y dt[\tilde{\Phi}\{\dot{\Phi}+\Gamma(-\nabla^2\Phi+\tilde{t}\Phi+u\Phi^3)\}-\frac{1}{2}\Gamma\tilde{\Phi}^2]}. \tag{3.7}$$

Here the last term in the above action results from the noise, Γ is the dissipation coefficient, $\tilde{t}$ the mean field reduced temperature, and u the coupling constant for the Φ^4 term in the coarse-grained free energy functional. Solving the TDLG equation in the absence of noise gives us the classical profile Φ_c, and on physical grounds we expect the full functional form of Φ to be $\Phi_c(x - f(y,t)) \approx \Phi_c(x) - f(y,t)\Phi_c'(x)$. The idea now is to substitute this into the action and to expand the

response fields in terms of some complete set of eigenfunctions $\Psi_n(x)$:

$$\tilde{\Phi}(x,y,t) = \sum_n A_n \tilde{f}_n(y,t)\Psi_n(x), \tag{3.8}$$

where the $\{A_n\}$ are normalising constants. The set of eigenfunctions is chosen such that when the x dependence is integrated out of the action, it leaves behind an unambiguous equation for $f(y,t)$, obtained by integrating over the new response fields $\tilde{f}_n(y,t)$ in the path integral. For the Ising case, $f(y,t)$ can be shown to satisfy a noisy diffusion equation whose solution implies that fluctuations delocalise the interface for $d \leq 3$. A similar result for reaction fronts would have dramatic consequences.

Returning to the reaction-diffusion system, we expect the functional forms for the fields in our geometry to be $\psi(x - f_1(y,t))$ and $\phi(x - f_2(y,t))$, by analogy with the Ising case. Considering first the situation where we neglect noise in the system, we expand the above functional forms, giving

$$\phi \approx \phi(x) - f_2(y,t)\phi'(x) \Rightarrow \phi \approx \frac{1}{2}\bar{J}|x| \mp \frac{1}{2}\bar{J}f_2 \qquad (x = \pm L) \tag{3.9}$$

$$\psi = \psi(x) - f_1(y,t)\psi'(x) \Rightarrow \psi = -\frac{1}{2}\bar{J}x + \frac{1}{2}\bar{J}f_1. \tag{3.10}$$

Hence $a = (1/2)\bar{J}(f_1 - f_2)$ and $b = \bar{J}x - (1/2)\bar{J}(f_1 + f_2)$ at $x = L$, and $a = -\bar{J}x + (1/2)\bar{J}(f_1 + f_2)$ and $b = (1/2)\bar{J}(f_2 - f_1)$ at $x = -L$. In the absence of noise a and b represent the (positive) particle densities, so we must have $f_1 = f_2$.

However, if we include the noise term then this argument is invalid, and we proceed, as in the Ising case, by inserting the expanded functional forms for ϕ and ψ into the action (2.20), giving

$$S = \int dx d^{d-1}y dt' [2\bar{\phi}\{\phi_c'[-\dot{f}_2 + \nabla_\perp^2 f_2] + 2\bar{\lambda}\psi_c\psi_c'(f_1 - f_2)\}$$
$$+2\bar{\psi}\{\psi_c'[-\dot{f}_1 + \nabla_\perp^2 f_1]\} + \bar{\lambda}(\bar{\phi}^2 - \bar{\psi}^2)(\phi_c^2 - \psi_c^2)], \tag{3.11}$$

where we have made the approximation $\phi \to \phi_c$, and then used the classical equations to simplify the expression. In our case it is now appropriate to Fourier expand the $\bar{\psi}$ and $\bar{\phi}$ fields, i.e.

$$\bar{\psi} = \sum_n \zeta_n(y,t)\theta_n(x) \qquad \bar{\phi} = \sum_n \xi_n(y,t)\theta_n(x), \tag{3.12}$$

where $\theta_n = \sin(n\pi x/L)$ for $n > 0$, $\theta_n = 1/2$ for $n = 0$, and $\theta_n = \cos(n\pi x/L)$ for $n < 0$. Inserting this into the noise term and performing the x integration, we have

$$\int \bar{\psi}^2(\phi_c^2 - \psi_c^2)dx = \sum_{n,m} \zeta_n\zeta_m \int_{-L}^{L} \theta_n\theta_m(\phi_c^2 - \psi_c^2)dx = \sum_{n,m} \zeta_n X_{nm}\zeta_m, \tag{3.13}$$

where X_{nm} is a symmetric matrix which we now diagonalise. Using $\hat{\zeta}_n = D_{nm}\zeta_m$, but such that $\hat{\zeta}_0 = \zeta_0$, we rewrite (3.13) as

$$\sum_{n,m} \hat{\zeta}_n \Lambda_{nm} \hat{\zeta}_m, \tag{3.14}$$

where $\mathbf{\Lambda}$ is a diagonal, and $\mathbf{D}$ a diagonalising, matrix. Bearing in mind the symmetries of the classical solutions, we can perform the x integration within the action to arrive at the path integral:

$$\int \mathcal{D}f_1\mathcal{D}f_2 \prod_n \mathcal{D}\hat{\zeta}_n\mathcal{D}\xi_n \exp\left[-\int d^{d-1}y dt' \left\{2\sum_{n>0} \xi_n[A_n(-\dot{f}_2 + \nabla_\perp^2 f_2) \right.\right. \tag{3.15}$$
$$\left.\left. +2\bar{\lambda}B_n(f_1 - f_2)] + \bar{\lambda}\sum_{n,m} \xi_n\xi_m X_{nm} + 2\hat{\zeta}_0 C_0[-\dot{f}_1 + \nabla_\perp^2 f_1] - \bar{\lambda}\sum_n \hat{\zeta}_n\Lambda_{nn}\hat{\zeta}_n \right\}\right],$$

with

$$A_n = \int_{-L}^{L} \theta_n\phi_c' dx, \qquad B_n = \int_{-L}^{L} \theta_n\psi_c\psi_c' dx, \qquad C_0 = \int_{-L}^{L} \theta_0\psi_c' dx \sim \bar{J}L. \tag{3.16}$$

Integrating over $\hat{\zeta}_0$ and f_1 gives the equation

$$-\dot{f}_1 + \nabla_\perp^2 f_1 + \eta = 0, \tag{3.17}$$

where η is a noise variable with a Gaussian distribution:

$$P(\eta) \sim e^{-(\eta^2 C_0^2/\bar{\lambda}|\Lambda_{00}|)} \tag{3.18}$$

If we also diagonalise the noise term involving the ξ fields, then the relevant part of the action is transformed to

$$2\sum_{n>0} W_n \hat{\xi}_n [A_n(\dot{g} - \nabla_\perp^2 g - \eta) - 2\bar{\lambda} B_n g] + \bar{\lambda} \sum_n \hat{\xi}_n \Lambda_{nn} \hat{\xi}_n, \tag{3.19}$$

where $g = f_1 - f_2$, and the equation for f_1 (3.17) has been added into the action. The $\{W_n\}$ are coefficients generated by writing ξ_n in terms of $\{\hat{\xi}_m\}$. Finally, performing the integrations over $\hat{\xi}_n$ and g, we find equations for g which can only be mutually consistent for different n if $g = 0$, or in other words, if $f_1 = f_2 = f$. From (3.13) we see that $\Lambda_{00} \sim \bar{J}\bar{\lambda}^{-1}$, and so

$$-\dot{f} + \nabla_\perp^2 f + \eta = 0, \tag{3.20}$$

where η is a Gaussian noise variable with probability distribution:

$$P(\eta) \sim e^{-(const.)L^2 \bar{J}\eta^2}. \tag{3.21}$$

We now proceed to calculate the mean square fluctuation $\langle f^2 \rangle - \langle f \rangle^2$. This can be done in a straightforward manner, solving the noisy diffusion equation satisfied by f using a Green function method. The results are

$$\langle f(y,t)^2 \rangle - \langle f(y,t) \rangle^2 \sim \begin{cases} \frac{\Lambda^{d-3}\bar{J}^{-1}}{L_\parallel^2} & \text{for } d \geq 4 \\ \frac{\ln(L_\perp \Lambda)\bar{J}^{-1}}{L_\parallel^2} & \text{for } d = 3 \\ \frac{L_\perp \bar{J}^{-1}}{L_\parallel^2} & \text{for } d = 2, \end{cases} \tag{3.22}$$

where the system has physical dimensions $L_\parallel \times L_\perp^{d-1}$, and Λ is now the large k

momentum cut-off. So we expect that interface fluctuations will be unimportant if

$$\langle f^2 \rangle - \langle f \rangle^2 \sim \begin{cases} \frac{\Lambda^{d-3}}{L_\parallel^2 JD^{-1}} \ll L_\parallel^2 & \Rightarrow \quad \frac{L_\parallel^2 (JD^{-1})^{1/2}}{\Lambda^{(d-3)/2}} \gg 1 \quad \text{for } d \geq 4 \\ \frac{\ln(L_\perp \Lambda)}{L_\parallel^2 JD^{-1}} \ll L_\parallel^2 & \Rightarrow \quad \frac{L_\parallel^2 (JD^{-1})^{1/2}}{(\ln(L_\perp \Lambda))^{1/2}} \gg 1 \quad \text{for } d = 3 \\ \frac{L_\perp}{L_\parallel^2 JD^{-1}} \ll L_\parallel^2 & \Rightarrow \quad \frac{L_\parallel^2 (JD^{-1})^{1/2}}{L_\perp^{1/2}} \gg 1 \quad \text{for } d = 2. \end{cases} \tag{3.23}$$

Hence, for $d \geq 2$ fluctuations resulting from internal noise do not delocalise the front. However, in $d = 1$, the situation is rather different and we conclude that, in an infinite one dimensional system, the front is completely unpinned and free to perform a random walk. This follows from equation (3.20) which has the form

$$\dot{f} = \eta \tag{3.24}$$

in one dimension. This indicates that we must treat the one dimensional case in a somewhat different way from higher dimensions. Note, however, that in finite systems, with appropriate boundary conditions, the above "zero mode" fluctuations are actually forbidden. Nevertheless, the analysis of section 3.3.2 will show that higher order fluctuation harmonics can still have a dramatic effect on the reaction front profile.

Our results can now be applied to the problem of the late time behaviour of an initially homogeneous distribution of A and B particles [18, 19, 55, 57, 58], where it has been shown that the reactants segregate asymptotically [13, 18, 19, 55]. We assume here that we can access the quasistatic time dependent regime by simply replacing our currents J by their time dependent analogues. In this homogeneous system the densities decay at late times as $t^{-d/4}$, whereas the length scale of the segregated zones grows diffusively as $t^{1/2}$. Hence the time dependent inward currents towards the domain interfaces scale as $J \sim t^{-(d+2)/4}$. So on the basis of our assumption, we can insert the appropriate time dependencies into

(3.23) for $d \geq 2$, and use equation (3.24) to calculate the fluctuations in $d = 1$. It is then easily seen that these fluctuations are unimportant at large enough times in dimensions where segregation occurs ($d < 4$).

3.3 The Reaction Front in One Dimension

As we have noted in the last section we must treat the $1d$ reaction front in a rather different manner to other spatial dimensionalities, owing to the existence of centre of mass fluctuations. We shall begin by describing the results of some $1d$ numerical simulations.

3.3.1 Simulation Details

Previous one dimensional reaction-diffusion simulations have usually employed an infinite reaction rate, which enforces complete segregation between the two species (see for example [28, 29]). Furthermore, often only single occupancy of a given lattice site for a particular species has been permitted. In our simulations we relax these restrictions by simulating a system with both multiple site occupancy and an adjustable, finite, reaction rate λ. This model will turn out to be closer to that used in the analytic RG calculations, which we will describe later in this chapter.

Our model consists of a one dimensional lattice with L sites on which particles of types A and B are located. In addition to this the model features reservoirs containing either A or B particles. The total number of particles of each species was set equal: $N_A = N_B = N/2$. Three distinct processes occur:

(1) A and B particles located on the lattice hop to neighboring sites in each direction with a hopping rate h, which we set equal to 1 (corresponding to $D = 1$

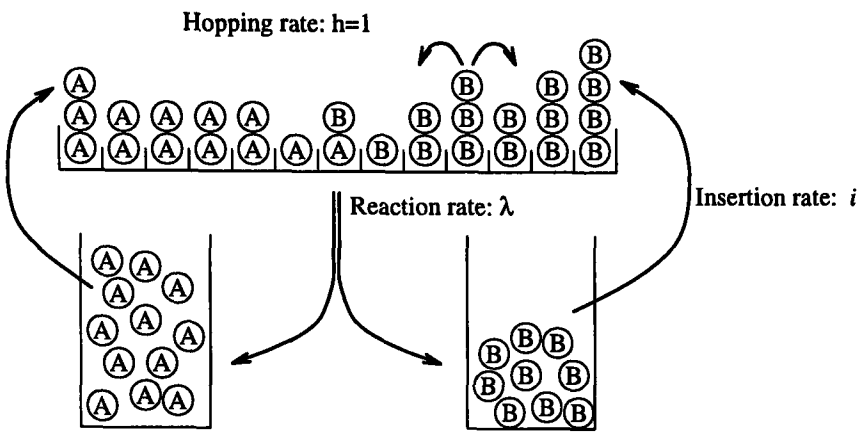

Figure 3.1: In our model A and B particles are located on a one-dimensional lattice. Three processes occur: particles can hop one lattice site to the left or right with rate $h = 1$; each pair of A and B particles at the same site can react with a rate λ, after which they are moved to their respective reservoirs; and A (B) particles enter the lattice on the left (right) sides with an insertion rate i.

in the continuum theory).

(2) Each A particle can react with each B particle on the same lattice site with a reaction rate λ. After each reaction both particles are removed from the lattice and placed in their respective reservoirs.

(3) Each A (B) particle in the reservoir is inserted onto the leftmost (rightmost) site in the lattice with an insertion rate i. Clearly $J = N_{res} \cdot i$, where N_{res} is the number of particles in the reservoir. The purpose of these reservoirs is to break up correlations between particle annihilation inside the reaction front and particle reinsertion at the boundaries - the larger the reservoirs the smaller the correlations. The same effect can be achieved by increasing the system size, but this is computationally far less efficient, as in that case particles have to hop large distances before they can reach the reaction zone.

We carry out the simulations using rare-event dynamics (RED). In this Monte

Carlo method the time increment is determined by the current configuration: if many changes in the configuration are likely, then the time increment is small, whereas if the configuration is very stable, the time increment is large. In RED, a list is made of all possible changes to the configuration (events), together with the expected time after which each event will occur. So we have $4L - 2$ events for A and B particle hops, L events for recombination of a pair, and 2 events for insertion of a particle of either type; altogether $5L$ events.

One step in a RED simulation consists of incrementing the time scale with $\Delta t = 1/\sum_j(r_j)$, where r_j is the rate for event j, and then allowing selection (and execution) of an event. The probability that event i is chosen is equal to $p_i = r_i/\sum_j(r_j)$.

For an efficient implementation the events are organized in a binary tree, where each branch contains one event and has a weight equal to the rate of that event. The weight of a parent node is equal to the sum of the weights of its children. As the root node contains the sum of all rates, the time increment Δt is easily obtained: it is the inverse of the weight of the root node. To select a particular event i with a probability proportional to its rate r_i, we start in the root node, descend to either its left or its right child with a probability proportional to their weights, and iterate this process until we have reached the bottom of the tree. The selected event is then executed and the weights in the tree of all events whose rates have changed, plus their parents, grandparents, etc. are updated. The use of the binary tree assures that the CPU time required for one step in the RED simulation scales with the logarithm of the size of the tree.

The initial configuration for each simulation consisted of linear density profiles for the A and B species, which decreased from the left and the right hand edges to

the system centre. In all our simulations, we chose L such that no A particle ever penetrated the B-rich region to within 10 sites of the lattice boundary, and vice versa. Correlation and thermalisation times varied with J, N, λ and L, and the tails of the reaction front required more thermalisation than the middle section. The necessary thermalisation time never exceeded 10^7 events. To be safe, we thermalised our system in all runs over 10^8 events.

3.3.2 One Dimensional Results

We consider first the regime $\lambda J^{-1/2} D^{-1/2} \ll 1$, where the mean field reaction front width $w_{mf} \sim (\lambda J/D^2)^{-1/3}$ is much larger than the predicted fluctuation modified width $\sim (J/D)^{-1/2}$. In this case we expect that the behavior of the system should be close to mean field. The mean field reaction front $R_{mf} = \lambda ab$ has the form

$$R_{mf} = J(\lambda J/D^2)^{1/3} S([\lambda J/D^2]^{1/3} x). \tag{3.25}$$

Hence the mean-field solution predicts that measured data for the reaction front should collapse if $R/[J(\lambda J/D^2)^{1/3}]$ is plotted as a function of $(\lambda J/D^2)^{1/3}x$, as shown in figure 3.2. In this case the number of particles N (which varied from between 1300 to 12000) was tuned to obtain the desired J. Note that in many previous simulations this mean field regime was completely inaccessible, since in those cases the reaction rate was taken to be infinite.

The collapsed data is in good agreement with the mean field prediction, although there is a slight tendency for our simulation data to lie to the right of R_{mf} for the largest values of $(\lambda J/D^2)^{1/3}x$. In this region, where the number of minority particles is small, we expect that noise from the reaction front will again become important leading to a widening of the profile. Note that these simulation results

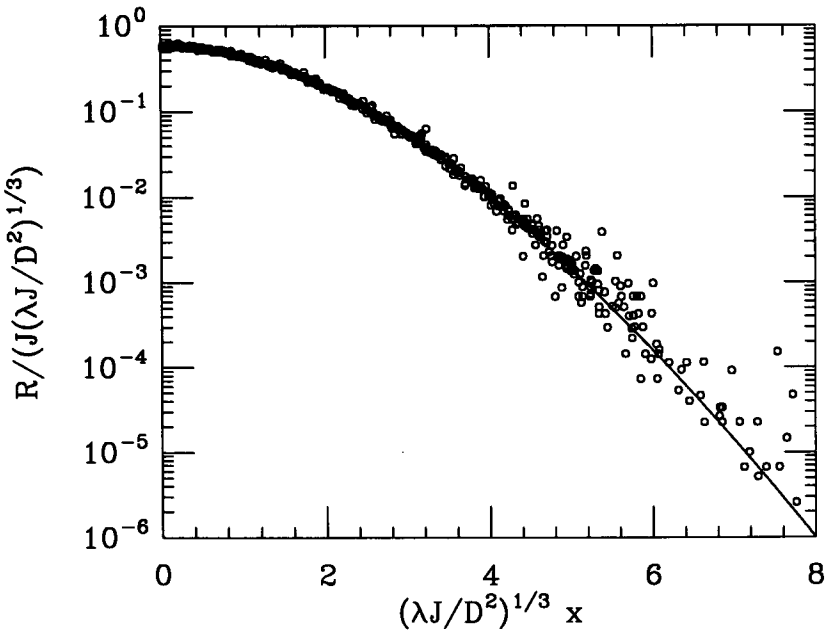

Figure 3.2: Collapsed data in the regime $\lambda J^{-1/2} D^{-1/2} \ll 1$. Solid line: mean field prediction. Squares: simulation results for runs over 10^9 events and $i = 1000$, with $D = 1$, $\lambda = 0.001, 0.01, 0.1$, and $J = 0.1, 0.2, 0.5, 1.0$.

were found not to depend on the inclusion of reservoirs in our model, implying that the existence of correlations between particle annihilation and reinjection was unimportant in this case.

In the limit $\lambda J^{-1/2} D^{-1/2} \gg 1$ the mean field solution predicts that the reaction front will become increasingly narrow. However, the simulations disagree with this assertion - the reaction front keeps a finite width even if λ is made very large. Our analysis, described below, distinguishes two components of this width: one is intrinsic, and the other is caused by the ability of the centre of the front to wander. The intrinsic width is calculable using the RG approach, which we will discuss later in this chapter, whereas the front wandering can be understood by considering the fluctuations in the field $\psi = a - b$, whose zero may be taken as defining the centre of the front. Including the effects of reaction front noise (which is relevant in one dimension), the field theory leads to the following equation for ψ (see equation

(2.28)):

$$\frac{\partial \psi}{\partial t} = D\partial_x^2 \psi + \eta, \tag{3.26}$$

where we have left out terms due to the boundary conditions. Here η is the reaction front noise, satisfying $\langle \eta(x,t) \rangle = 0$ and

$$\langle \eta(x,t)\eta(x',t') \rangle = 2\delta(t-t')\delta(x-x')R, \tag{3.27}$$

where the reaction rate at the wandering front, with width w_g, has the form $R = (J/w_g)S(x/w_g)$. Note that the form of the noise written down in equation (3.27) is exact - a consequence of its derivation from an exact field theoretic action. It is also important to realise that, while ψ is on average equal to $\langle a \rangle - \langle b \rangle$, its fluctuations are *not* the same as those in the density difference. This arises from the non-trivial commutation properties of the bosonic creation and annihilation operators (a point which we discussed in chapter 2). This fact accounts for the non-conservative nature of the noise in equation (3.26). We may now decompose ψ into its mean field part together with higher order Fourier harmonics:

$$\psi = -(J/D)x + \sum_{n=0} \chi_n(t) \cos\left(\frac{(2n+1)\pi x}{L}\right) \tag{3.28}$$

for $-(L/2) \leq x \leq (L/2)$. These corrections are the most general possible which both couple to the noise (i.e. the harmonics have a non-zero amplitude at $x = 0$), and which are appropriate for the non-conservative nature of the noise. Furthermore the densities on the boundaries are kept constant by these additional terms. Note, however, that the zero mode fluctuations of the form considered in section 3.2 are excluded from the Fourier decomposition of ψ - this is a consequence of the boundary conditions. We can now insert the above expression into the noisy diffusion equation and use the following approximate form for the reaction front

noise:

$$\langle \eta(x',t')\eta(x,t)\rangle = \frac{2J}{w_g} S\left(\frac{x}{w_g}\right)\delta(x-x')\delta(t-t') \approx 2J\delta(t-t')\delta(x)\delta(x'). \quad (3.29)$$

Fourier expanding these delta functions yields an equation for the amplitudes χ_n:

$$\dot{\chi}_n = -\frac{(2n+1)^2\pi^2}{L^2}\chi_n + \frac{2\sqrt{2J}}{L}\eta, \quad (3.30)$$

where now

$$\langle \eta(t)\rangle = 0 \qquad \langle \eta(t)\eta(t')\rangle = \delta(t-t'). \quad (3.31)$$

Solving equation (3.30) in the large time limit gives

$$\chi_n(t) \approx \frac{2\sqrt{2J}}{L}\int_0^t \eta(t')\exp\left[\frac{(2n+1)^2\pi^2 D}{L^2}(t'-t)\right]dt'. \quad (3.32)$$

Clearly $\psi(x=0,t) = \sum \chi_n(t)$ is a Gaussian random variable with

$$\langle \psi(0,t)^2\rangle - \langle \psi(0,t)\rangle^2 = \sum_{n,m}\langle \chi_n(t)\chi_m(t)\rangle \quad (3.33)$$

$$= \sum_{n,m}\frac{8J}{L^2}\int_0^t dt'\int_0^t dt'' \exp\left(-\frac{(2n+1)^2\pi^2}{L^2}(t-t')\right)$$
$$\times \exp\left(-\frac{(2m+1)^2\pi^2}{L^2}(t-t'')\right)\langle \eta(t')\eta(t'')\rangle \quad (3.34)$$

$$= \sum_{n,m}\frac{8J}{\pi^2[(2n+1)^2+(2m+1)^2]} \quad (3.35)$$

$$\sim \frac{J}{\pi D}\ln\left(\frac{cL}{w_g}\right), \quad (3.36)$$

in the large time limit, with c a constant, and where the upper limit of the summation is provided by the finite width w_g of the wandering reaction front. Assuming that the fluctuations of ψ are small in comparison with the system size, then the gradient of ψ at $x = 0$ remains approximately equal to $-(J/D)$. Hence, to leading order, we expect the position of the zero of the ψ field to be a Gaussian random variable with width w_g, given by the recursive relation:

$$w_g = \left[\frac{\ln(cL/w_g)}{\pi(J/D)}\right]^{\frac{1}{2}} \quad (3.37)$$

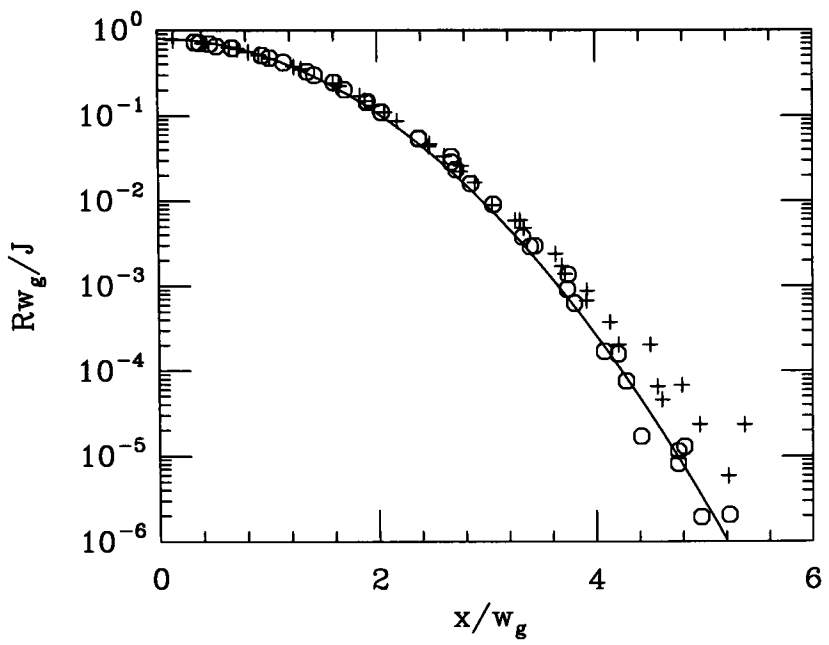

Figure 3.3: Collapsed data in the regime $\lambda J^{-1/2} D^{-1/2} \gg 1$. Solid line: normalized Gaussian; Data points: simulation results over 10^9 events with $D = 1$, $\lambda = 1000$, $i = 1000$, $J = 0.1, 0.2, 0.5, 1.0$, and $N = 100$ (0), 1000 (+).

From our simulation data (in the limit $\lambda J^{-1/2} D^{-1/2} \gg 1$) we have plotted Rw_g/J as a function of x/w_g, where in (3.37) we used $c = 0.5$ (see figure 3.3). The collapsed data is well described by a normalised Gaussian with width 1, in good agreement with our theory. This indicates that any higher order non-Gaussian corrections to the distribution of the zero of the ψ field are indeed small. Note that the logarithmic factor in (3.37) is essential for a good fit to the data.

We can clearly see from figure 3.3 that, in the appropriate limit, the wandering Gaussian dominates over the intrinsic profile (which we will discuss in succeeding sections) to form the overwhelming component of the front in $1d$. Notice also that we find a basic $(J/D)^{-1/2}$ scaling, in agreement with earlier predictions [24, 29, 54, 55]. Previously, however, only the *intrinsic* part of the front was being analysed, whereas we have been studying the *wandering* piece. The scaling agreement is simply a consequence of dimensional analysis - any quantity with the

dimensions of length, which is independent of λ, must scale as $(J/D)^{-1/2}$. We may also generalise our calculation to the time dependent case, where a reaction front is formed quasistatically between initially entirely segregated reactants. In this situation we find $w_g \sim t^{\alpha}(\ln t)^{1/2}$, where $\alpha = 1/4$. The presence of the logarithm may explain the slow convergence found in measurements of the exponent α [29].

In summary, we now have a good understanding of the Gaussian nature of the front in $1d$ - it is simply a result of the centre of mass fluctuations of the reaction front. Next we turn to a consideration of the intrinsic front in $1d$, and the overall front profile in higher dimensions.

3.4 Summary of Results for the Intrinsic Front

We first present our results for the asymptotic forms of the densities and the (intrinsic) reaction front profile. Since the associated calculations are quite long, we will, for convenience, group together our results below. It will be shown that a zero loop field theoretic calculation yields a stretched exponential dependence, which we include in the following summary even though we expect its effects to be overwhelmed by leading and subleading power law terms. In addition, for $d < 2$, we do not rule out the possibility of logarithms in higher order terms summing to give a modification to the leading power law given below (which results from the straightforward evaluation of the one loop contributions). So we find asymptotically, as $|x| \to \infty$, for $d < 2$:

$$\begin{Bmatrix} \langle a \rangle \\ \langle b \rangle \end{Bmatrix} = (J/D)|x| \begin{Bmatrix} \theta(-x) \\ \theta(x) \end{Bmatrix} + A_1 |x|^{(7-5d)/12} e^{-A_2|x|^{(d+1)/2}} + A_3 |x|^{-5+2\epsilon} + \dots \quad (3.38)$$

$$R = \lambda \langle ab \rangle = A_4 |x|^{(7d-5)/12} e^{-A_2|x|^{(d+1)/2}} + A_5 |x|^{-7+2\epsilon} + \dots \quad (3.39)$$

where

$$A_1 = 0.3787\frac{(J/D)^{7/12}}{(4\pi\epsilon)^{5/12}} \qquad A_2 = \frac{2}{3}(4\pi\epsilon)^{1/2}(J/D)^{1/2} \qquad A_3 = \frac{1}{32\pi^2(J/D)\epsilon} \tag{3.40}$$

$$A_4 = 0.3787(J/D)^{19/12}\frac{(4\pi\epsilon)^{7/12}}{(9/D)}(d+1)^2 \qquad A_5 = \frac{(2d+1)(2d+2)}{32\pi^2(J/D^2)\epsilon}; \tag{3.41}$$

for $d = 2$:

$$\begin{Bmatrix}\langle a\rangle \\ \langle b\rangle\end{Bmatrix} = (J/D)|x|\begin{Bmatrix}\theta(-x) \\ \theta(x)\end{Bmatrix} + B_1(\ln|x|)^{\frac{5}{12}}|x|^{-\frac{1}{4}}e^{-B_2(\ln|x|)^{-1/2}|x|^{3/2}} + B_3|x|^{-5}\ln|x| + \ldots \tag{3.42}$$

$$R = B_4(\ln|x|)^{-7/12}|x|^{3/4}e^{-B_2(\ln|x|)^{-1/2}|x|^{3/2}} + B_5|x|^{-7}\ln|x| + \ldots \tag{3.43}$$

where

$$B_1 = 0.3787\frac{(J/D)^{7/12}}{(4\pi)^{5/12}} \qquad B_2 = \frac{2}{3}(4\pi(J/D))^{1/2} \qquad B_3 = \frac{(J/D)^{-1}}{32\pi^2} \tag{3.44}$$

$$B_4 = 0.3787(4\pi)^{7/12}D(J/D)^{19/12} \qquad B_5 = \frac{15(J/D)^{-1}}{16\pi^2/D}; \tag{3.45}$$

and finally, for $d > 2$:

$$\begin{Bmatrix}\langle a\rangle \\ \langle b\rangle\end{Bmatrix} = (J/D)|x|\begin{Bmatrix}\theta(-x) \\ \theta(x)\end{Bmatrix} + C_1|x|^{-1/4}e^{-C_2|x|^{3/2}} + C_3|x|^{-d-3} + \ldots \tag{3.46}$$

$$R = C_4|x|^{3/4}e^{-C_2|x|^{3/2}} + C_5|x|^{-d-5} + \ldots \tag{3.47}$$

where

$$C_1 = 0.3787\frac{(J/D)^{7/12}}{(\lambda/D)^{5/12}} \qquad C_2 = \frac{2}{3}(\lambda J/D^2)^{1/2} \tag{3.48}$$

$$C_3 = (\lambda J/D^2)^{-1}2^{-1-d}\pi^{-(d+1)/2}(d-1)\Gamma\left(\frac{d-1}{2}\right) \qquad C_4 = 0.3787\lambda\frac{(J/D)^{19/12}}{(\lambda/D)^{5/12}} \tag{3.49}$$

$$C_5 = \lambda(\lambda/D)^{-2}(J/D)^{-1}2^{-1-d}\pi^{-(d+1)/2}\Gamma\left(\frac{d-1}{2}\right)(d-1)(d+3)(d+4). \tag{3.50}$$

Although these results are for the case of equal diffusion constants, we note that our calculations could be repeated for $D_A \neq D_B$. However, we do not expect

that such a modification will make a qualitative difference, at least for the case where both diffusion constants remain non-zero [59]. Evidence for this comes from a similar calculation by Lee and Cardy [19] for the same two species reaction, but with homogeneous initial conditions. They found that unequal diffusion constants led only to modified amplitudes for the densities, whilst leaving the density decay exponent unchanged.

3.5 Field Theory Formulations

Our goal is now to use our field theoretic techniques to calculate the intrinsic front profile. In what follows it will be convenient to develop two parallel field theories - one given by the action already described in (2.20), and another to be described below, formed by writing $\phi = \phi_c + \phi_1$ and $\psi = \psi_c + \psi_1$. In particular, whilst the second theory is more useful for calculations, the cancellation of divergences after renormalisation, and the identification of leading terms in an expansion in powers of the coupling constant, are easier to see in the first theory.

3.5.1 Propagators and Vertices

First of all we give the natural canonical dimensions for the various quantities appearing in the action (2.20), noting that the coupling becomes dimensionless at the postulated value of the critical dimension [54]:

$$[\bar{t}] = k^{-2} \qquad [a, b] = k^d \qquad [\bar{a}, \bar{b}] = k^0 \qquad [\bar{\lambda}] = k^{2-d} \qquad [\bar{J}] = k^{d+1}. \tag{3.51}$$

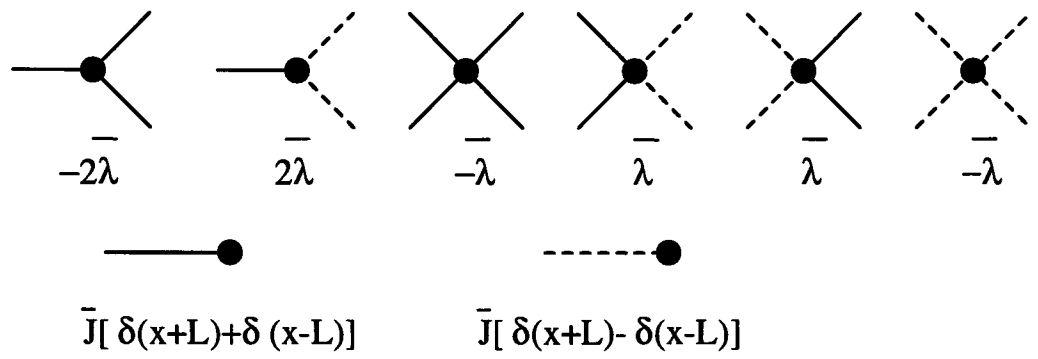

Figure 3.4: Vertices for Field Theory I.

The propagators for the first of the two theories described above (which we shall call Field Theory I) are (from (2.20))

$$G_{\phi\bar{\phi}}(k,\bar{t}) = G_{\psi\bar{\psi}}(k,\bar{t}) = \frac{1}{2}e^{-k^2\bar{t}}, \tag{3.52}$$

in $(k,\bar{t})$ space. In (k,s) space, where a Laplace transform of time has been performed, we have

$$G_{\phi\bar{\phi}}(k,s) = G_{\psi\bar{\psi}}(k,s) = \frac{1/2}{k^2+s}. \tag{3.53}$$

The vertices are shown in figure 3.4, where the ϕ propagators are represented by solid lines and ψ propagators by dotted lines.

For Field Theory II, we split the ϕ and ψ fields into their classical and non-classical components, which leads to a modified action

$$\begin{aligned} S = \int dx d^{d-1}y d\bar{t} \Big\{ & 2\bar{\phi}(\partial_{\bar{t}} - \nabla^2 + 2\bar{\lambda}\phi_c)\phi_1 + 2\bar{\psi}(\partial_{\bar{t}} - \nabla^2)\psi_1 \\ & + 2\bar{\lambda}\bar{\phi}(\phi_1^2 - \psi_1^2 - 2\psi_c\psi_1) + \bar{\lambda}(\bar{\phi}^2 - \bar{\psi}^2)(\phi_c^2 + 2\phi_c\phi_1 + \phi_1^2 - \psi_c^2 - 2\psi_c\psi_1 - \psi_1^2)\Big\}, \end{aligned} \tag{3.54}$$

where the classical equations have been used to simplify its form somewhat. We can now substitute for the exact value of $\psi_c = -(\bar{J}/2)x$ and for the functional form of the ϕ_c field (from (2.25))

$$\phi_c = (\bar{J}^2/\bar{\lambda})^{1/3} f[(\bar{\lambda}\bar{J})^{1/3}x]. \tag{3.55}$$

If we also make the rescaling in the action of

$$\tilde{x} = (\bar{\lambda}\bar{J})^{1/3}x \quad \tilde{y} = (\bar{\lambda}\bar{J})^{1/3}y \quad \tilde{t} = (\bar{\lambda}\bar{J})^{2/3}\bar{t}, \tag{3.56}$$

then it is transformed to

$$\begin{aligned} S = \int d\tilde{x}d^{d-1}\tilde{y}d\tilde{t}(\bar{\lambda}\bar{J})^{-\frac{d}{3}} \Big[& 2\bar{\phi}(\partial_{\tilde{t}} - \tilde{\nabla}^2 + 2f(\tilde{x}))\phi_1 + 2\bar{\psi}(\partial_{\tilde{t}} - \tilde{\nabla}^2)\psi_1 \\ & +2(\bar{\lambda}/\bar{J}^2)^{1/3}\bar{\phi}(\phi_1^2 - \psi_1^2) + 2\bar{\phi}\tilde{x}\psi_1 \\ & +(\bar{\phi}^2 - \bar{\psi}^2)\left((\bar{J}^2/\bar{\lambda})^{\frac{1}{3}}h(\tilde{x}) + 2f(\tilde{x})\phi_1 + \tilde{x}\psi_1 + (\bar{\lambda}/\bar{J}^2)^{\frac{1}{3}}(\phi_1^2 - \psi_1^2)\right)\Big], \end{aligned} \tag{3.57}$$

where

$$h(\tilde{x}) = [f(\tilde{x})]^2 - \frac{1}{4}\tilde{x}^2, \tag{3.58}$$

which is essentially just the classical profile of the reaction front. The form of the propagators is now

$$G_{\phi_1\bar{\phi}} = \frac{1}{2}(\bar{\lambda}\bar{J})^{d/3}G(\tilde{x}, \tilde{x}', \tilde{\mathbf{y}}, \tilde{\mathbf{y}}', \tilde{t}), \tag{3.59}$$

where

$$[\partial_{\tilde{t}} - \tilde{\nabla}^2 + 2f(\tilde{x})]G(\tilde{x}, \tilde{x}', \tilde{\mathbf{y}}, \tilde{\mathbf{y}}', \tilde{t}) = \delta(\tilde{x} - \tilde{x}')\delta(\tilde{\mathbf{y}} - \tilde{\mathbf{y}}')\delta(\tilde{t} - \tilde{t}'); \tag{3.60}$$

and

$$G_{\psi_1\bar{\psi}}(\tilde{k}, \tilde{s}) = \frac{1}{2}(\bar{\lambda}\bar{J})^{d/3}\frac{1}{\tilde{k}^2 + \tilde{s}}, \tag{3.61}$$

in $(\tilde{k}, \tilde{s})$ space, or

$$G_{\psi_1\bar{\psi}}(\tilde{x} - \tilde{x}', \tilde{k}_\perp, \tilde{s}) = (\bar{\lambda}\bar{J})^{d/3}\frac{e^{-(\tilde{k}_\perp^2 + \tilde{s})^{1/2}|\tilde{x} - \tilde{x}'|}}{4(\tilde{k}_\perp^2 + \tilde{s})^{1/2}}, \tag{3.62}$$

in $(\tilde{x}, \tilde{k}_\perp, \tilde{s})$ space, where the perpendicular directions are defined to be those perpendicular to the applied currents. Unfortunately the equation for G (3.60) is too hard to solve exactly, as we do not have an analytic form for ϕ_c. Consequently we must rely on the approximation $f(\tilde{x}) \sim \frac{1}{2}|\tilde{x}|$, valid at large $|\tilde{x}|$, in order to make

the equation tractable. If we also Laplace transform time, and Fourier transform to momentum space for spatial dimensions perpendicular to the applied currents, then we obtain

$$\left(\tilde{s} + \tilde{k}_\perp^2 - \partial_{\tilde{x}}^2 + |\tilde{x}|\right) G(\tilde{x}, \tilde{x}', \tilde{k}_\perp, \tilde{s}) = \delta(\tilde{x} - \tilde{x}'). \tag{3.63}$$

In appendix A, we show that for $\tilde{x} \approx \tilde{x}' \gg 0$, this gives

$$G_{\phi_1\bar{\phi}}(\tilde{x}, \tilde{x}', \tilde{k}_\perp, \tilde{s}) = \frac{1}{4}(\bar{\lambda}\bar{J})^{d/3}(\tilde{x} + \tilde{k}_\perp^2 + \tilde{s})^{-1/2} e^{-(\tilde{x}+\tilde{k}_\perp^2+\tilde{s})^{1/2}|\tilde{x}-\tilde{x}'|}. \tag{3.64}$$

The important point to notice here is that for $\tilde{x}$ sufficiently close to $\tilde{x}'$, the Green function decays only as a power law.

Finally, we note that each occurrence of a propagator is associated with a factor of $(\bar{\lambda}\bar{J})^{d/3}$. If we also extract a factor of $(\bar{\lambda}\bar{J})^{-(d+2)/3}$ from each vertex then we can use the vertices shown in figure 3.5, provided we multiply any given diagram by a factor of

$$(\bar{\lambda}\bar{J})^{\frac{1}{3}pd - \frac{v}{3}(d+2)}, \tag{3.65}$$

where p is the number of propagators and v is the number of vertices. Again in figure 3.5, ϕ propagators are solid lines and ψ propagators are dotted lines. Note the simple form of the vertices (h) to (m).

3.5.2 Renormalisation

The renormalisation of the theory proceeds in a similar vein to that described in [38] for the reaction $A + A \to \emptyset$ - our field theory differs fundamentally only in the nature of the boundary conditions. Again the only renormalisation required is coupling constant renormalisation, as the set of vertices for Field Theory I allows no diagrams which dress the propagator. Hence we have no field renormalisation and the bare propagators are the full propagators for the theory.

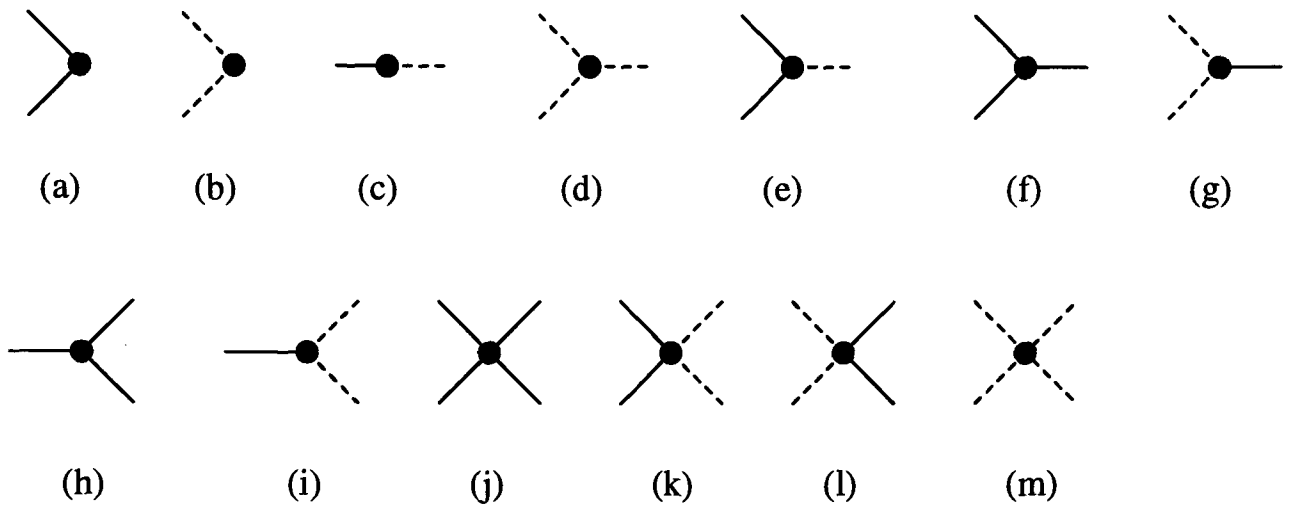

Figure 3.5: Vertices for Field Theory II. The couplings associated with each of the above diagrams are: (a). $-\bar{\lambda}^{1/3}\bar{J}^{4/3}h(\tilde{x})$ (b). $\bar{\lambda}^{1/3}\bar{J}^{4/3}h(\tilde{x})$ (c). $-2(\bar{\lambda}\bar{J})^{2/3}\tilde{x}$ (d). $(\bar{\lambda}\bar{J})^{2/3}\tilde{x}$ (e). $-(\bar{\lambda}\bar{J})^{2/3}\tilde{x}$ (f). $-2(\bar{\lambda}\bar{J})^{2/3}f(\tilde{x})$ (g). $2(\bar{\lambda}\bar{J})^{2/3}f(\tilde{x})$ (h). $-2\bar{\lambda}$ (i). $2\bar{\lambda}$ (j). $-\bar{\lambda}$ (k). $\bar{\lambda}$ (l). $\bar{\lambda}$ (m). $-\bar{\lambda}$.

Renormalisation of the Coupling

The temporally extended vertex function is given by the sum of diagrams shown in figure 3.6. This sum may be calculated exactly, as in [38]. In $(k, \bar{t})$ space the sum is given by

$$\bar{\lambda}(k, \bar{t}_2 - \bar{t}_1) = \bar{\lambda}\delta(\bar{t}_2 - \bar{t}_1) - 2\bar{\lambda}^2 I(k, \bar{t}_2 - \bar{t}_1) + 4\bar{\lambda}^3 \int_{\bar{t}_1}^{\bar{t}_2} d\bar{t}' I(k, \bar{t}_2 - \bar{t}') I(k, \bar{t}' - \bar{t}_1) - \ldots \tag{3.66}$$

where we have included factors of 2 resulting from the presence of two different types of propagator, and where $I(k, \bar{t})$ is the integral

$$I(k, \bar{t}) = 2 \int \frac{d^d p}{(2\pi)^d} \frac{1}{2} e^{-p^2 \bar{t}} \frac{1}{2} e^{-(k-p)^2 \bar{t}}. \tag{3.67}$$

This integral can easily be evaluated, and the series in equation (3.66) summed exactly by taking the Laplace transform $\bar{\lambda}(k, s) = \int_0^\infty d\bar{t} e^{-s\bar{t}} \bar{\lambda}(k, \bar{t})$. We finally end

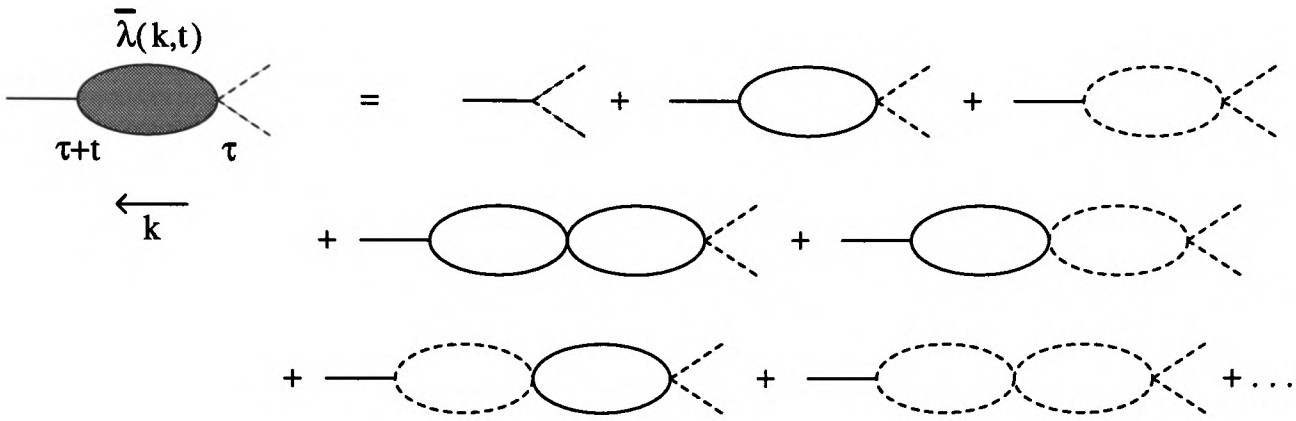

Figure 3.6: The sum of diagrams contributing to the primitively divergent vertex function $\bar{\lambda}(k,t)$.

up with

$$\bar{\lambda}(k,s) = \frac{\bar{\lambda}}{1 + \frac{1}{2}\bar{\lambda}B_2\Gamma(\epsilon/2)(s + \frac{1}{2}k^2)^{-\epsilon/2}}, \tag{3.68}$$

where $B_2 = 2/(8\pi)^{d/2}$ and $\epsilon = 2 - d$. If we take $s = 0$ this becomes

$$\bar{\lambda}(k) = \frac{\bar{\lambda}}{1 + \frac{1}{2}\bar{\lambda}B_2\Gamma(\epsilon/2)2^{\epsilon/2}k^{-\epsilon}}. \tag{3.69}$$

The vertex function can now be used to define the renormalised coupling, with $k = \kappa$ as the normalisation point. Hence we have

$$g_R = \kappa^{-\epsilon}\bar{\lambda}(k)|_{k=\kappa} \qquad g_0 = \kappa^{-\epsilon}\bar{\lambda}, \tag{3.70}$$

for the dimensionless renormalised and bare couplings respectively. The β function is defined by

$$\beta(g_R) \equiv \kappa\frac{\partial}{\partial\kappa}g_R = -\epsilon g_R + \frac{1}{2}\epsilon g_R^2 B_2\Gamma(\epsilon/2)2^{\epsilon/2}, \tag{3.71}$$

and we have a fixed point $\beta(g_R^*) = 0$ when

$$g_R^* = \{2^{-d/2}B_2\Gamma(\epsilon/2)\}^{-1}. \tag{3.72}$$

Notice that the fixed point is $O(\epsilon)$. Finally, the expansion of g_0 in powers g_R is given by:

$$g_0 = g_R + \frac{g_R^2}{g_R^*} + \dots \tag{3.73}$$

Callan-Symanzik Equation

We now write down the renormalisation group equation for $\langle\phi_1\rangle_R$ (the renormalised value of $\langle\phi_1\rangle$), expressing its lack of dependence on the normalisation scale:

$$\left(\kappa\frac{\partial}{\partial\kappa} + \beta(g_R)\frac{\partial}{\partial g_R}\right)\langle\phi_1\rangle_R(x, g_R, \kappa, \bar{J}) = 0. \tag{3.74}$$

In addition, dimensional analysis implies

$$\left(\kappa\frac{\partial}{\partial\kappa} - x\frac{\partial}{\partial x} + (d+1)\bar{J}\frac{\partial}{\partial\bar{J}}\right)\langle\phi_1\rangle_R(x, g_R, \kappa, \bar{J}) = d\langle\phi_1\rangle_R(x, g_R, \kappa, \bar{J}). \tag{3.75}$$

Eliminating the terms involving κ, we have

$$\left(x\frac{\partial}{\partial x} - (d+1)\bar{J}\frac{\partial}{\partial\bar{J}} + \beta(g_R)\frac{\partial}{\partial g_R} + d\right)\langle\phi_1\rangle_R(x, g_R, \kappa, \bar{J}) = 0. \tag{3.76}$$

This can be solved by the method of characteristics, with solution

$$\langle\phi_1\rangle_R(x, g_R, \kappa, \bar{J}) = (\kappa x)^{-d}\langle\phi_1\rangle_R(\kappa^{-1}, \tilde{g}_R(\kappa^{-1}), \kappa, \tilde{\bar{J}}(\kappa^{-1})), \tag{3.77}$$

and associated characteristics

$$x\frac{\partial\tilde{g}_R}{\partial x} = \beta(\tilde{g}_R) \qquad \tilde{g}_R(x) = g_R \tag{3.78}$$

$$x\frac{\partial\tilde{\bar{J}}}{\partial x} = -(d+1)\tilde{\bar{J}} \qquad \tilde{\bar{J}}(x) = \bar{J}. \tag{3.79}$$

These equations have the exact solutions:

$$\tilde{\bar{J}}(x') = \left(\frac{x}{x'}\right)^{d+1}\bar{J} \tag{3.80}$$

$$\tilde{g}_R(x') = g_R^* \left(1 + \frac{g_R^* - g_R}{g_R \left(\frac{x}{x'}\right)^{\epsilon}}\right)^{-1}, \tag{3.81}$$

where in the large $|x|$ limit $\tilde{g}_R \rightarrow g_R^*$.

We can make use of the mechanics developed above by first calculating an expansion in powers of g_0, which can be converted into an expansion in powers of g_R via (3.73). Provided that the expansion is non-singular in ϵ, we can relate the g_R expansion to an ϵ expansion using (3.77), where for large $|x|$ we can take $\tilde{g}_R \rightarrow g_R^*$.

Tree Diagrams

At this point we need to identify the leading terms in an expansion in powers of g_0 - something which can be done in a very similar fashion to [38], using Field Theory I. For the calculation of $\langle\phi\rangle$, tree diagrams are of order $g_0^i \bar{J}^{1+i}$, for integer i. Diagrams with j loops will be of order $g_0^i \bar{J}^{1+i-j}$. As the addition of loops makes the power of g_0 higher relative to the power of $\bar{J}$, we see that the number of loops will give an indicator of the order of the diagram.

We are now in a position to develop two tree level quantities - namely the classical density and the classical response function. Diagrammatically, we represent the classical densities by wavy lines and the classical response functions by thick lines. The tree level density $\langle\phi\rangle$ is given by the sum of all tree diagrams which end with a $G_{\phi\bar{\phi}}$ propagator, as shown in figure 3.7(b). This is equivalent to the mean field equation, as may be seen by acting on both sides of the graphical equation by the inverse Green function $2(\partial_{\bar{t}} - \nabla^2)$. Similarly, acting on the much simpler tree level diagram for $\langle\psi\rangle$ (figure 3.7(a)) with the inverse Green function, gives its classical equation.

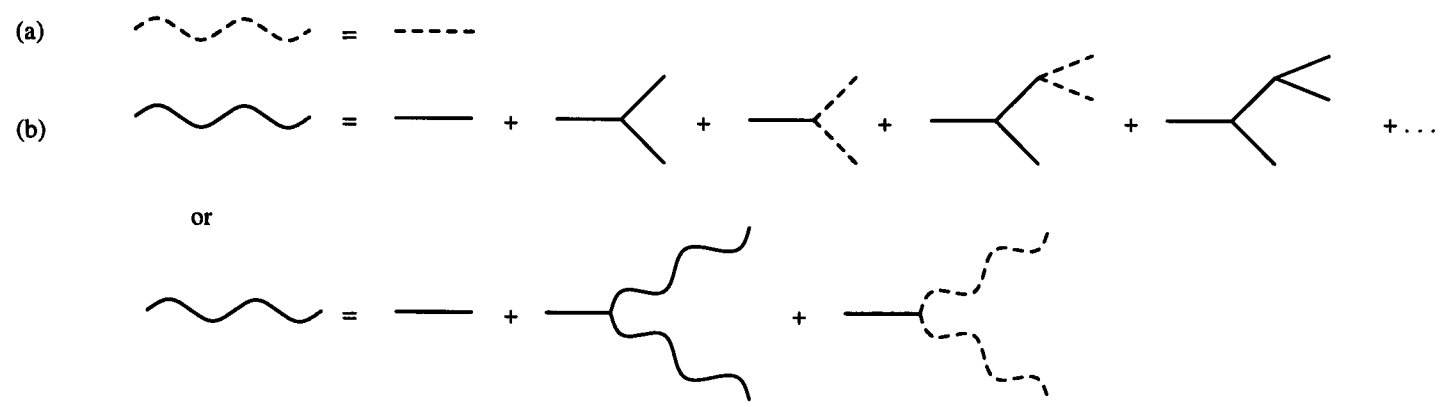

Figure 3.7: Tree level diagrams for (a) $\langle\psi\rangle$, and (b) $\langle\phi\rangle$.

We now define the three response functions for the theory:

$$\langle\psi(x,-k_\perp,-s)\bar{\psi}(x',k_\perp,s)\rangle^{(1)} \qquad \langle\phi(x,-k_\perp,-s)\bar{\phi}(x',k_\perp,s)\rangle^{(1)}$$
$$\langle\phi(x,-k_\perp,-s)\bar{\psi}(x',k_\perp,s)\rangle^{(1)}, \tag{3.82}$$

where the superscript '1' indicates that they are defined in Field Theory I. Their diagrammatic sums are shown in figure 3.8. The first one $\langle\psi(x,-k_\perp,-s)\bar{\psi}(x',k_\perp,s)\rangle^{(1)}$ is simply the propagator $G^{(2)}_{\psi_1\bar{\psi}}$, where the superscript '2' indicates that it belongs to the second field theory. It is also easy to show that the second response function $\langle\phi(x,-k_\perp,-s)\bar{\phi}(x',k_\perp,s)\rangle^{(1)}$ is equivalent to the propagator $G^{(2)}_{\phi_1\bar{\phi}}$. To do this we rearrange the unrescaled equation for $G^{(2)}_{\phi_1\bar{\phi}}$:

$$2(s + k_\perp^2 - \partial_x^2)G^{(2)}_{\phi_1\bar{\phi}}(x,x',k_\perp,s) = -4\bar{\lambda}\phi_c(x)G^{(2)}_{\phi_1\bar{\phi}}(x,x',k_\perp,s) + \delta(x-x'). \tag{3.83}$$

Including a delta function integration in the first term on the right hand side, and acting on both sides with the inverse Green function, we obtain

$$G^{(2)}_{\phi_1\bar{\phi}}(x,x',k_\perp,s) = G^{(1)}_{\phi\bar{\phi}} - 4\bar{\lambda}\int G^{(1)}_{\phi\bar{\phi}}(x,x_1,k_\perp,s)\phi_c(x_1)G^{(2)}_{\phi_1\bar{\phi}}(x_1,x',k_\perp,s)dx_1, \tag{3.84}$$

where $G^{(1)}_{\phi\bar{\phi}}$ is the ϕ propagator for the first field theory. Iteration now generates the appropriate tree level expansion for $\langle\phi(x,-k_\perp,-s)\bar{\phi}(x',k_\perp,s)\rangle^{(1)}$, and we have

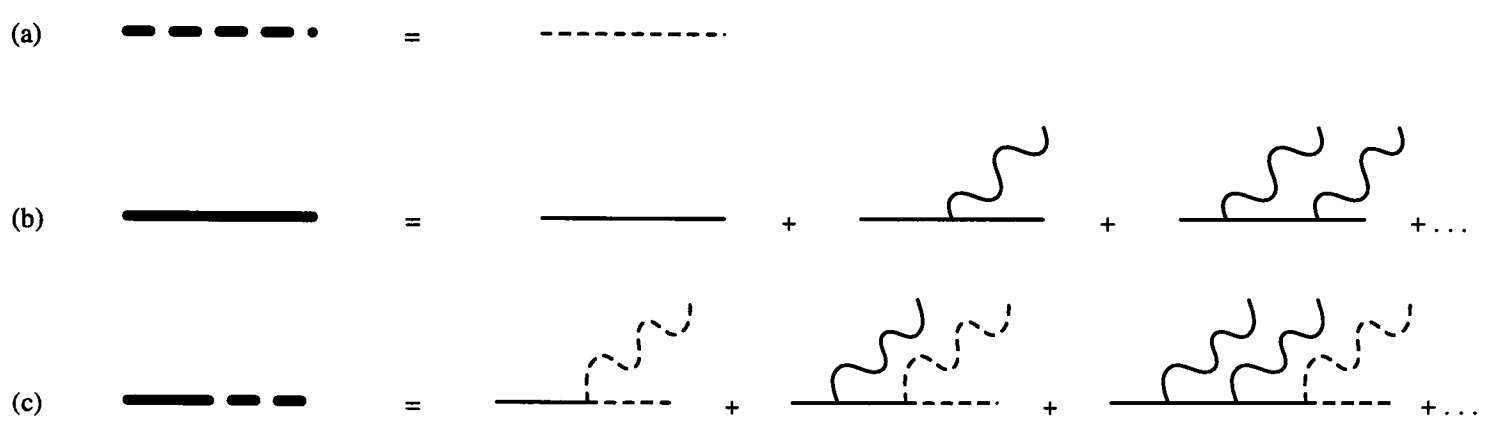

Figure 3.8: Response functions for Field Theory I: (a) $\langle \psi\bar{\psi} \rangle^{(1)}$, (b) $\langle \phi\bar{\phi} \rangle^{(1)}$, and (c) $\langle \phi\bar{\psi} \rangle^{(1)}$.

$G^{(2)}_{\phi_1\bar{\phi}} = \langle \phi\bar{\phi} \rangle^{(1)}$. The remaining response function $\langle \phi\bar{\psi} \rangle^{(1)}$ is, as would be expected, equivalent in the second field theory to the two point vertex sandwiched between a ϕ propagator and a ψ propagator.

3.6 Density and Reaction Front Calculations

We first note that we cannot draw diagrams which terminate with a ψ_1 propagator in Field Theory II. Consequently we conclude that $\langle \psi_1 \rangle = 0$, and hence that $\langle \psi \rangle = \psi_c$. This also follows from averaging equation (2.28). We now turn to the asymptotic evaluation of $\langle \phi \rangle$. Inserting the classical (tree level) solution (3.5) into the Callan-Symanzik solution (3.77), and making the leading order replacements $\bar{\lambda} \to g_R \kappa^\epsilon$, and for large $|x|$, $\tilde{g}_R \to g_R^*$, we obtain

$$\langle \phi \rangle = \frac{1}{2}\bar{J}|x| + 0.3787 \frac{\bar{J}^{7/12}}{g_R^{*\,5/12}} |x|^{(7-5d)/12} e^{-(2/3) g_R^{*1/2} \bar{J}^{1/2} |x|^{(d+1)/2}} + \ldots \qquad (3.85)$$

If we use the explicit value of g_R^* from (3.72), then

$$\langle \phi \rangle = \frac{1}{2}\bar{J}|x| + 0.3787 \frac{\bar{J}^{7/12}}{(4\pi\epsilon)^{5/12}} |x|^{(7-5d)/12} e^{-(2/3)(4\pi\epsilon)^{1/2} \bar{J}^{1/2} |x|^{(d+1)/2}} + \ldots \qquad (3.86)$$

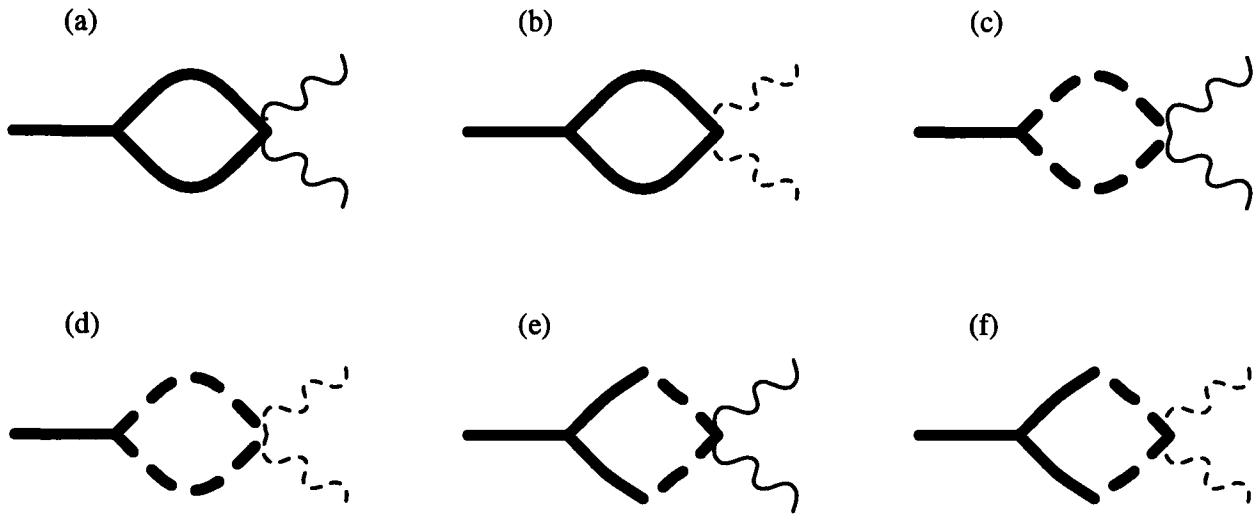

Figure 3.9: One loop diagrams in Field Theory I.

So the tree level expression consists of the expected linear term, which must be present if the boundary conditions are to be satisfied, together with a stretched exponential component.

3.6.1 One Loop Contributions

According to our earlier arguments, we expect the next order contributions to $\langle\phi\rangle$ (in Field Theory I) to contain one loop embedded somewhere in the tree diagram. The diagrams corresponding to this prescription are shown in figure 3.9. However, we have shown that we may translate these diagrams into Field Theory II by replacing response functions by propagators. This is convenient as we have analytic expressions for the Green functions in the second field theory (at least asymptotically), and so performing calculations becomes easier. The equivalent diagrams for Field Theory II are shown in figure 3.10. Notice that the density lines present in the diagrams for Field Theory I have been absorbed into the vertices for Field Theory II, where a factor of $\phi_c^2 - \psi_c^2$ is present at the source vertex.

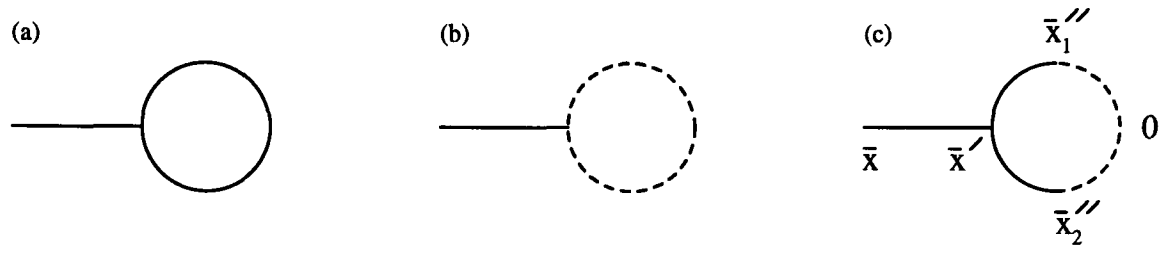

Figure 3.10: One loop diagrams in Field Theory II.

We begin by calculating the third diagram of figure 3.10. At this level of approximation we replace the source (the incoming classical density lines at the rightmost vertex in Field Theory I) by a delta function at the origin, with a weight equal to the area under the classical reaction front:

$$\phi_c^2 - \psi_c^2 \rightarrow \left(\int (\phi_c^2 - \psi_c^2) dx' \right) \delta(x). \tag{3.87}$$

This will be valid provided $\langle \phi \rangle$ decays much more slowly than the classical reaction front - an assumption that will be shown to be justified *a posteriori.* By integrating the classical equations we also have the relation

$$\bar{\lambda} \int (\phi_c^2 - \psi_c^2) dx' = \bar{\lambda}^{1/3} \bar{J}^{4/3} \int h[(\bar{\lambda}\bar{J})^{1/3} x'] dx' = \bar{J}, \tag{3.88}$$

which is simply saying that, classically, the number of particles entering the system is the same as the number being annihilated at the reaction front. After we have performed the rescaling $\tilde{x}' = (\bar{\lambda}\bar{J})^{1/3} x'$, this becomes

$$\int h(\tilde{x}') d\tilde{x}' = 1. \tag{3.89}$$

So the vertex factor at the source is replaced by:

$$\bar{\lambda}^{1/3} \bar{J}^{4/3} h(\tilde{x}) \rightarrow \bar{\lambda}^{1/3} \bar{J}^{4/3} \left(\int h(\tilde{x}') d\tilde{x}' \right) \delta(\tilde{x}) = \bar{\lambda}^{1/3} \bar{J}^{4/3} \delta(\tilde{x}). \tag{3.90}$$

The evaluation of the diagram is presented in appendix B, where it is shown that part of the result cancels off the (divergent) diagram shown in figure 3.10(b). The net result of these two diagrams is then:

$$-(\bar{\lambda}\bar{J})^{-1}2^{-1-d}\pi^{-(d+1)/2}(1-d)\Gamma\left(\frac{d-1}{2}\right)x^{-d-3}. \tag{3.91}$$

We may now insert this into the Callan-Symanzik solution (3.77), and use the results for the running current/coupling (3.80)/(3.81), and for the coupling fixed point (3.72). This leads to the 1 loop density correction

$$\frac{x^{-2d-1}}{32\pi^2\bar{J}\epsilon}, \tag{3.92}$$

which justifies the use of the delta function approximation for the source. The one remaining diagram in figure 3.10 consists entirely of ϕ propagators, and so asymptotically we expect an exponential dependence which we neglect in comparison with the power law. So to this level of accuracy we have

$$\langle\phi\rangle = \frac{1}{2}\bar{J}|x| + 0.3787\frac{\bar{J}^{7/12}}{(4\pi\epsilon)^{5/12}}|x|^{(7-5d)/12}e^{-\frac{2}{3}(4\pi\epsilon)^{1/2}\bar{J}^{1/2}|x|^{(d+1)/2}} + \frac{|x|^{-2d-1}}{32\pi^2\bar{J}\epsilon} + \ldots \tag{3.93}$$

Using the relation (2.32) it is also straightforward to calculate the form of the intrinsic reaction front profile:

$$R = \lambda\langle\phi^2 - \psi^2\rangle = 0.3787\bar{J}^{\frac{19}{12}}\frac{(4\pi\epsilon)^{7/12}}{9/D}(d+1)^2|x|^{(7d-5)/12}e^{-\frac{2}{3}(4\pi\epsilon)^{1/2}\bar{J}^{1/2}|x|^{(d+1)/2}} + \frac{(2d+1)(2d+2)|x|^{-2d-3}}{32\pi^2\epsilon\bar{J}/D} + \ldots, \tag{3.94}$$

where only the leading terms generated by the differentiation of each of the component parts of (3.93) have been retained.

Finally, we consider the cancellation of divergences at 1 loop which, as we mentioned earlier, can most easily be seen in the formalism of Field Theory I. We

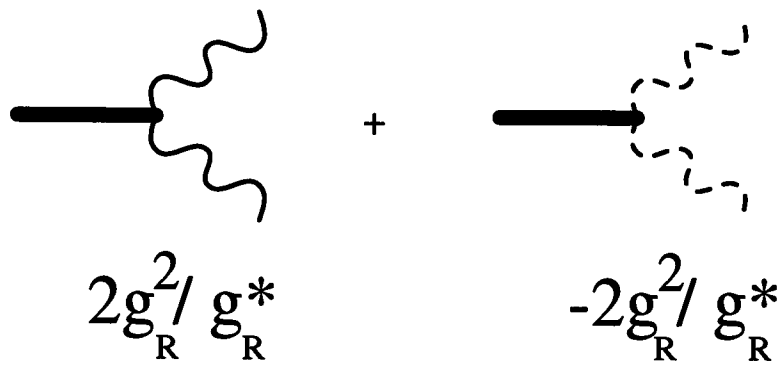

Figure 3.11: Divergences at one loop. The factor underneath each diagram is associated with the vertex.

expect divergent contributions from the 1 loop diagrams a,b,c and d in figure 3.9, in the limit where the position of the loop's left vertex tends towards that of the right vertex. In this limit, where no insertions are possible into the response functions, it is appropriate to replace the loop of ϕ response functions with one of ψ response functions. Evaluating this loop gives the result $1/2g_R^*$, and the diagrams become as shown in figure 3.11. However, if we consider the corrections to the tree level due to subleading terms in $g_0(g_R)$ (from (3.73)), we have the same diagrams but with opposite signs, which exactly cancel the 1 loop divergences.

Two Loops

Whilst we have not calculated in full the contributions to the density from the two loop diagrams, a remark concerning their general nature, and of the nature of our perturbation expansion, is in order. A sample of these two loop diagrams is shown in figure 3.12.

The easiest diagrams to evaluate are the first and second of those in figure 3.12,

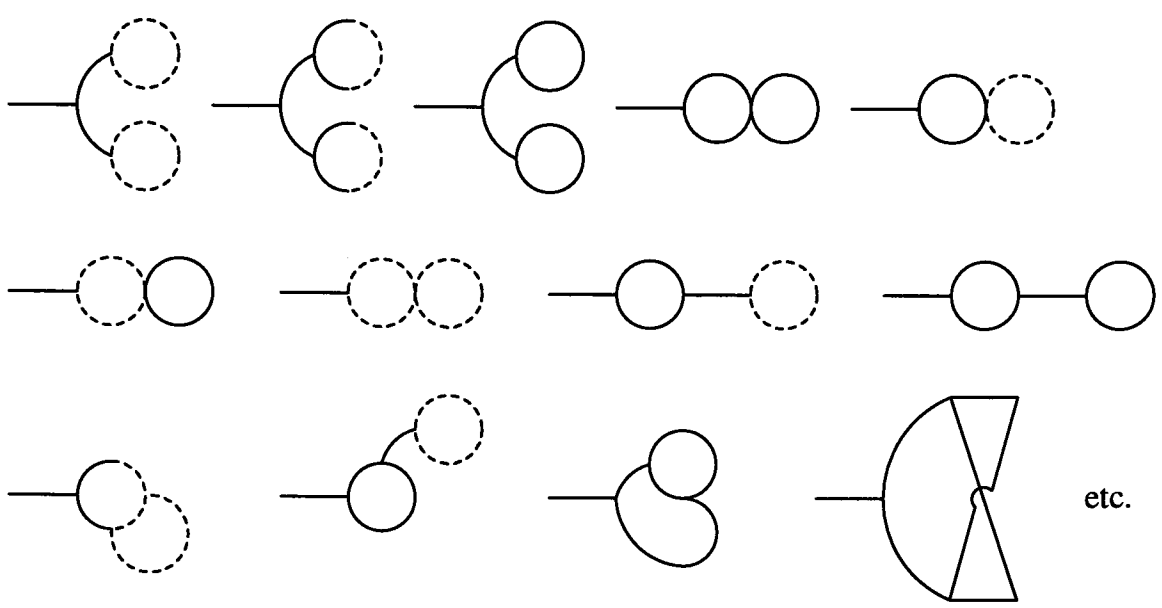

Figure 3.12: A sample of the two loop diagrams for $\langle \phi_1 \rangle$.

for which it is easy to check that they have the form

$$\sim \frac{|x|^{-4d-3}\bar{J}^{-3}}{\epsilon^2} \sim \epsilon^{-1/2}|x|^{-d}[\bar{J}|x|^{d+1}\epsilon^{1/2}]^{-3} \tag{3.95}$$

Hence the perturbative expansion for the power law contributions to $\langle \phi \rangle$ would appear to have the form:

$$\langle \phi \rangle \sim \epsilon^{-\frac{1}{2}}|x|^{-d}[\bar{J}|x|^{d+1}\epsilon^{1/2}] + \epsilon^{-\frac{1}{2}}|x|^{-d}[\bar{J}|x|^{d+1}\epsilon^{1/2}]^{-1} + \epsilon^{-\frac{1}{2}}|x|^{-d}[\bar{J}|x|^{d+1}\epsilon^{1/2}]^{-3} + \ldots \tag{3.96}$$

Consequently, we see that the condition for our field theory to be valid is that the dimensionless parameter $\bar{J}|x|^{d+1}$ be $\gg 1$. It should also be noted that subleading power laws from the loop integrals will be smaller than their leading term by factors of $(\bar{J}|x|^{d+1})^{-1/3}$.

3.6.2 $d \geq d_c$

At the upper critical dimension for the system, in this case $d = 2$, we expect logarithmic corrections to the $d > 2$ results, owing to the presence of the marginally

irrelevant parameter $\bar{\lambda}$. The Callan-Symanzik solution (3.77) is still valid, although with a different running coupling, which we calculate by taking $\epsilon \to 0$ in (3.71). This gives the result

$$\tilde{g}_R(\kappa^{-1}) = \frac{g_R}{1 + \frac{g_R}{4\pi}\ln(\kappa x)}. \tag{3.97}$$

The behaviour of the running current is as previously calculated. Using the asymptotic form $\tilde{g}_R \sim 4\pi/\ln(\kappa x)$, we obtain

$$\langle\phi\rangle = \frac{1}{2}\bar{J}|x| + 0.3787\bar{J}^{\frac{7}{12}}\left(\frac{\ln|x|}{4\pi}\right)^{\frac{5}{12}}|x|^{-\frac{1}{4}}e^{-\frac{2}{3}(4\pi\bar{J})^{1/2}(\ln|x|)^{-1/2}|x|^{3/2}} + \frac{|x|^{-5}\ln|x|}{32\pi^2\bar{J}} + \ldots, \tag{3.98}$$

where higher order corrections will be only $O[(\ln|x|)^{-1}]$ smaller, so the asymptotic regime will be accordingly hard to reach. Finally, for the reaction front, we have

$$R = 0.3787D\frac{(4\pi)^{7/12}\bar{J}^{19/12}}{(\ln|x|)^{7/12}}|x|^{3/4}e^{-\frac{2}{3}(4\pi\bar{J})^{1/2}(\ln|x|)^{-1/2}|x|^{3/2}} + \frac{15D\bar{J}^{-1}|x|^{-7}\ln|x|}{16\pi^2} + \ldots \tag{3.99}$$

For dimensions higher than the critical dimension, the expressions from the evaluation of the Feynman diagrams can be used directly without being inserted into the Callan-Symanzik solution. This gives us the following results, valid for $d > 2$, and in the regime $(J^2\lambda/D^3)|x|^{d+4} \gg 1$:

$$\langle\phi\rangle = \frac{1}{2}\bar{J}|x| + 0.3787\frac{\bar{J}^{7/12}}{\bar{\lambda}^{5/12}}|x|^{-1/4}e^{-\frac{2}{3}(\bar{\lambda}\bar{J})^{1/2}|x|^{3/2}} - (\bar{\lambda}\bar{J})^{-1}2^{-1-d}\pi^{-(d+1)/2}(1-d)\Gamma\left(\frac{d-1}{2}\right)|x|^{-d-3} + \ldots \tag{3.100}$$

and

$$R = 0.3787\bar{J}^{19/12}\bar{\lambda}^{7/12}D|x|^{3/4}e^{-\frac{2}{3}(\bar{\lambda}\bar{J})^{1/2}|x|^{3/2}} \tag{3.101}$$
$$-D\bar{\lambda}^{-1}\bar{J}^{-1}2^{-1-d}\pi^{-(d+1)/2}\Gamma\left(\frac{d-1}{2}\right)(1-d)(d+3)(d+4)|x|^{-d-5} + \ldots$$

3.7 Discussion

The main results of these last few sections have been expansions for the asymptotic behaviour of the densities and the intrinsic reaction front profile for dimensions above, below, and equal to the critical dimension. We can now compare our results with previously published simulations (see for example [28, 29, 45, 48, 49, 54]). Note that in all of these papers except [54], the initial conditions were those of complete particle segregation - so the particle currents at later times were time dependent. The remaining reference [54] contains the results of simulations in the steady state. Our calculations could, in principle, be redone for the time dependent case. However, this would lead to an analytic calculation of greatly increased complexity, as the quantities involved in the calculation (including the Green functions, the response functions, and the mean field reaction front) would acquire additional time dependence. Fortunately, simple one loop considerations for $\langle \psi^2 \rangle$ indicate that the dominant contributions to the integrals originate from large times. At these times the reaction front is formed quasistatically, and so we expect to be able to relate to the steady state case by making the correspondence $J \sim t^{-1/2}$ [29, 55] (but see below for occasions where this breaks down). In addition, most earlier work employs an infinite reaction rate (which considerably simplifies the simulations). However, as we have already pointed out, this leads to complete species segregation at all later times - a feature which is not in accord with our field theoretic/RG calculation scheme.

Furthermore, previous $1d$ simulations are dominated by the wandering Gaussian reaction front, which makes a verification of our intrinsic calculation difficult. In addition, in higher dimensions, previous simulations lack sufficient detail for

a comparison to be made with our results. However, Cornell and Droz [54] do present evidence for the validity of their scaling hypothesis (3.6) in dimensions $d = 1, 2, 3$ for regions close to the reaction front centre. Returning to the $1d$ case, if we wish to study the intrinsic component of the front (in the non-mean field limit $\lambda J^{-1/2} D^{-1/2} \gg 1$), we must find a way of suppressing the dominance of the wandering Gaussian part. One way in which this can be achieved is to measure the reaction rate R_r as a function of $|x - x_p|$, the distance between successive reaction events at x_p and x. This enables the intrinsic profile to be studied, as the front centre has little time to move on such short time scales. These reaction events are effectively uncorrelated, so that the relative reaction rate R_r is given by

$$R_r(\tilde{x}) = \int R(x) P(x_p) \delta(x - x_p - \tilde{x}) dx dx_p, \tag{3.102}$$

where $P(x_p)dx_p = R(x_p)dx_p / \int R(x_p)dx_p$ is the probability that the previous reaction occurred between x_p and $x_p + dx_p$. In our simulations of R_r we kept the boundary insertion rate i small, and hence many particles were present in the reservoirs (see section 3.3.1). We were therefore able to effectively simulate a much bigger system with a large number of particles. This ensured that correlations between annihilation and reinsertion, which would otherwise have modified the intrinsic profile, were kept to a minimum. Our simulation data is shown in figure 3.13, which shows a convincing data collapse of $R_r(J/D)^{-1/2}/J$ plotted against $|x - x_p|(J/D)^{1/2}$. As we are now studying the intrinsic profile, this result finally confirms the scaling predictions of [24, 54, 55] for the intrinsic front in $1d$. For large values of $|x - x_p|(J/D)^{1/2}$ we also find a tail which is consistent with the RG improved tree level prediction $\log(R) \sim -B(J/D)^{1/2}|x|$ (implying $\log(R_r) \sim -B(J/D)^{1/2}|\tilde{x}|$). Unfortunately our data provides no clear indication of the predicted power law tails. However, such tails would be very hard to see in measurements of the relative reaction rate R_r, as

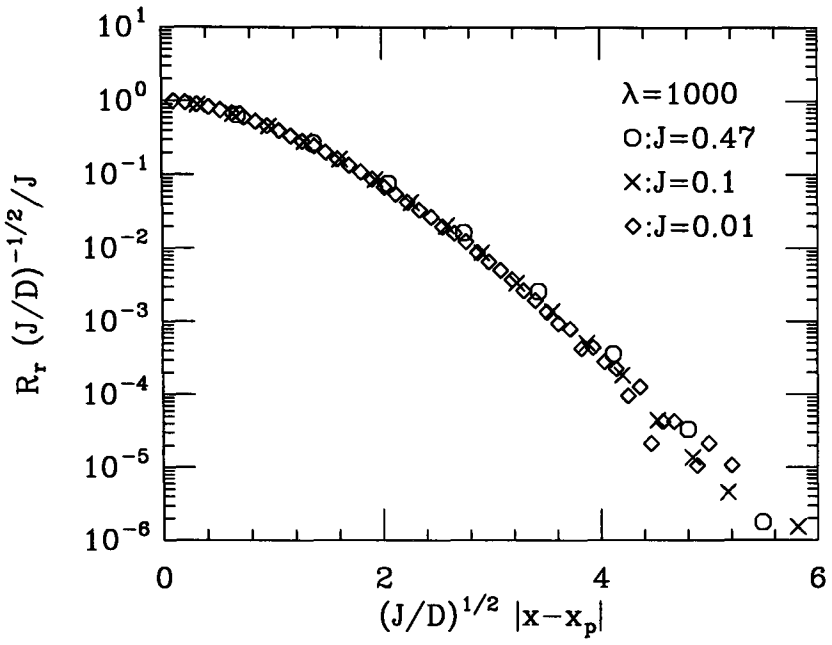

Figure 3.13: Collapsed data plot for the relative reaction rate in the regime $\lambda J^{-1/2} D^{-1/2} \gg 1$. Simulations were for 10^{10} events, with $D = 1$, $N = 200, 1100, 10100$.

the power law exponent would be large $(7 - 2\epsilon + O(\epsilon^2))$. We have also performed simulations in the mean field regime. In this case $R_r/[J(\lambda J/D^2)^{1/3}]$ was found to collapse when plotted against small values of $(\lambda J/D^2)^{1/3}|x - x_p|$. However, for larger values, the collapse no longer worked well, probably due to the increased importance of fluctuations in the asymptotic regime.

We now turn to a consideration of the spatial moments of the intrinsic reaction front profile, where there has been a recent controversy over the existence of multiscaling (see Araujo *et al* [28] and Cornell [29]). In fact, our calculations suggest that multiscaling does indeed occur for high enough moments in the time dependent version of our model, starting from completely segregated initial conditions. However, in $1d$ such behaviour will be especially hard to observe due to the dominance of the Gaussian wandering front. Furthermore, the size of the power law exponents is large, indicating that their effects will only become important in

an extremely asymptotic region. Nevertheless, for the steady state situation, the existence of the asymptotic power laws found above implies that the moments:

$$x^{(q)} = \left(\frac{\int_{-\infty}^{\infty} |x|^q R(x) dx}{\int_{-\infty}^{\infty} R(x) dx} \right)^{1/q} \tag{3.103}$$

do not exist for $q \geq \mu + 1$, where μ is defined by $R \sim (\text{constant}) \times |x|^{-\mu-2}$ in the reaction front tail. However, in the time dependent case, these moments *must* exist due to the presence of a diffusive cutoff at $x_D \sim t^{1/2}$ [60]. Therefore, for the calculation of the spatial moments $x^{(q)}$ for large enough q, we cannot relate the steady state case to the time dependent case by simply applying the scaling substitution $J \sim t^{-1/2}$. We can make these remarks more quantitative by performing the calculation of the spatial moments in the time dependent situation. Separate arguments must be applied for $d < 2$, when our RG arguments imply that the steady state profile has a scaling form (3.94), and for $d > 2$, when (3.101) shows that the fluctuation induced power law tails do not scale. For $d < 2$, we have:

$$x^{(q)}(t) \sim \left(\frac{\int_{-\infty}^{\infty} |x|^q t^{-\beta} S\left(\frac{x}{t^\alpha}\right) F\left(\frac{x}{t^{1/2}}\right) dx}{\int_{-\infty}^{\infty} t^{-\beta} S\left(\frac{x}{t^\alpha}\right) F\left(\frac{x}{t^{1/2}}\right) dx} \right)^{1/q}, \tag{3.104}$$

where α and β are defined in the usual way (see equation (3.3)). Here $F(y)$ is a function which provides a cutoff at $y \sim O(1)$, but whose inclusion does not affect the calculation of moments which are finite even in the absence of a cutoff. For $q < \mu + 1$, where the qth moment of S is finite (even without a cutoff), we can therefore neglect the effects of F. However, for $q > \mu + 1$ the qth moment is infinite without the cutoff so the integral will now be dominated by the region $(x/t^{1/2}) \sim O(1)$, where the asymptotic result $S \sim (x/t^\alpha)^{-\mu-2}$ may be used. These considerations lead to the result $x^{(q)}(t) \sim t^{\alpha q}$, where (neglecting any logarithmic

corrections for $q = \mu + 1$):

$$\alpha_q = \begin{cases} \alpha & \text{for } q < \mu + 1 \\ \frac{1}{2} + \frac{(\mu+1)(\alpha-1/2)}{q} & \text{for } q > \mu + 1. \end{cases} \tag{3.105}$$

Hence we have a cusp at $q = \mu + 1$, above which α_q tends towards $1/2$ for large q. Note that this value of $1/2$ is specific to a diffusive cutoff of the form $F(x/t^{1/2})$. For $d = 2$ we also expect logarithmic corrections to the above power laws.

For $d > 2$ we must carry out a slightly different calculation, as although the classical (tree level) reaction front obeys scaling, (3.101) reveals that the one loop power law correction does not (violating the scaling hypothesis (3.6)). However, for moments which exist without a cutoff, it turns out that the classical terms still give the dominant contribution in the scaling limit. For these terms we have, in the steady state case:

$$\int_{-\infty}^{\infty} |x|^q R_c(x, \lambda, J) dx \sim \lambda^{1/3} J^{4/3} \int_{-\infty}^{\infty} |x|^q S_c[(\lambda J)^{1/3} x] dx \sim \lambda^{-q/3} J^{1-q/3} \tag{3.106}$$

However, for the non-scaling power law we must consider:

$$(\lambda J)^{-1} \int_{(\lambda J^2)^{-1/(d+4)}}^{\infty} \frac{x^q dx}{x^{d+5}} \sim \lambda^{-q/(d+4)} J^{1-2q/(d+4)}, \tag{3.107}$$

where we have imposed a lower cutoff in the integral derived from the expansion parameter of the $d > 2$ asymptotic series (3.101). Comparing the J dependence of the two results above, we see that the first of these will dominate in the scaling limit $J \to 0$. Substituting $J \sim t^{-1/2}$ and normalising, we end up with $\alpha_q = \alpha = 1/6$, for $q < d + 4$. For the higher moments ($q > d + 4$) we need to introduce the cutoff function F, so the integral will be dominated by the region $(x/t^{1/2}) \sim O(1)$, where we can use the asymptotic power law from (3.101):

$$x^{(q)} \sim \frac{(\lambda t^{-1/2})^{-1}}{t^{-1/2}} \int_0^{\infty} dx \frac{x^q}{x^{d+5}} F(x/t^{1/2}) \sim \lambda^{-1} t^{(q-2-d)/2} \tag{3.108}$$

Consequently, we have the result $x^{(q)} \sim t^{\alpha_q}$, where (neglecting logarithmic corrections for $q = d + 4$):

$$\alpha_q = \begin{cases} \frac{1}{6} & \text{for } q < d+4 \\ \frac{1}{2} - \frac{d+2}{2q} & \text{for } q > d+4. \end{cases} \tag{3.109}$$

In this case we have a discontinuity at $q = d + 4$, a result of the power law term being unimportant for $q < d+4$, but dominant for $q > d+4$. Once again we stress that the limiting behaviour $\alpha_q \to 1/2$ as $q \to \infty$ is dependent on the diffusive form of the cutoff.

Thus we predict the existence of multiscaling in the time dependent case in qualitative agreement with Araujo *et al.*, even though we are considering a different model. In general power law tails in the steady state reaction front profile should *always* lead to dynamic multiscaling whatever their origin. These arguments are similar to those of Cornell *et al.* [60], who find evidence for multiscaling in the reaction $nA + mB \to \emptyset$ with $(n, m) \neq (1, 1)$. However, in that case the solutions of the mean field rate equations already gave power laws even without the addition of fluctuation effects.

In summary, our ability to adjust the reaction rate has enabled us to find two regimes for the $A + B \to \emptyset$ front in one dimension. For $\lambda J^{-1/2} D^{-1/2} \ll 1$ mean field predictions work well, whereas for $\lambda J^{-1/2} D^{-1/2} \gg 1$ the front is dominated by a Gaussian profile, a result of fluctuation induced wandering. Our theoretical prediction for this shape agrees well with simulations. Furthermore, we have made analytic predictions for the shape of the intrinsic profile. Our $1d$ simulations are again in agreement with these calculations. Finally, our prediction of power law tails in the intrinsic front profile has lead us to propose the existence of multiscaling in high enough order spatial moments of the time dependent reaction front. However, this behaviour has been rather hard to observe due to the dominance of

the Gaussian front in $1d$, and also the large size of the power law exponents.

3.8 Appendix A: Derivation of the Green Function $G(\tilde{x}, \tilde{x}', \tilde{k}_\perp, \tilde{s})$

In this appendix we find a solution to equation (3.63) in the region $\tilde{x}' > 0$, and accurate for large $|\tilde{x}|$, i.e. when $|x| \gg (\bar{\lambda}\bar{J})^{-1/3}$:

$$G(\tilde{x}, \tilde{x}', \tilde{k}_\perp, \tilde{s}) = \begin{cases} \alpha Ai[-\tilde{x} + \tilde{k}_\perp^2 + \tilde{s}] & \text{when } \tilde{x} \leq 0 \\ \beta Ai[\tilde{x} + \tilde{k}_\perp^2 + \tilde{s}] + \gamma Bi[\tilde{x} + \tilde{k}_\perp^2 + \tilde{s}] & \text{when } 0 \leq \tilde{x} \leq \tilde{x}' \\ \delta Ai[\tilde{x} + \tilde{k}_\perp^2 + \tilde{s}] & \text{when } \tilde{x} \geq \tilde{x}'. \end{cases} \tag{3.110}$$

Considering the boundary conditions at $\tilde{x}'$ (continuity in G and a discontinuity in its derivative), we have

$$\beta Ai(\tilde{x}' + \tilde{k}_\perp^2 + \tilde{s}) + \gamma Bi(\tilde{x}' + \tilde{k}_\perp^2 + \tilde{s}) = \delta Ai(\tilde{x}' + \tilde{k}_\perp^2 + \tilde{s}) \tag{3.111}$$

$$\beta Ai'(\tilde{x}' + \tilde{k}_\perp^2 + \tilde{s}) + \gamma Bi'(\tilde{x}' + \tilde{k}_\perp^2 + \tilde{s}) - \delta Ai'(\tilde{x}' + \tilde{k}_\perp^2 + \tilde{s}) = 1. \tag{3.112}$$

These equations can be solved for γ with the result that $\gamma = \pi Ai(\tilde{x}' + \tilde{k}_\perp^2 + \tilde{s})$. The final boundary condition ($G \to 0$ as $\tilde{x} \to -\infty$) will (in principle) give a further relation between β and γ, as well as specifying α. But to use this condition we need to know the behaviour of G in regions near the origin, where our asymptotic approximation breaks down. Consequently we must rely on numerical solutions, which reveal that for our purposes we may neglect the βAi term in (3.111). Solving for δ we obtain:

$$G(\tilde{x}, \tilde{x}', \tilde{k}_\perp^2, \tilde{s}) = \begin{cases} \pi Ai(\tilde{x}' + \tilde{k}_\perp^2 + \tilde{s}) Bi(\tilde{x} + \tilde{k}_\perp^2 + \tilde{s}) & \text{for } 0 \ll \tilde{x} \leq \tilde{x}' \\ \pi Bi(\tilde{x}' + \tilde{k}_\perp^2 + \tilde{s}) Ai(\tilde{x} + \tilde{k}_\perp^2 + \tilde{s}) & \text{for } \tilde{x} \geq \tilde{x}' \gg 0. \end{cases} \tag{3.113}$$

We can now use the asymptotic form of the Airy function [36] to simplify these expressions further:

$$Ai(z) \sim \frac{1}{2\sqrt{\pi}} z^{-1/4} e^{-(2/3)z^{3/2}}, \qquad Bi(z) \sim \frac{1}{\sqrt{\pi}} z^{-1/4} e^{(2/3)z^{3/2}} \tag{3.114}$$

Hence, for $0 \ll \tilde{x} < \tilde{x}'$,

$$G = \frac{1}{2}(\tilde{x}' + \tilde{k}_\perp^2 + \tilde{s})^{-1/4}(\tilde{x} + \tilde{k}_\perp^2 + \tilde{s})^{-1/4} e^{-(2/3)[(\tilde{x}'+\tilde{k}_\perp^2+\tilde{s})^{3/2} - (\tilde{x}+\tilde{k}_\perp^2+\tilde{s})^{3/2}]}, \tag{3.115}$$

with a similar expression for $\tilde{x} > \tilde{x}' \gg 0$. For $\tilde{x} \approx \tilde{x}' \gg 0$, we may expand the terms inside the exponential to obtain

$$G_{\phi_1\bar{\phi}}(\tilde{x}, \tilde{x}', \tilde{k}_\perp, \tilde{s}) = \frac{1}{4}(\bar{\lambda}\bar{J})^{d/3}(\tilde{x} + \tilde{k}_\perp^2 + \tilde{s})^{-1/2} e^{-(\tilde{x}+\tilde{k}_\perp^2+\tilde{s})^{1/2}|\tilde{x}-\tilde{x}'|}. \tag{3.116}$$

3.9 Appendix B: Evaluation of the One Loop Diagrams

The loop contained in the diagram in figure 3.10(c) is given by the integral

$$2\bar{\lambda}^{-1/3}\bar{J}^{2/3}(\bar{\lambda}\bar{J})^{d/3} \int \frac{e^{-(\tilde{k}_\perp^2+i\tilde{s})^{1/2}|\tilde{x}_1''|}}{4(\tilde{k}_\perp^2 + i\tilde{s})^{1/2}} \frac{e^{-(\tilde{k}_\perp^2-i\tilde{s})^{1/2}|\tilde{x}_2''|}}{4(\tilde{k}_\perp^2 - i\tilde{s})^{1/2}} \frac{e^{-(\tilde{x}'+\tilde{k}_\perp^2+i\tilde{s})^{1/2}|\tilde{x}'-\tilde{x}_1''|}}{4(\tilde{x}' + \tilde{k}_\perp^2 + i\tilde{s})^{1/2}}$$
$$\times \frac{e^{-(\tilde{x}'+\tilde{k}_\perp^2-i\tilde{s})^{1/2}|\tilde{x}'-\tilde{x}_2''|}}{4(\tilde{x}' + \tilde{k}_\perp^2 - i\tilde{s})^{1/2}} (2\tilde{x}_1'')(2\tilde{x}_2'') d\tilde{x}_1'' d\tilde{x}_2'' \frac{d^{d-1}\tilde{k}_\perp d\tilde{s}}{(2\pi)^d}, \tag{3.117}$$

where the prefactor of '2' is a symmetry factor, and the s integration is along the real axis. In the integral we have used the form of the propagator for the ϕ field valid for $\tilde{x}_1'', \tilde{x}_2'', \tilde{x}' \gg 0$, and $\tilde{x}_1'', \tilde{x}_2'' \approx \tilde{x}'$, the region from which we expect the dominant contribution (as here the ϕ propagator falls off only as a power law). The $\tilde{x}_1''$ and $\tilde{x}_2''$ integrations are elementary, giving

$$2\bar{\lambda}^{-1/3}\bar{J}^{2/3}(\bar{\lambda}\bar{J})^{d/3} \frac{1}{16} \int e^{-(\tilde{k}_\perp^2+i\tilde{s})^{1/2}\tilde{x}'} e^{-(\tilde{k}_\perp^2-i\tilde{s})^{1/2}\tilde{x}'} \left[(\tilde{k}_\perp^2 + i\tilde{s})^{-1/2} - \frac{2}{\tilde{x}'^2}\right]$$
$$\left[(\tilde{k}_\perp^2 - i\tilde{s})^{-1/2} - \frac{2}{\tilde{x}'^2}\right] \frac{d^{d-1}\tilde{k}_\perp d\tilde{s}}{(2\pi)^d}. \tag{3.118}$$

However, we notice that the leading $\tilde{x}'$ part of the integral is in fact a divergent power law. Furthermore, this divergence cannot be cancelled by the renormalisation of the theory, as any such cancellation would have to arise from coupling constant renormalisation at the tree level (using (3.73)). As the renormalised tree level result is still an exponential, cancellation with a power law cannot occur. Consequently, we must find another mechanism for the removal of the divergence, and this is provided by its cancellation with the divergent loop shown in figure 3.10(b). Turning now to the next to leading $\tilde{x}'$ term in the above integral, we have

$$-\bar{\lambda}^{-1/3}\bar{J}^{2/3}(\bar{\lambda}\bar{J})^{d/3}\frac{1}{4\tilde{x}'^2}\int e^{-(\tilde{k}_\perp^2+i\tilde{s})^{1/2}\tilde{x}'}e^{-(\tilde{k}_\perp^2-i\tilde{s})^{1/2}\tilde{x}'} \times\left[\frac{1}{(\tilde{k}_\perp^2+i\tilde{s})^{1/2}}+\frac{1}{(\tilde{k}_\perp^2-i\tilde{s})^{1/2}}\right]\frac{d^{d-1}\tilde{k}_\perp d\tilde{s}}{(2\pi)^d}. \tag{3.119}$$

This can be rewritten as

$$\bar{\lambda}^{-1/3}\bar{J}^{2/3}(\bar{\lambda}\bar{J})^{d/3}\frac{2}{\tilde{x}'^2}\frac{\partial}{\partial\tilde{x}'}\int\frac{2e^{-(\tilde{k}_\perp^2+i\tilde{s})^{1/2}\tilde{x}'-(\tilde{k}_\perp^2-i\tilde{s})^{1/2}\tilde{x}'}}{4(\tilde{k}_\perp^2+i\tilde{s})^{1/2}4(\tilde{k}_\perp^2-i\tilde{s})^{1/2}}\frac{d^{d-1}\tilde{k}_\perp d\tilde{s}}{(2\pi)^d}, \tag{3.120}$$

i.e. a constant times the derivative of the ψ propagator loop integral. Rewriting the ψ propagators entirely in momentum space, and performing a contour integration for $\tilde{s}$, we end up with

$$\bar{\lambda}^{-1/3}\bar{J}^{2/3}(\bar{\lambda}\bar{J})^{d/3}\frac{1}{\tilde{x}'^2}\frac{\partial}{\partial\tilde{x}'}\int\frac{e^{i\tilde{p}\tilde{x}'}}{\tilde{\mathbf{k}}^2+(\tilde{p}-\tilde{\mathbf{k}})^2}\frac{d^d\tilde{\mathbf{k}}d\tilde{p}}{(2\pi)^{d+1}}. \tag{3.121}$$

This integral may be done exactly using some standard results from [61], with the result

$$\bar{\lambda}^{-1/3}\bar{J}^{2/3}(\bar{\lambda}\bar{J})^{d/3}2^{-1-d}\pi^{-(d+1)/2}(1-d)\Gamma\left(\frac{d-1}{2}\right)\tilde{x}'^{-d-2}. \tag{3.122}$$

To evaluate the contribution to $\langle\phi\rangle$ we now need to include the leftmost vertex and propagator:

$$-(\bar{\lambda}\bar{J})^{d/3}2^{-2-d}\pi^{-(d+1)/2}(1-d)\Gamma\left(\frac{d-1}{2}\right)\int\tilde{x}'^{-d-2}\tilde{x}^{-1/2}e^{-\tilde{x}^{1/2}|\tilde{x}-\tilde{x}'|}d\tilde{x}', \tag{3.123}$$

giving the leading order result

$$-(\bar{\lambda}\bar{J})^{-1}2^{-1-d}\pi^{-(d+1)/2}(1-d)\Gamma\left(\frac{d-1}{2}\right)x^{-d-3}. \tag{3.124}$$

Chapter 4

A Multispecies Reaction-Diffusion System

4.1 Introduction

In this chapter we set out to study fluctuation effects in a system with three competing irreversible reactions:

$$A + A \to \emptyset \qquad B + B \to \emptyset \qquad A + B \to \emptyset.$$

At $t = 0$ the A and B particles are distributed randomly (according to a Poisson distribution), such that on large scales both densities are initially homogeneous. Our goal is to calculate density decay exponents and amplitudes taking into account fluctuation effects. In pursuit of this aim, we analyse the system using both the Smoluchowski approximation and the field theory approach, and we show that the two methods are closely related. However, whereas it is unclear how the Smoluchowski approach may be improved, the field theory provides a systematic way to obtain successively more accurate values for the asymptotic density decay expo-

nents and amplitudes. We shall concentrate on situations where one of the two species is greatly in the majority (as is almost always the case asymptotically) - so, for example, if the A species is predominant, then we can safely neglect the reaction $B + B \rightarrow \emptyset$. This kind of assumption will lead to a considerable simplification in our analysis.

Previous work on this problem includes use of the Smoluchowski approximation [31], as well as exact $1d$ results obtained by Derrida *et al.* [32, 33, 34] for the special case of *immobile* minority particles. Derrida *et al.* were, in fact, studying a different problem, namely the probability that a given spin has never flipped in the zero temperature Glauber dynamics of the q-state Potts model in one dimension. By solving that model exactly [33, 34] they showed that this probability decreased as a power law: $t^{-3/8}$ for the Ising ($q = 2$) case. However, in one dimension, the Ising spin flip problem and the decay rate for the immobile impurity in our reaction-diffusion system are exactly equivalent problems (see figure 4.1), and hence this exact decay rate also holds in our case.

We also mention one other previous result for the immobile impurity problem, due to Cardy [62]. Using renormalisation group methods similar to those employed in this thesis, it was shown that the density of the minority species decays away as a universal power law: $t^{-\beta}$ for $d < 2$, where $\beta = \frac{1}{2} + O(\epsilon)$ and $\epsilon = 2 - d$. The case where the *majority* species is immobile has also been solved (see [35]). In this case the decay rate for the minority species is dominated by minority impurity particles existing in regions where there happen to be very few of the majority particles. Since these majority particles are strictly stationary, this situation is not describable using a rate equation approach, and it turns out that the minority species decays away as $\exp\left(-t^{d/(d+2)}\right)$, a result which is not accessible by perturbative

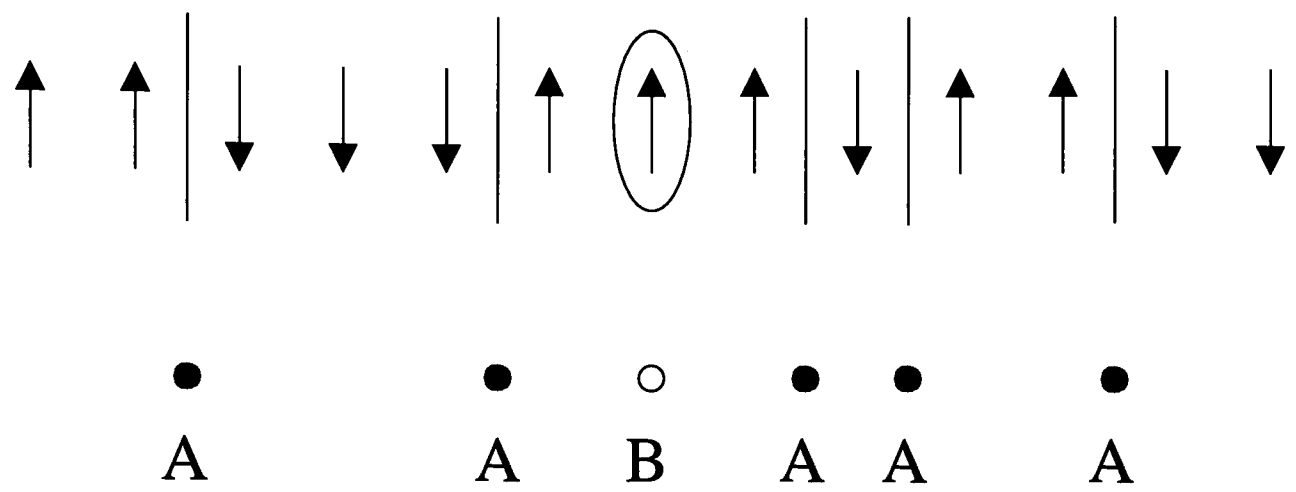

Figure 4.1: The mapping from the spin flip problem to the multispecies reaction-diffusion system.

methods.

For convenience, we now present a complete summary of our results for the density decay rates. In what follows we define n_A, n_B to be the initial density of A, B particles, and $\delta = (D_B/D_A) \leq 1$ to be the ratio of the diffusion constants. For $d < d_c = 2$, $n_A \gg n_B$ and $n_A^{-2/d} D_A^{-1} \ll t \ll t_1$ (where t_1 is a crossover time derived in section 4.4), we have (as in [38]):

$$\langle a \rangle \sim \left(\frac{1}{4\pi\epsilon} + \frac{2\ln 8\pi - 5}{16\pi} + O(\epsilon) \right) (D_A t)^{-d/2}. \tag{4.1}$$

For the minority species, we find, from the RG improved tree level approximation in the field theory:

$$\langle b \rangle \sim F(D_A t)^{-\beta} \tag{4.2}$$

where

$$\beta \approx \frac{d}{2} \left(\frac{\delta + 1}{2} \right)^{d/2} \qquad F \approx n_B \left(\frac{\Gamma(\epsilon/2)}{n_A (8\pi)^{d/2}} \right)^{\left(\frac{\delta+1}{2}\right)^{d/2}} \tag{4.3}$$

These decay exponents are identical with the Smoluchowski results. Performing a strict ϵ expansion on this RG improved tree level result gives an exponent $\beta =$

$\frac{1}{2}+O(\epsilon)$ for the immobile impurity case ($\delta = 0$). This is in agreement with previous RG calculations by Cardy [62]. If we now go beyond the tree level calculation by including one loop diagrams, then we obtain an improved value for the exponent β using an ϵ expansion:

$$\beta = \left(\frac{1+\delta}{2}\right)\left(1 - \frac{\epsilon}{2}\left[\frac{3}{2} + \ln\left(\frac{1+\delta}{2}\right) - \frac{\delta(1+\delta)}{4}\left[1 + 2\ln\left(\frac{1+\delta}{2}\right)\right]\right.\right.$$
$$\left.\left. -\frac{1}{4}(\delta^2-1)\left(1 + (1+\delta)\left[f\left\{\frac{2}{1+\delta}\right\} - \frac{\pi^2}{6}\right]\right)\right]\right) + O(\epsilon^2), \tag{4.4}$$

where

$$f\{x\} = -\int_1^x \frac{\ln u}{u-1} du \tag{4.5}$$

is the dilogarithmic function [36]. This exponent is found to be in good agreement with simulations [31] and exact results [34] in $d = 1$.

However, for $\delta < 1$, the system crosses over to a second regime where $\langle b \rangle \gg \langle a \rangle$. This situation is similar to the case where we begin with $n_B \gg n_A$. In that regime, at times $D_B t \gg n_B^{-2/d}$, and for $n_B \gg n_A$, $\delta \neq 0$ and $d < 2$, we have:

$$\langle b \rangle \sim \left(\frac{1}{4\pi\epsilon} + \frac{2\ln 8\pi - 5}{16\pi} + O(\epsilon)\right)(D_B t)^{-d/2}, \tag{4.6}$$

for the majority species. Using the RG improved tree level result for the minority species, we obtain:

$$\langle a \rangle \sim E(D_B t)^{-\alpha}, \tag{4.7}$$

with

$$\alpha \approx \frac{d}{2}\left(\frac{1+\delta^{-1}}{2}\right)^{d/2} \qquad E \approx n_A\left(\frac{\Gamma(\epsilon/2)}{n_B(8\pi)^{d/2}}\right)^{\left(\frac{1+\delta^{-1}}{2}\right)^{d/2}} \tag{4.8}$$

The exponent is again in agreement with the Smoluchowski result. If we attempt to improve this calculation to one loop accuracy, then we obtain:

$$\alpha = \left(\frac{1+\delta^{-1}}{2}\right)\left(1 - \frac{\epsilon}{2}\left[\frac{3}{2} + \ln\left(\frac{1+\delta^{-1}}{2}\right) - \frac{\delta^{-1}(1+\delta^{-1})}{4}\left[1 + 2\ln\left(\frac{1+\delta^{-1}}{2}\right)\right]\right.\right.$$

$$-\frac{1}{4}(\delta^{-2}-1)\left(1+(1+\delta^{-1})\left[f\left\{\frac{2}{1+\delta^{-1}}\right\}-\frac{\pi^2}{6}\right]\right)\Bigg]\Bigg)+O(\epsilon^2). \tag{4.9}$$

This exponent is only valid for δ quite close to unity, and even in this region it may be less accurate than the (non ϵ-expanded) RG improved tree level result given above. This point will be discussed further in section 4.4.2.

We next give results valid for $d = 2$, where we find extra logarithmic factors multiplying the power law decay rates. Treating first the case $\langle a\rangle \gg \langle b\rangle$ and $\delta \leq 1$, we have, from the RG improved tree level, an initial regime with:

$$\langle a\rangle \sim \frac{\ln t}{8\pi D_A t} \tag{4.10}$$

$$\langle b\rangle = O\left(\left(\frac{\ln t}{t}\right)^{\left(\frac{1+\delta}{2}\right)}\right) \tag{4.11}$$

However, for $\delta < 1$, the system again crosses over to a second regime where $\langle b\rangle \gg \langle a\rangle$. In this second regime the density decay exponents (though not the amplitudes) are the same as for the case where we begin with $n_B \gg n_A$. In that case we have, for $\delta \neq 0$:

$$\langle b\rangle \sim \frac{\ln t}{8\pi D_B t} \tag{4.12}$$

$$\langle a\rangle = O\left(\left(\frac{\ln t}{t}\right)^{\left(\frac{1+\delta^{-1}}{2}\right)}\right) \tag{4.13}$$

Crossover times for these cases are given in section 4.4.3.

We now give a brief description of the layout of this chapter. In the next section we analyse the system using the mean field/Smoluchowski approach. We then set up the necessary formalism for our field theory in section 4.3, and use it to perturbatively calculate values for the density exponents and amplitudes in section 4.4. Finally, we give some conclusions and prospects for future work in section 4.5.

4.2 The Mean Field & Smoluchowski Approach

The simplest description of a reaction-diffusion process is provided by the mean field rate equations. For the system we are considering with densities a and b, they take the form:

$$\frac{da}{dt} = -2\lambda_{AA}a^2 - \lambda_{AB}ab \tag{4.14}$$

$$\frac{db}{dt} = -2\lambda_{BB}b^2 - \lambda_{AB}ab, \tag{4.15}$$

where λ_{AA}, λ_{BB}, and λ_{AB} are the reaction rates, and where we impose initial conditions of the form $a|_{t=0} = n_A$ and $b|_{t=0} = n_B$. In this approach we have, of course, completely neglected the effects of fluctuations - below an upper critical dimension d_c, where fluctuations become relevant, this sort of approximation will break down.

Nevertheless, even at the mean field level, the complete solution set for these rate equations is quite complicated. In what follows we shall restrict our analysis to the case where $2\lambda_{BB} < \lambda_{AB} < 2\lambda_{AA}$. The solution for this particular parameter set will be required for our later field theoretic analysis. As we demonstrate in Appendix A (see also [31]), it is easy to show (by forming a rate equation for the concentration ratio) that $(a/b) \to 0$ as $t \to \infty$. Thus, if we begin with initial conditions where $n_A \gg n_B$, we can identify two distinct regimes - an early time regime where $a \gg b$ and, after a crossover, a late time (true asymptotic) regime where $b \gg a$. Treating the early time regime first, we find (after some algebra):

$$a \sim (2\lambda_{AA}t)^{-1} \tag{4.16}$$

$$b \sim \frac{n_B}{(2n_A\lambda_{AA}t)^{\lambda_{AB}/2\lambda_{AA}}}. \tag{4.17}$$

Note that the A particles are decaying away more quickly than the B's, so eventu-

ally we crossover to a second regime:

$$b \sim (2\lambda_{BB}t)^{-1} \tag{4.18}$$

$$a \sim \frac{n_A}{(2n_B\lambda_{BB}t)^{\lambda_{AB}/2\lambda_{BB}}}\left(1+\frac{(\lambda_{AB}-2\lambda_{AA})}{(2\lambda_{BB}-\lambda_{AB})}\frac{n_A}{n_B}\right)^{-1-\frac{\lambda_{AB}(\lambda_{AB}-2\lambda_{BB})}{2\lambda_{BB}(\lambda_{AB}-2\lambda_{AA})}} \tag{4.19}$$

More details of these derivations can be found in appendix A. Alternatively, if we begin with $n_B \gg n_A$, then we have a single asymptotic regime:

$$b \sim (2\lambda_{BB}t)^{-1} \tag{4.20}$$

$$a \sim \frac{n_A}{(2n_B\lambda_{BB}t)^{\lambda_{AB}/2\lambda_{BB}}}. \tag{4.21}$$

By using these solutions to compare the relative sizes of the reaction terms in the mean field rate equations (4.14) and (4.15), it is also easy to derive crossover times for the various regimes.

However, if we now wish to extend our results at or below the upper critical dimension, we must attempt to include some of the fluctuation effects. The simplest way in which this can be done is to employ the Smoluchowski approximation [4, 31, 63]. The essential idea of this approach is to relate the effective reaction rates $\lambda^{eff}_{\{ij\}}$ to the diffusion constants D_A, D_B. Suppose we want to calculate the reaction rate λ^{eff}_{AB}. We begin by choosing a (fixed) A species target "trap", which is surrounded by B particles. When a B particle approaches within a distance R of the target, a reaction is deemed to have occurred. Consequently, the reaction rate may be obtained by solving a diffusion equation with boundary conditions of fixed density as $r \to \infty$, and absorption at $r = R$. The flux of B particles across the d dimensional sphere of radius R around the target is then proportional to an effective microscopic reaction rate. If we now generalise to the case where both the A and B species are mobile, then we find (in dimension $d < 2$ and in the large time

limit):

$$\lambda_{AB}^{eff} \sim (\text{const.})(D_A + D_B)^{d/2} t^{d/2-1}. \tag{4.22}$$

For $d = 2$ we obtain logarithmic corrections:

$$\lambda_{AB}^{eff} \sim \frac{(\text{const.})(D_A + D_B)}{\ln((D_A + D_B)t)}. \tag{4.23}$$

More details of these derivations can be found in appendix B. The Smoluchowski reaction rates for λ_{AA}^{eff} and λ_{BB}^{eff} are obtained in a similar fashion. Note that above $d = 2$ the reaction rate approaches a limiting (constant) value, and we see that the Smoluchowski approach predicts a critical dimension of $d_c = 2$ for this system. This is simply related to the reentrancy property of random walks in $d \leq 2$. It is the inclusion of this effect which accounts for the improvement introduced by the Smoluchowski approach.

If we now substitute these modified reaction rates into the rate equations, we can obtain the Smoluchowski improved density exponents. For the case where $n_A \gg n_B$, we find an initial regime with

$$a = O(t^{-d/2}) \tag{4.24}$$

$$b = O\left(t^{-\frac{d}{2}\left(\frac{1+\delta}{2}\right)^{d/2}}\right) \tag{4.25}$$

Once again, since the A particles are decaying away faster than the B's, we cross over to a second regime, where (for $0 < \delta < 1$)

$$b = O(t^{-d/2}) \tag{4.26}$$

$$a = O\left(t^{-\frac{d}{2}\left(\frac{1+\delta^{-1}}{2}\right)^{d/2}}\right) \tag{4.27}$$

This second set of exponents is the same as for the case where we begin with $n_B \gg n_A$ and $\delta \neq 0$. In this situation no crossover occurs and the exponents

are valid for all asymptotic times. These exponents can be compared favourably with both simulations [31], and exact results [34]. For example, the decay rate for immobile minority impurities is given by Smoluchowski to be $\approx t^{-0.354}$. This compares well with the exact decay rate of $t^{-0.375}$.

Turning to the case $d = d_c = 2$ and $n_A \gg n_B$, we obtain, for the initial regime:

$$a = O\left(\frac{\ln t}{t}\right) \tag{4.28}$$

$$b = O\left(\left(\frac{\ln t}{t}\right)^{\left(\frac{1+\delta}{2}\right)} (\ln t)^{\left(\frac{1+\delta}{2}\right)\ln\left(\frac{1+\delta}{2}\right)}\right) \tag{4.29}$$

We again eventually crossover to a second regime, where (for $0 < \delta < 1$):

$$b = O\left(\frac{\ln t}{t}\right) \tag{4.30}$$

$$a = O\left(\left(\frac{\ln t}{t}\right)^{\left(\frac{1+\delta^{-1}}{2}\right)} (\ln t)^{\left(\frac{1+\delta^{-1}}{2}\right)\ln\left(\frac{1+\delta^{-1}}{2}\right)}\right) \tag{4.31}$$

This second set of exponents is again valid (for all asymptotic times) in the case where we begin with $n_B \gg n_A$ and $\delta \neq 0$.

Note that the Smoluchowski approach can also be employed for $d > d_c$, where again we will find (time independent) reaction rates which depend on the diffusion constants. However, our later field theoretic analysis shows that there is no strict justification for this procedure. Nevertheless, a recent Smoluchowski based study has been made of a system with heterogeneous single species annihilation [31]. In this situation we have only one fundamental reaction process, but different reaction rates may still arise, for example, by having two or more different particle masses (and hence two or more different diffusion constants). In this case it is physically reasonable to suppose that the exponents for $d > d_c$ (which are ratios of reaction rates) may again depend only on the diffusivity ratios, with any other parameters

cancelling out. However, in the general case, where the reaction processes are genuinely distinct this will not be the case.

Overall, we have seen that the Smoluchowski approach is a simple way to incorporate some fluctuation effects into the rate equation approach. Unfortunately, it is not at all clear how these methods may be systematically improved. It is for this reason that we turn to the main purpose of this chapter - the development of an alternative field theoretic framework.

4.3 The Field Theory Approach

Our starting point is the field theoretic action (2.41), derived in section 2.3:

$$S = \int d^d x \left(\int dt \left[\bar{a}(\partial_t - \nabla^2)a + \bar{b}(\partial_t - \delta\nabla^2)b + 2\lambda_{AA}\bar{a}a^2 + \lambda_{AA}\bar{a}^2a^2 \right.\right. \quad (4.32)$$
$$\left.\left. +2\lambda_{BB}\bar{b}b^2 + \lambda_{BB}\bar{b}^2b^2 + \lambda_{AB}\bar{a}ab + \lambda_{AB}\bar{b}ab + \lambda_{AB}\bar{a}\bar{b}ab \right] - \bar{a}n_A - \bar{b}n_B \right).$$

Here we have defined $\delta = (D_B/D_A) \leq 1$, and also rescaled time t, together with the reaction rates $\lambda_{\{ij\}}$, to absorb the diffusion constant D_A.

Performing power counting on the action S, we can now give the natural canonical dimensions for the various parameters appearing in the action:

$$[t] \sim k^{-2} \qquad [a], [b], [n_A], [n_B] \sim k^d \qquad [\bar{a}], [\bar{b}] \sim k^0 \qquad [\lambda_{\{ij\}}] \sim k^{2-d}. \quad (4.33)$$

Notice that the reaction rates become dimensionless in $d = 2$, which we therefore postulate as the upper critical dimension for the system, in agreement with the Smoluchowski prediction.

From the action S, we can see that the propagators for the theory are given by

$$G_{a\bar{a}}(k, t - t') = \begin{cases} e^{-k^2(t-t')} & \text{for } t > t' \\ 0 & \text{for } t < t' \end{cases} \quad (4.34)$$

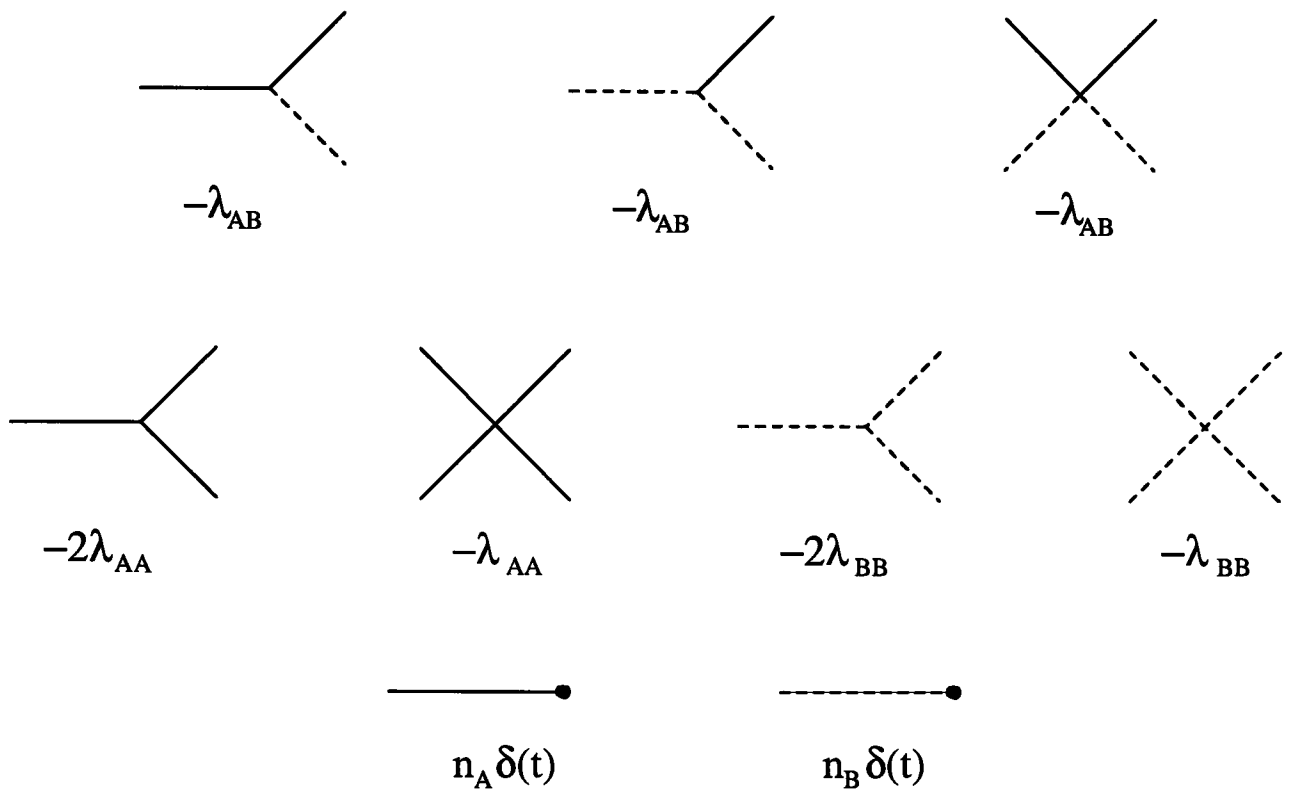

Figure 4.2: Vertices for the field theory.

$$G_{b\bar{b}}(k, t-t') = \begin{cases} e^{-k^2(t-t')\delta} & \text{for } t > t' \\ 0 & \text{for } t < t'. \end{cases} \tag{4.35}$$

Diagrammatically, we represent $G_{a\bar{a}}$ by a thin solid line and $G_{b\bar{b}}$ by a thin dotted line. The vertices for the theory are given in figure 4.2.

4.3.1 Renormalisation

One of the most important features of this theory, as we have previously mentioned, is the relative simplicity of its renormalisation. Examination of the vertices given in figure 4.2 reveals that it is again not possible to draw diagrams which dress the propagators. Hence the bare propagators are the full propagators for the theory. Consequently, the only renormalisation needed involves the reaction rates $\lambda_{\{ij\}}$, and in particular the diffusion constants (or δ) are *not* renormalised.

The temporally extended vertex functions for the reaction rates are given by

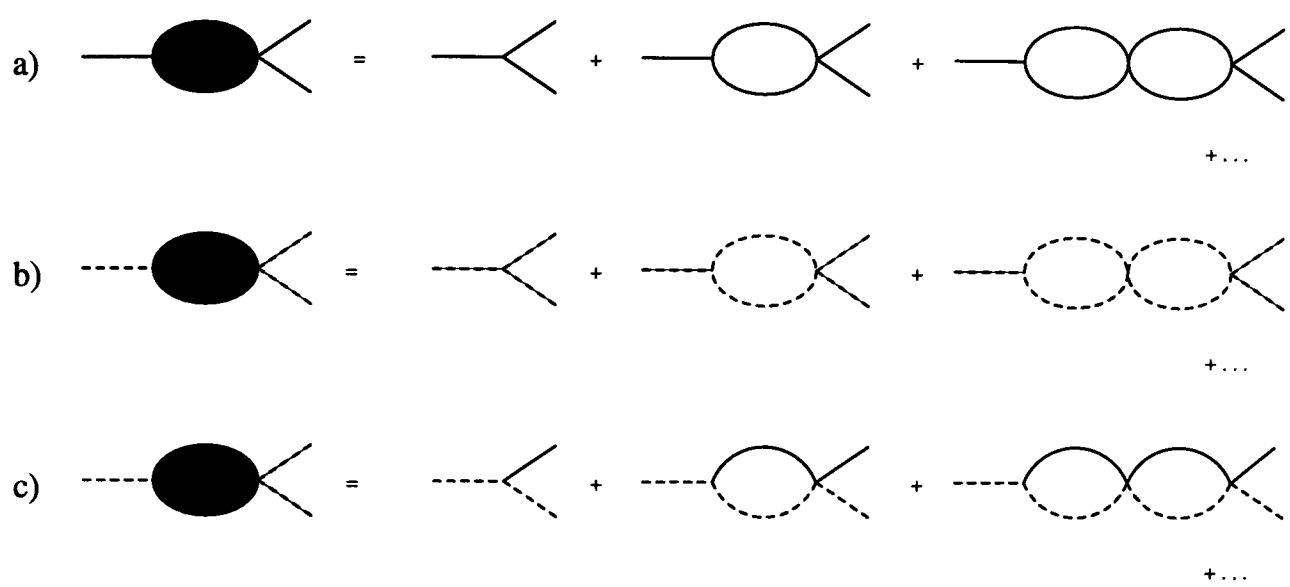

Figure 4.3: The temporally extended vertex functions (a) $\lambda_{AA}(k,s)$, (b) $\lambda_{BB}(k,s)$, and (c) $\lambda_{AB}(k,s)$.

the diagrammatic sums given in figure 4.3. As is the case in similar theories (see chapter 3 and also [19, 24, 38]), these sums may be evaluated exactly using Laplace transforms:

$$\lambda_{AA}(k,s) = \frac{\lambda_{AA}}{1+\lambda_{AA}C\Gamma(\epsilon/2)(s+\frac{1}{2}k^2)^{-\epsilon/2}} \tag{4.36}$$

$$\lambda_{BB}(k,s) = \frac{\lambda_{BB}}{1+\lambda_{BB}C\Gamma(\epsilon/2)\delta^{-1}(s/\delta+\frac{1}{2}k^2)^{-\epsilon/2}} \tag{4.37}$$

$$\lambda_{AB}(k,s) = \frac{\lambda_{AB}}{1+\lambda_{AB}2^{-\epsilon/2}C\Gamma(\epsilon/2)(1+\delta)^{-d/2}(s+k^2\delta/(1+\delta))^{-\epsilon/2}}, \tag{4.38}$$

where $C = 2/(8\pi)^{d/2}$ and s is the Laplace transformed time variable.

We can now use these vertex functions to define the three dimensionless renormalised and bare couplings, with $s = \kappa^2$, $k = 0$ as the normalisation point:

$$g_{R_{\{ij\}}} = \kappa^{-\epsilon}\lambda_{\{ij\}}(k,s)|_{s=\kappa^2,k=0} \qquad g_{0_{\{ij\}}} = \kappa^{-\epsilon}\lambda_{\{ij\}}. \tag{4.39}$$

Consequently, we can define three β functions:

$$\beta(g_{R_{AA}}) = \kappa\frac{\partial}{\partial\kappa}g_{R_{AA}} = -\epsilon g_{R_{AA}} + \epsilon C\Gamma(\epsilon/2)g_{R_{AA}}^2 \tag{4.40}$$

$$\beta(g_{R_{BB}}) = \kappa\frac{\partial}{\partial\kappa}g_{R_{BB}} = -\epsilon g_{R_{BB}} + \epsilon C\Gamma(\epsilon/2)\delta^{-d/2}g^2_{R_{BB}} \tag{4.41}$$

$$\beta(g_{R_{AB}}) = \kappa\frac{\partial}{\partial\kappa}g_{R_{AB}} = -\epsilon g_{R_{AB}} + 2^{-\epsilon/2}\epsilon C\Gamma(\epsilon/2)(1+\delta)^{-d/2}g^2_{R_{AB}}, \tag{4.42}$$

and three fixed points $\beta(g^*_{R_{\{ij\}}}) = 0$:

$$g^*_{R_{AA}} = (C\Gamma(\epsilon/2))^{-1} \tag{4.43}$$

$$g^*_{R_{BB}} = (C\Gamma(\epsilon/2)\delta^{-d/2})^{-1} \tag{4.44}$$

$$g^*_{R_{AB}} = \left(C\Gamma(\epsilon/2)\frac{1}{2}\left(\frac{1+\delta}{2}\right)^{-d/2}\right)^{-1} \tag{4.45}$$

Finally, we see from (4.36), (4.37), and (4.38) that the expansion of $g_{0_{\{ij\}}}$ in powers of $g_{R_{\{ij\}}}$ is given by:

$$g_{0_{\{ij\}}} = g_{R_{\{ij\}}} + \frac{g^2_{R_{\{ij\}}}}{g^*_{R_{\{ij\}}}} + \dots \tag{4.46}$$

4.3.2 Callan-Symanzik Equation

We now exploit the fact that physical quantities calculated using the field theory must be independent of the choice of normalisation point. This leads us to a Callan-Symanzik equation:

$$\left[\kappa\frac{\partial}{\partial\kappa} + \beta(g_{R_{AA}})\frac{\partial}{\partial g_{R_{AA}}} + \beta(g_{R_{BB}})\frac{\partial}{\partial g_{R_{BB}}} + \beta(g_{R_{AB}})\frac{\partial}{\partial g_{R_{AB}}}\right]\langle a\rangle_R = 0. \tag{4.47}$$

However dimensional analysis implies

$$\left[\kappa\frac{\partial}{\partial\kappa} - 2t\frac{\partial}{\partial t} + dn_A\frac{\partial}{\partial n_A} + dn_B\frac{\partial}{\partial n_B} - d\right]\langle a\rangle_R(t, n_A, n_B, g_{R_{\{ij\}}}, \delta, \kappa) = 0. \tag{4.48}$$

Exactly similar equations hold for $\langle b\rangle_R$. Eliminating the terms involving κ and solving by the method of characteristics, we find:

$$\langle a\rangle_R(t, n_A, n_B, g_{R_{\{ij\}}}, \delta, \kappa) = (\kappa^2 t)^{-d/2}\langle a\rangle_R(\kappa^{-2}, \tilde{n}_A(\kappa^{-2}), \tilde{n}_B(\kappa^{-2}), \tilde{g}_{R_{\{ij\}}}(\kappa^{-2}), \delta, \kappa), \tag{4.49}$$

with the characteristic equations:

$$2t\frac{\partial \tilde{n}_A}{\partial t} = -d\tilde{n}_A \qquad 2t\frac{\partial \tilde{n}_B}{\partial t} = -d\tilde{n}_B \qquad 2t\frac{\partial \tilde{g}_{R_{\{ij\}}}}{\partial t} = \beta(\tilde{g}_{R_{\{ij\}}}), \tag{4.50}$$

and initial conditions:

$$\tilde{n}_A(t) = n_A \quad \tilde{n}_B(t) = n_B \tag{4.51}$$

$$\tilde{g}_{R_{AA}}(t) = g_{R_{AA}} \quad \tilde{g}_{R_{BB}}(t) = g_{R_{BB}} \quad \tilde{g}_{R_{AB}}(t) = g_{R_{AB}}. \tag{4.52}$$

These equations have the exact solutions:

$$\tilde{n}_A(t') = \left(\frac{t}{t'}\right)^{d/2} n_A \qquad \tilde{n}_B(t') = \left(\frac{t}{t'}\right)^{d/2} n_B, \tag{4.53}$$

and

$$\tilde{g}_{R_{\{ij\}}}(t') = g^*_{R_{\{ij\}}} \left(1 + \frac{g^*_{R_{\{ij\}}} - g_{R_{\{ij\}}}}{g_{R_{\{ij\}}}(t/t')^{\epsilon/2}}\right)^{-1} \tag{4.54}$$

In the large t limit $\tilde{g}_{R_{\{ij\}}} \to g^*_{R_{\{ij\}}}$, a relationship which will allow us to relate an expansion in powers of the renormalised couplings $g_{R_{\{ij\}}}$ to an ϵ expansion using (4.49). In our later density calculations we will assume that this asymptotic regime has been reached.

4.3.3 Tree Diagrams

In order to perform systematic ϵ expansion calculations we now need to identify the leading and subleading terms in an expansion in powers of $g_{0_{\{ij\}}}$. In calculating $\langle a \rangle$ and $\langle b \rangle$ contributions from tree diagrams are of order $g^q_{0_{\{ij\}}} n^{1+q}_{\{i\}}$, for integer q, and densities $n_{\{i\}} = \{n_A, n_B\}$. However, diagrams with l loops will be of order $g^q_{0_{\{ij\}}} n^{1+q-l}_{\{i\}}$. The addition of loops makes the power of $g_{0_{\{ij\}}}$ higher relative to the power of the densities - so we conclude that the number of loops again gives the order of the diagram.

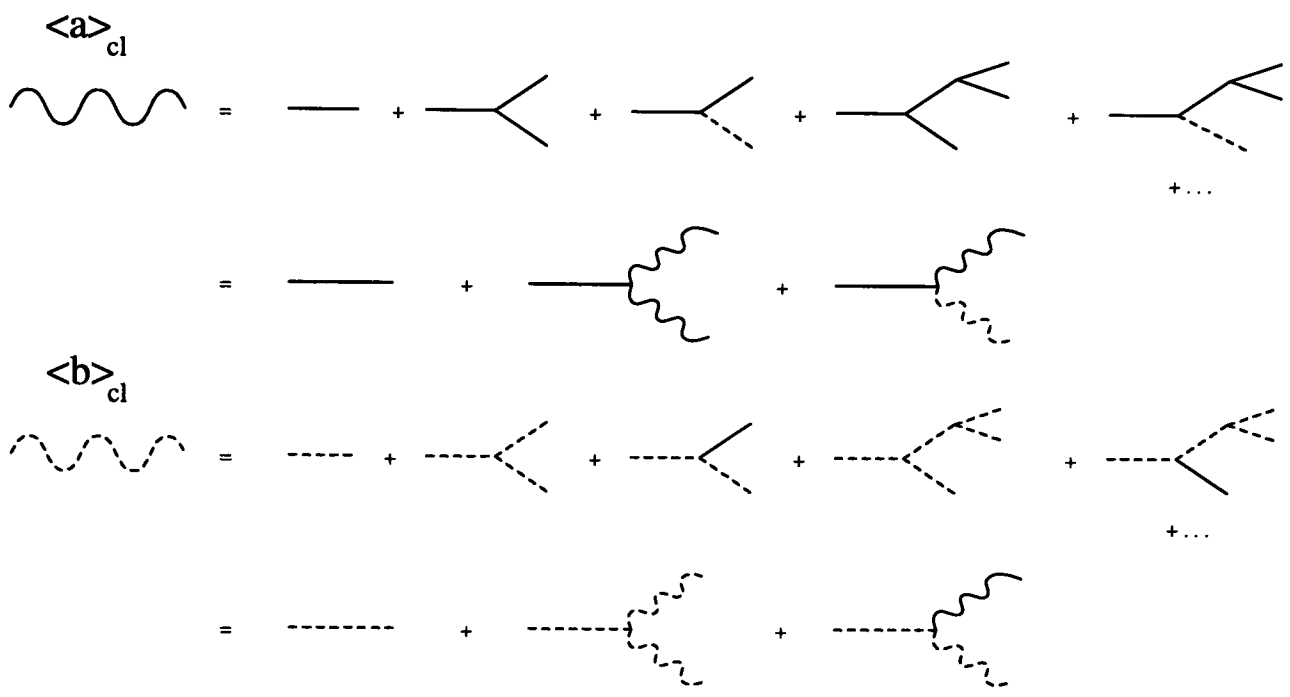

Figure 4.4: Tree level diagrams for the densities $\langle a \rangle$ and $\langle b \rangle$.

The lowest order diagrams contributing to $\langle a \rangle$ and $\langle b \rangle$ are the tree diagrams shown in figure 4.4. We represent the classical (tree level) density $\langle a \rangle_{cl}$ by a wavy solid line, and $\langle b \rangle_{cl}$ by a wavy dotted line. These sets of diagrams are equivalent to the mean field rate equations, as may be seen by acting on each by their respective inverse Green functions.

The second tree level quantities appearing in the theory are the response functions:

$$L(k, t_2, t_1) = \langle a(-k, t_2)\bar{a}(k, t_1)\rangle \tag{4.55}$$

$$M(k, t_2, t_1) = \langle b(-k, t_2)\bar{a}(k, t_1)\rangle \tag{4.56}$$

$$N(k, t_2, t_1) = \langle b(-k, t_2)\bar{b}(k, t_1)\rangle \tag{4.57}$$

$$P(k, t_2, t_1) = \langle a(-k, t_2)\bar{b}(k, t_1)\rangle, \tag{4.58}$$

which we represent diagrammatically by the thick lines shown in figure 4.5. These functions can be evaluated analytically, but only in the limit $\langle a \rangle \gg \langle b \rangle$, or $\langle b \rangle \gg$

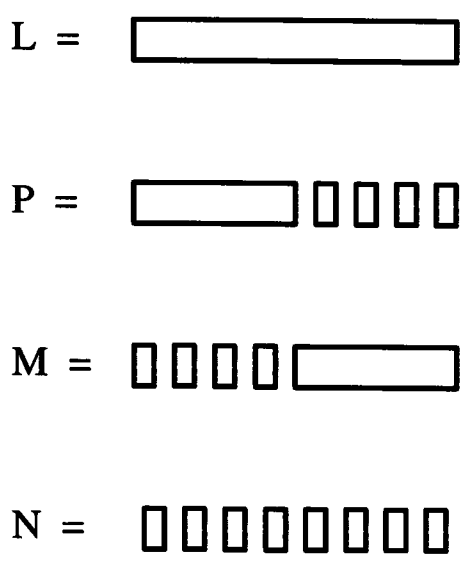

where, for example :

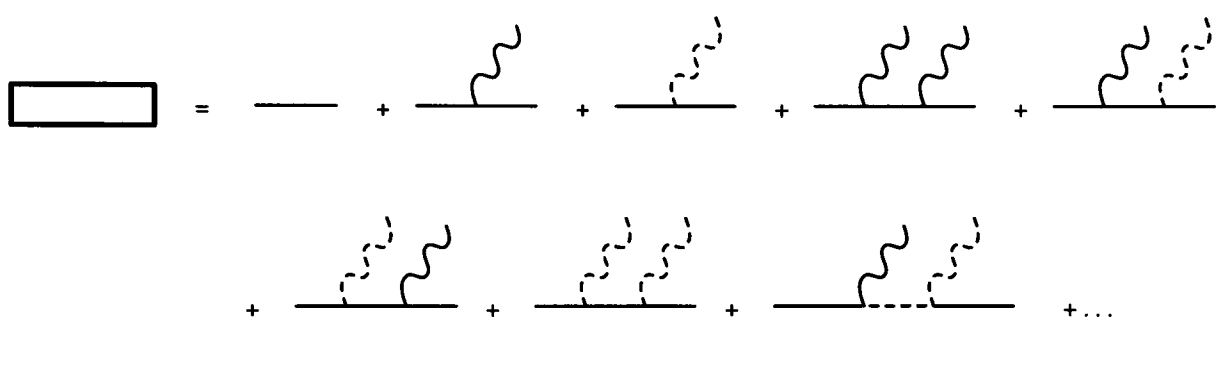

Figure 4.5: The response functions.

$\langle a \rangle$. The details of this calculation are presented in appendix C, where the following results are derived (for $\langle a \rangle \gg \langle b \rangle$):

$$L(k,t_2,t_1) = \left(\frac{1+2\lambda_{AA}n_A t_1}{1+2\lambda_{AA}n_A t_2}\right)^2 \exp\left(-k^2(t_2-t_1)\right) \tag{4.59}$$

$$N(k,t_2,t_1) = \left(\frac{1+2\lambda_{AA}n_A t_1}{1+2\lambda_{AA}n_A t_2}\right)^{\lambda_{AB}/2\lambda_{AA}} \exp\left(-k^2(t_2-t_1)\delta\right) \tag{4.60}$$

$$P(k,t_2,t_1) = -\lambda_{AB}n_A \frac{(1+2\lambda_{AA}n_A t_1)^{\lambda_{AB}/2\lambda_{AA}}}{(1+2\lambda_{AA}n_A t_2)^2} \exp\left(-k^2(t_2-t_1\delta)\right) \times \int_{t_1}^{t_2} \frac{\exp\left(k^2(1-\delta)t'\right)}{(1+2\lambda_{AA}n_A t')^{-1+\lambda_{AB}/2\lambda_{AA}}} dt' \tag{4.61}$$

$$M(k,t_2,t_1) = -\lambda_{AB}n_B \frac{(1+2\lambda_{AA}n_A t_1)^2}{(1+2\lambda_{AA}n_A t_2)^{\lambda_{AB}/2\lambda_{AA}}} \exp\left(-k^2(t_2\delta-t_1)\right)$$

$$\times \int_{t_1}^{t_2} \frac{\exp\left(-k^2(1-\delta)t'\right)}{(1+2\lambda_{AA}n_A t')^2} dt'. \tag{4.62}$$

An extra check on the validity of these response functions is provided by the relations:

$$L(0,t,0) = \frac{\partial\langle a(t)\rangle}{\partial n_A} \qquad N(0,t,0) = \frac{\partial\langle b(t)\rangle}{\partial n_B} \tag{4.63}$$

$$P(0,t,0) = \frac{\partial\langle a(t)\rangle}{\partial n_B} \qquad M(0,t,0) = \frac{\partial\langle b(t)\rangle}{\partial n_A}, \tag{4.64}$$

which follow from the definition of the response functions, and from the initial condition terms in the action S. It is easy to check that the above response functions do indeed satisfy these relations.

For the opposite situation where $n_B \gg n_A$ (and hence $\langle b\rangle \gg \langle a\rangle$), we could use a formalism similar to the above for the density calculations. However, it is much simpler to map this case onto the $\langle a\rangle \gg \langle b\rangle$ regime by swapping the labels on the A and B particles, and then transforming:

$$n_A \leftrightarrow n_B \quad \lambda_{AA} \leftrightarrow \lambda_{BB} \quad D_A \leftrightarrow D_B.$$

We can then obtain the exponents and amplitudes for this second regime with no extra work.

This concludes our discussion of the field theory formalism. The framework we have built up allows (in principle) the systematic calculation of fluctuation effects in all circumstances. However, it is only in the case where one of the species is greatly in the majority where the equations (for the tree level densities and response functions) are sufficiently simple for analytic progress to be made. We now turn to make use of the field theory in calculating the fluctuation modified densities.

4.4 Density Calculations

4.4.1 Tree Level

The first step in using our field theory to include fluctuation effects is to insert the mean field (tree level) solution into the Callan-Symanzik solution (4.49), using the results for the running densities/couplings (4.53), (4.54). Since the fixed points for the couplings obey $2g^*_{R_{BB}} < g^*_{R_{AB}} < 2g^*_{R_{AA}}$ (when $\delta < 1$) it is appropriate to use the mean field solutions derived in section 4.2. For the case where $n_A \gg n_B$, this gives:

$$\langle a \rangle \sim \left(\frac{\Gamma(\epsilon/2)}{(8\pi)^{d/2}} \right) (D_A t)^{-d/2}, \tag{4.65}$$

and

$$\langle b \rangle \sim F(D_A t)^{-\beta}, \tag{4.66}$$

with

$$\beta \approx \frac{d}{2}\left(\frac{1+\delta}{2}\right)^{d/2} \qquad F \approx n_B \left(\frac{\Gamma(\epsilon/2)}{n_A (8\pi)^{d/2}} \right)^{\left(\frac{1+\delta}{2}\right)^{d/2}} \tag{4.67}$$

valid for $n_A^{-2/d} D_A^{-1} \ll t \ll t_1$, where

$$D_A t_1 \approx \left(\frac{n_B}{n_A^{\left(\frac{1+\delta}{2}\right)^{d/2}}} \right)^{\frac{2}{d}\left(\left(\frac{1+\delta}{2}\right)^{d/2}-1\right)^{-1}} \tag{4.68}$$

These modified crossover times are obtained by using the expressions for the running couplings/densities in the mean field crossovers. Notice that the density decay exponents derived here are the same as those obtained from the Smoluchowski approach. However, as we are performing an ϵ expansion, we are only strictly justified in retaining leading order ϵ terms. Consequently we find, for the minority species density decay exponent and amplitude:

$$\beta = \left(\frac{1+\delta}{2}\right) + O(\epsilon) \qquad F = n_B \left(\frac{1}{4\pi\epsilon n_A} + O(\epsilon^0) \right)^{\left(\frac{1+\delta}{2}\right)+O(\epsilon)} \tag{4.69}$$

Eventually, however, as the A particles are decaying away more quickly than the B particles (due to their greater diffusivity when $\delta < 1$), we crossover to a second regime where $\langle b \rangle \gg \langle a \rangle$. For $0 < \delta < 1$, we have:

$$\langle b \rangle \sim \left(\frac{\Gamma(\epsilon/2)}{(8\pi)^{d/2}} \right) (D_B t)^{-d/2} \tag{4.70}$$

$$\langle a \rangle \sim E(D_B t)^{-\alpha}, \tag{4.71}$$

with

$$\alpha \approx \frac{d}{2} \left(\frac{1+\delta^{-1}}{2} \right)^{d/2} = \left(\frac{1+\delta^{-1}}{2} \right) + O(\epsilon) \tag{4.72}$$

$$E \approx n_A f(d) \left(\frac{\Gamma(\epsilon/2)}{n_B (8\pi)^{d/2}} \right)^{\left(\frac{1+\delta^{-1}}{2}\right)^{d/2}} = n_A f(2) \left(\frac{1}{4\pi\epsilon n_B} + O(\epsilon^0) \right)^{\left(\frac{1+\delta^{-1}}{2}\right)+O(\epsilon)} \tag{4.73}$$

where

$$f(d) = \left(1 + \frac{[((1+\delta)/2)^{d/2} - 1] n_A}{[\delta^{d/2} - ((1+\delta)/2)^{d/2}] n_B} \right)^{-1-\left(\frac{1+\delta^{-1}}{2}\right)^{d/2} \left(\frac{((1+\delta)/2)^{d/2} - \delta^{d/2}}{((1+\delta)/2)^{d/2} - 1} \right)} \tag{4.74}$$

This result is valid for $t \gg t_2$, where

$$D_B t_2 \approx \left(\frac{n_A f(d) (1+\delta^{-1})^{d/2}}{n_B^{((1+\delta^{-1})/2)^{d/2}}} \right)^{\frac{2}{d}\left(\left(\frac{1+\delta^{-1}}{2}\right)^{d/2} - 1\right)^{-1}} \tag{4.75}$$

Note that for $\delta = 1$ the first crossover time $t_1 \to \infty$ - in this case the two species decay away at the same rate, and so no further crossover occurs. Alternatively if $\delta = 0$, then the first regime is left, but the second crossover time $t_2 \to \infty$. In that case the minority species finally decays away in the exponential fashion predicted in [35]. For the intermediate case where δ is small, but nonzero, the decay exponent for the minority species becomes large in the final regime. The explanation for this result lies in the relatively large diffusivity of the minority A species (if D_A is large) and/or the increased density amplitude for the majority B particles (if D_B is small). Both these effects will lead to an increased rate of decay for the A species.

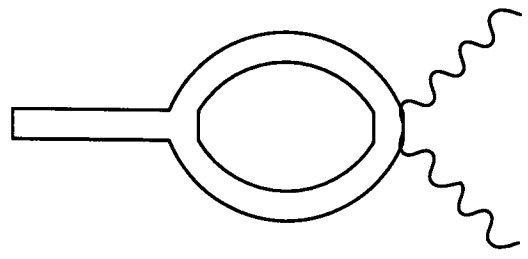

Figure 4.6: One loop diagram for $\langle a \rangle$ (when $\langle a \rangle \gg \langle b \rangle$).

Finally, if the initial conditions are changed such that now $n_B \gg n_A$, with $\delta \neq 0$, then we obtain the same results as for the second of the above regimes for $D_B t \gg n_B^{-2/d}$, with $f \approx 1$.

4.4.2 One Loop Results

We now describe the one loop improvements to the tree level result. In the regime $\langle a \rangle \gg \langle b \rangle$, the dominant diagrams will be those where the minimum possible number of $\langle b \rangle_{cl}$ insertions are made. For the majority A species the appropriate diagram is shown in figure 4.6, where there are no $\langle b \rangle_{cl}$ insertions. This is identical to the one loop diagram for $A+A \to \emptyset$ evaluated in [38], which gives, in conjunction with the subleading terms from the tree level:

$$\langle a \rangle \sim \left(\frac{1}{4\pi\epsilon} + \frac{2\ln 8\pi - 5}{16\pi} + O(\epsilon) \right) (D_A t)^{-d/2}. \tag{4.76}$$

In addition, for that subset of diagrams with no $\langle b \rangle_{cl}$ insertions, the decay exponent is exact. More details of this calculation, including a demonstration of the cancellation of divergences, can be found in [38].

Turning now to the one loop calculation for the minority species, the appropriate diagrams are the three shown in figure 4.7, each of which contains just one $\langle b \rangle_{cl}$

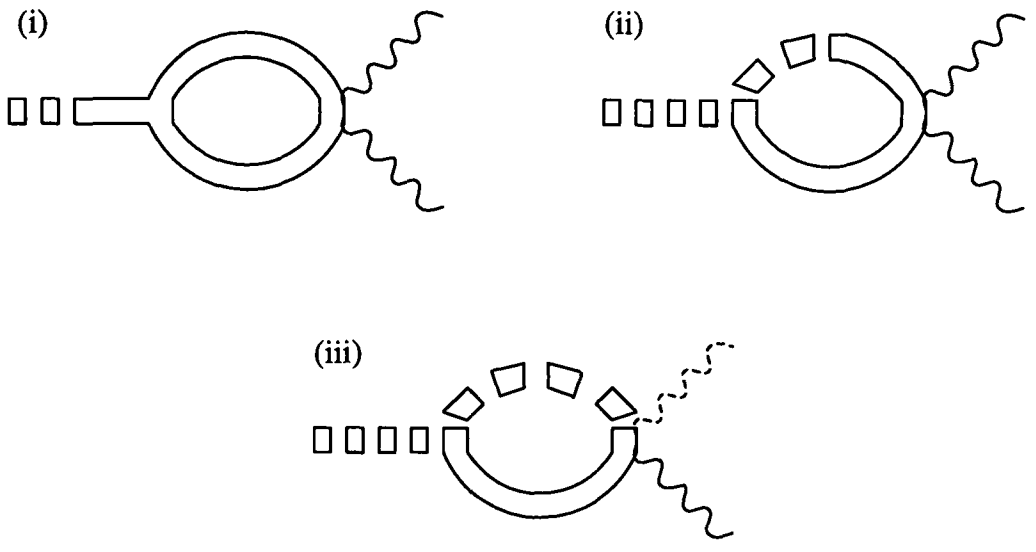

Figure 4.7: One loop diagrams for $\langle b \rangle$ (when $\langle a \rangle \gg \langle b \rangle$).

insertion:

$$(i) \qquad \frac{-4\lambda_{AB}\lambda_{AA}^2 n_A^2 n_B}{(2\lambda_{AA}n_A t)^{1+\lambda_{AB}/2\lambda_{AA}}} \int \frac{d^d k}{(2\pi)^d} \int_0^t dt_2 \int_0^{t_2} dt_1 (t - t_2) \times \frac{(1 + 2\lambda_{AA}n_A t_1)^2}{(1 + 2\lambda_{AA}n_A t_2)^3} \exp\left[-2k^2(t_2 - t_1)\right] \qquad (4.77)$$

$$(ii) \qquad \frac{-2\lambda_{AB}^2 \lambda_{AA} n_A^2 n_B}{(2\lambda_{AA}n_A t)^{\lambda_{AB}/2\lambda_{AA}}} \int \frac{d^d k}{(2\pi)^d} \int_0^t dt_2 \int_0^{t_2} dt_1 \int_{t_1}^{t_2} dt' \frac{(1 + 2\lambda_{AA}n_A t_1)^2}{(1 + 2\lambda_{AA}n_A t_2)^2} \times \frac{1}{(1 + 2\lambda_{AA}n_A t')^2} \exp\left[-k^2(t_2(1 + \delta) - 2t_1 + (1 - \delta)t')\right] \qquad (4.78)$$

$$(iii) \qquad \frac{\lambda_{AB}^2 n_A n_B}{(2\lambda_{AA}n_A t)^{\lambda_{AB}/2\lambda_{AA}}} \int \frac{d^d k}{(2\pi)^d} \int_0^t dt_2 \int_0^{t_2} dt_1 \frac{(1 + 2\lambda_{AA}n_A t_1)}{(1 + 2\lambda_{AA}n_A t_2)^2} \times \exp\left[-k^2(1 + \delta)(t_2 - t_1)\right]. \qquad (4.79)$$

The detail of the evaluation of these diagrams is rather subtle. Essentially we are interested in extracting the most divergent parts of these integrals, which will turn out to be pieces of $O(\epsilon^{-1})$ and $O(\epsilon^0)$. However, we must be careful not to confuse genuine bare divergences (of $O(\epsilon^{-1})$ which must be removed by the renormalisation of the theory), with logarithmic pieces, which we must retain. The divergences arise in diagrams (i) and (iii) as the difference in time $t_2 - t_1$ between

the beginning and end of the loops tends to zero (in $d = 2$). After the process of renormalisation we find corrections of the form:

$$1 + (\text{constant})\epsilon \ln((\text{constant})t^{d/2}) + O(\epsilon^2). \tag{4.80}$$

If this series is identified as the expansion of an exponential, then we find that our one loop diagrams (together with subleading components from the tree level) have provided $O(\epsilon)$ corrections to the exponents.

Diagrams (i) and (iii) are relatively straightforward to evaluate. The k and t_1 integrals are elementary, and the final t_2 integrals can also be done by parts to extract the necessary most divergent pieces (up to $O(\epsilon^0)$). The details are provided in appendix D. The second diagram of figure 4.7 is more complicated - and we also perform its evaluation in appendix D - although we are only able to extract the logarithmic piece of $O(t^{-\lambda_{AB}/2\lambda_{AA}}\, t^{\epsilon/2} \ln t)$. There will be corrections to this of $O(t^{-\lambda_{AB}/2\lambda_{AA}}\, t^{\epsilon/2})$ (contributing to a modified amplitude) which we have been unable to calculate. We find asymptotically:

$$(i)\ \frac{-\lambda_{AB} n_B}{8\pi(2\lambda_{AA} n_A t)^{\lambda_{AB}/2\lambda_{AA}}} \left(\frac{2t^{\epsilon/2}(\ln(2\lambda_{AA} n_A t) - 1)}{\epsilon} + t^{\epsilon/2}(\ln(2\lambda_{AA} n_A t) - 1)\ln(8\pi) \right.$$
$$\left. + \frac{15t^{\epsilon/2}}{4} - \frac{3}{2} t^{\epsilon/2} \ln(2\lambda_{AA} n_A t) - \int_0^t t_2^{-1+\epsilon/2} \ln(1 + 2\lambda_{AA} n_A t_2) dt_2 + O(\epsilon) \right) \tag{4.81}$$

$$(ii)\ \frac{-\lambda_{AB}^2 n_B}{32\pi\lambda_{AA}(2\lambda_{AA} n_A t)^{\lambda_{AB}/2\lambda_{AA}}} \left(\delta + \frac{1}{2}(\delta^2 - 1) \left[\ln\left(\frac{1-\delta}{1+\delta}\right) \right.\right. \tag{4.82}$$
$$\left.\left. - \int_{-1}^{\frac{1-\delta}{1+\delta}} dv \frac{(1+v)^2}{v^2} \ln(1+v) \right] + O(\epsilon) \right) t^{\epsilon/2} \ln(2\lambda_{AA} n_A t)$$

$$(iii)\ \frac{\lambda_{AB}^2 n_B (4\pi(1+\delta))^{-1}}{2\lambda_{AA}(2\lambda_{AA} n_A t)^{\lambda_{AB}/2\lambda_{AA}}} \left(\frac{2t^{\epsilon/2} \ln(2\lambda_{AA} n_A t)}{\epsilon} + t^{\epsilon/2} \ln(2\lambda_{AA} n_A t) \ln(4\pi(1+\delta)) \right. \tag{4.83}$$
$$\left. - t^{\epsilon/2}(\ln(2\lambda_{AA} n_A t) - 1) - \int_0^t t_2^{-1+\epsilon/2} \ln(1 + 2\lambda_{AA} n_A t_2) dt_2 + O(\epsilon) \right).$$

To one loop accuracy we can make the replacement: $\lambda_{\{ij\}} = \kappa^\epsilon g_{0_{\{ij\}}} \to \kappa^\epsilon g_{R_{\{ij\}}}$. These results must now be combined with the subleading terms from the tree level. Using (4.46), we find

$$\langle b \rangle \sim \frac{n_B}{(2\lambda_{AA} n_A t)^{\lambda_{AB}/2\lambda_{AA}}} = \frac{n_B}{(2\kappa^\epsilon g_{R_{AA}} n_A t)^{g_{R_{AB}}/2g_{R_{AA}}}} \left(1 - \frac{g_{R_{AB}}}{2g^*_{R_{AA}}} - \frac{g^2_{R_{AB}}}{2g_{R_{AA}} g^*_{R_{AB}}} \ln(2\kappa^\epsilon g_{R_{AA}} n_A t) + \frac{g_{R_{AB}}}{2g^*_{R_{AA}}} \ln(2\kappa^\epsilon g_{R_{AA}} n_A t) + O(g_R^2)\right). \quad (4.84)$$

If we now insert explicit ϵ expanded values for the fixed points $g^*_{R_{\{ij\}}}$, then we discover that the bare divergences cancel between (4.81), (4.83), and (4.84). With insertion into the Callan-Symanzik solution (4.49), we find that the pieces we have left as integrals in (i) and (iii) (which are $O(t^{\epsilon/2}(\ln t)^2)$) also mutually cancel. Eventually we find:

$$\langle b \rangle \sim (\text{const.}) t^{-\frac{d}{2}\left(\frac{1+\delta}{2}\right)^{d/2}} \left(1 + \frac{\epsilon(1+\delta)}{8}\left[1 - 2(1+\delta)\left(\frac{\delta}{4} + \frac{\delta^2-1}{8}\left(\ln\left(\frac{1-\delta}{1+\delta}\right) - \int_{-1}^{\frac{1-\delta}{1+\delta}} dv \frac{(1+v)^2}{v^2}\ln(1+v)\right)\right)\right] \ln((\text{const.})t^{d/2}) + O(\epsilon^2)\right), \quad (4.85)$$

where we have neglected $O(\epsilon)$ pieces which, aside from the prefactor, are time *independent.* These terms contribute only to the density amplitude. We now evaluate the integral in (4.85), using

$$\int_{-1}^{\frac{1-\delta}{1+\delta}} \frac{\ln(1+v)}{v} dv = \int_0^{\frac{2}{1+\delta}} \frac{\ln u}{u-1} du = \int_0^1 \frac{\ln u}{u-1} du + \int_1^{\frac{2}{1+\delta}} \frac{\ln u}{u-1} du$$
$$= \frac{\pi^2}{6} - f\left\{\frac{2}{1+\delta}\right\}, \quad (4.86)$$

where $f\{x\}$ is the dilogarithm function [36]. The other parts of the integral are elementary. The next step is to ϵ expand the RG improved tree level result:

$$\frac{d}{2}\left(\frac{1+\delta}{2}\right)^{d/2} = \left(\frac{1+\delta}{2}\right)\left(1 - \frac{\epsilon}{2}\left(1 + \ln\left(\frac{1+\delta}{2}\right)\right) + O(\epsilon^2)\right). \quad (4.87)$$

Then, exponentiating the ϵ expansion in (4.85), we find $\langle b \rangle = O(t^{-\beta})$, where

$$\beta = \left(\frac{1+\delta}{2}\right)\left(1 - \frac{\epsilon}{2}\left[\frac{3}{2} + \ln\left(\frac{1+\delta}{2}\right) - \frac{\delta(1+\delta)}{4}\left[1 + 2\ln\left(\frac{1+\delta}{2}\right)\right]\right.\right.$$
$$\left.\left. -\frac{1}{4}(\delta^2-1)\left(1 + (1+\delta)\left[f\left\{\frac{2}{1+\delta}\right\} - \frac{\pi^2}{6}\right]\right)\right]\right) + O(\epsilon^2). \quad (4.88)$$

β is plotted as a function of δ for $\epsilon = 1$ ($d = 1$) in figure 4.8. For the case where $\delta = 1$, we recover the decay rate $\langle b \rangle = O(t^{-d/2})$. This is to be expected, as when $\delta = 1$ we are effectively again dealing with a single species reaction-diffusion system (at least for $d < 2$). In that case the density decay exponent is known to all orders in perturbation theory [38], and is in agreement with our result. For the case where $\delta = 0$ and $d = 1$, the decay exponent is also known exactly to be $\langle b \rangle = O(t^{-0.375})$ [34]. This can be compared with our result, where we find

$$\beta = \frac{1}{16} + \frac{1}{4}\ln 2 + \frac{\pi^2}{64} \approx 0.39 \qquad (\delta = 0). \quad (4.89)$$

Consequently, this answer is a modest improvement over the Smoluchowski result derived in section 4.2, and also in [31]. Our expression for the one loop exponent (4.88) is also in good agreement with the results of numerical simulations [31].

For the case $n_B \gg n_A$ (and hence $\langle b \rangle \gg \langle a \rangle$), we could follow the same route as described above, by evaluating the one loop diagrams shown in figures 4.9 and 4.10. However, as we mentioned in the last section we can much more easily obtain these corrections by swapping the labels on the A and B particles, and then transforming:

$$n_A \leftrightarrow n_B \quad \lambda_{AA} \leftrightarrow \lambda_{BB} \quad D_A \leftrightarrow D_B.$$

Following this procedure, the majority species amplitude/exponent can be found by taking $D_A \to D_B$ in equation (4.76):

$$\langle b \rangle \sim \left(\frac{1}{4\pi\epsilon} + \frac{2\ln 8\pi - 5}{16\pi} + O(\epsilon)\right)(D_B t)^{-d/2}. \quad (4.90)$$

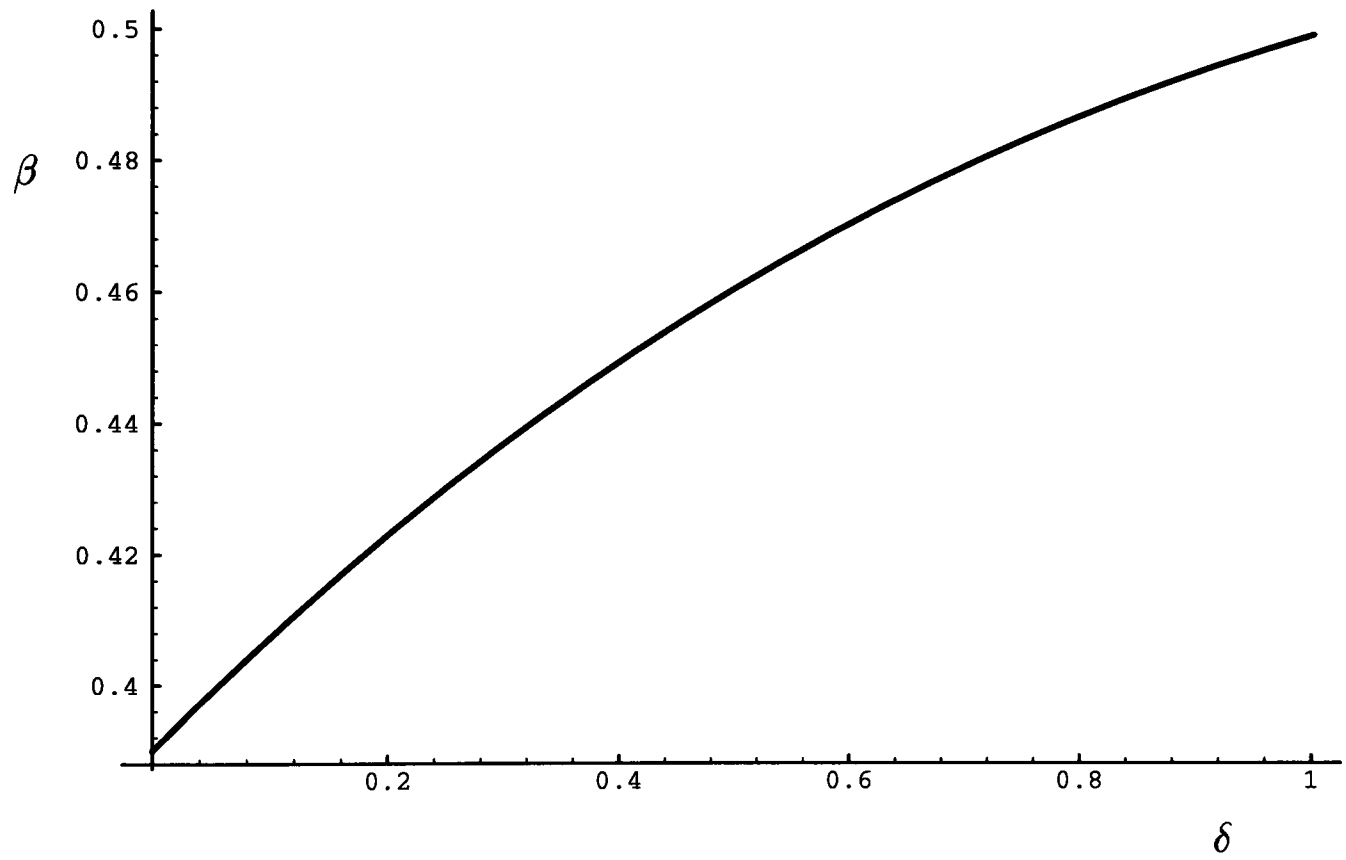

Figure 4.8: The one loop density decay exponent β for the minority B species ($\langle b \rangle = O(t^{-\beta})$) as a function of δ .

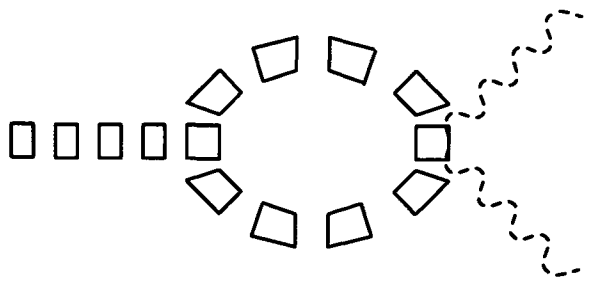

Figure 4.9: One loop diagram for $\langle b \rangle$ (when $\langle b \rangle \gg \langle a \rangle$).

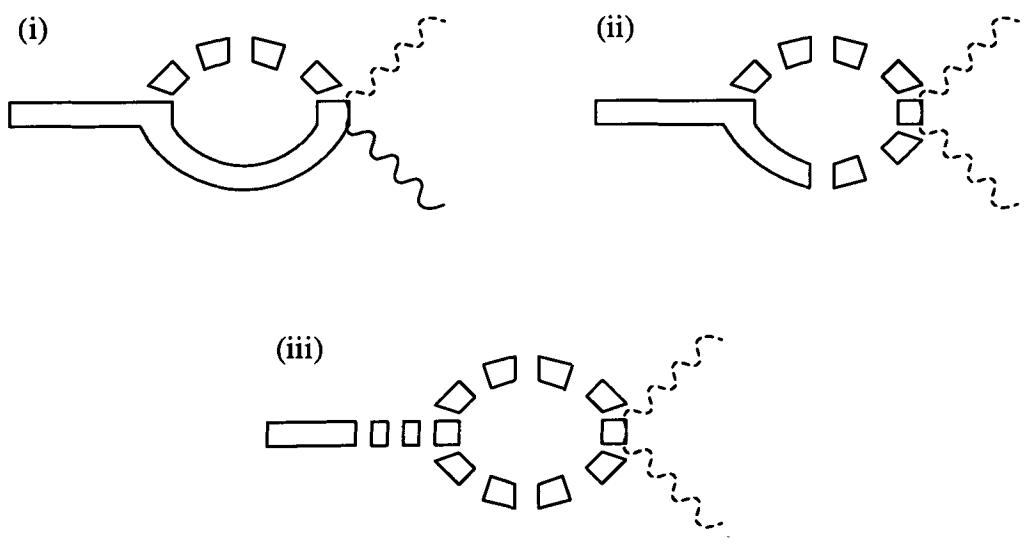

Figure 4.10: One loop diagrams for $\langle a \rangle$ (when $\langle b \rangle \gg \langle a \rangle$).

We can obtain the one loop minority species exponent by substituting $\delta \to \delta^{-1}$ in equation (4.88):

$$\langle a \rangle = O(t^{-\alpha}), \tag{4.91}$$

where

$$\alpha = \left(\frac{1+\delta^{-1}}{2}\right)\left(1 - \frac{\epsilon}{2}\left[\frac{3}{2} + \ln\left(\frac{1+\delta^{-1}}{2}\right) - \frac{\delta^{-1}(1+\delta^{-1})}{4}\left[1 + 2\ln\left(\frac{1+\delta^{-1}}{2}\right)\right]\right.\right.$$
$$\left.\left. -\frac{1}{4}(\delta^{-2}-1)\left(1 + (1+\delta^{-1})\left[f\left\{\frac{2}{1+\delta^{-1}}\right\} - \frac{\pi^2}{6}\right]\right)\right]\right) + O(\epsilon^2). \tag{4.92}$$

Notice, however, that in forming the one loop corrections for the minority species exponent, we have had to expand the RG improved tree level result:

$$\frac{d}{2}\left(\frac{1+\delta^{-1}}{2}\right)^{d/2} = \left(\frac{1+\delta^{-1}}{2}\right)\left(1 - \frac{\epsilon}{2}\left(1 + \ln\left(\frac{1+\delta^{-1}}{2}\right)\right) + O(\epsilon^2)\right). \tag{4.93}$$

The error arising from this expansion will become large as δ becomes small. Eventually this inaccuracy will cause the exponent to reach a maximum and then *decrease* as δ is further reduced - behaviour which is clearly unphysical. In order to reduce the error, and to ensure that the expansion in equation (4.93) is qualitatively correct, we need to retain the $O(\epsilon^2)$ terms. Hence the one loop exponent in equation (4.92) should be treated with some caution - terms of order $O(\epsilon^2)$ will probably be required for precise results. Consequently the (non ϵ expanded) RG improved tree level result given in the last section may be more accurate in this regime. In figure 4.11 we have plotted the one loop exponent α as a function of δ for $d = 1$ ($\epsilon = 1$) in the region $0.7 \leq \delta \leq 1$, where the exponent is still *increasing* for decreasing δ.

In principle, calculations can also be made for the case with $n_A \gg n_B$, but where we have crossed over to the regime $\langle b \rangle \gg \langle a \rangle$ (for $0 < \delta < 1$ and times $t \gg t_2$). However, a rigorous evaluation of the one loop diagrams is now much more difficult, as the functional forms for the densities and response functions will

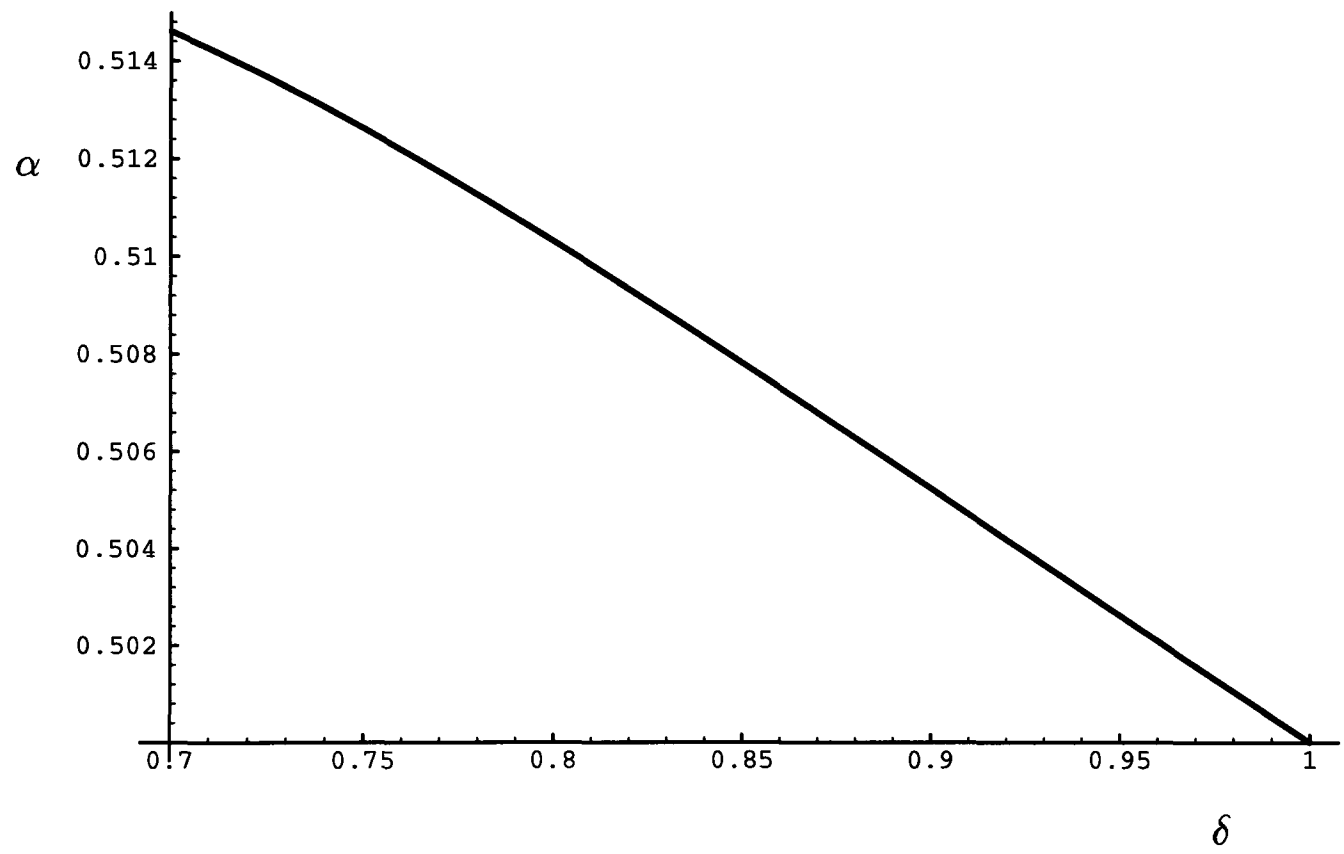

Figure 4.11: The one loop density decay exponent α for the minority A species ($\langle a \rangle = O(t^{-\alpha})$) as a function of δ (for $0.7 \leq \delta \leq 1$).

change over time. Nevertheless, since the above corrections to the exponents come from asymptotic logarithmic terms, it is plausible to suppose that the new exponent corrections will be dominated by contributions from the final asymptotic regime. If this is indeed the case, then the one loop exponents (though *not* the amplitudes) will be unchanged from the previous results (equations (4.90) to (4.92)). This calculation will, however, suffer from the same problem as described above.

4.4.3 $d = d_c$

For the case $d = d_c = 2$ we expect logarithmic corrections to the decay exponents, as the reaction rates $\lambda_{\{ij\}}$ are marginal parameters at the critical dimension. We can find the running couplings from the characteristic equation (4.50) by taking the limit $\epsilon \to 0$ in equations (4.40), (4.41), and (4.42):

$$\tilde{g}_{R_{AA}}(\kappa^{-2}) = \frac{g_{R_{AA}}}{1 + g_{R_{AA}} C \ln(\kappa^2 t)} \sim (C \ln t)^{-1} \tag{4.94}$$

$$\tilde{g}_{R_{BB}}(\kappa^{-2}) = \frac{g_{R_{BB}}}{1 + g_{R_{BB}} C \delta^{-1} \ln(\kappa^2 t)} \sim (C \delta^{-1} \ln t)^{-1} \tag{4.95}$$

$$\tilde{g}_{R_{AB}}(\kappa^{-2}) = \frac{g_{R_{AB}}}{1 + g_{R_{AB}} C (1+\delta)^{-1} \ln(\kappa^2 t)} \sim (C(1+\delta)^{-1} \ln t)^{-1}, \tag{4.96}$$

where we have taken the asymptotic limits. Corrections to the asymptotic running couplings will be an order $(\ln t)^{-1}$ smaller, and consequently these asymptotic expressions will only be correct at very large times. Hence, our expressions for the densities will only be valid when both this condition, and the crossover time constraints given below, are satisfied. In what follows we shall assume the validity of the first of these two conditions. Notice that the asymptotic running couplings are still ordered $2\tilde{g}_{R_{BB}} < \tilde{g}_{R_{AB}} < 2\tilde{g}_{R_{AA}}$ for $\delta < 1$, so we can use the mean field solutions derived in section 4.2 as the basis for the RG improved tree level exponents and amplitudes. Making use of the Callan-Symanzik solution (4.49) and the

above running couplings, we find for $\langle a \rangle \gg \langle b \rangle$:

$$\langle a \rangle \sim \frac{\ln t}{8\pi D_A t} \tag{4.97}$$

$$\langle b \rangle \sim \frac{n_B}{(8\pi n_A G D_A t/\ln t)^{(1+\delta)/2}}, \tag{4.98}$$

where $G = \exp\left(\frac{4\pi}{g_{R_{AA}}}\left(1 - \frac{(1+\delta)g_{R_{AA}}}{g_{R_{AB}}}\right)\right)$ is a non-universal amplitude correction. Note that the next order terms for the minority species are suppressed by a factor of only $(\ln\ln t)/(\ln t)$. Using our expressions for the running couplings/densities in the mean field crossovers, we find that these expressions are valid for times $D_A^{-1} n_A^{-1} \ln t \ll t \ll T_1$, where

$$(D_A T_1/\ln T_1) \approx \left(\frac{(G n_A)^{(1+\delta)/2}}{n_B}\right)^{\frac{2}{1-\delta}}. \tag{4.99}$$

For the case $\delta < 1$ the system will eventually enter a second regime, where now the B species will be in the majority. We have (for $\delta \neq 0$):

$$\langle b \rangle \sim \frac{\ln t}{8\pi D_B t} \tag{4.100}$$

$$\langle a \rangle \sim \frac{n_A K}{(8\pi n_B H D_B t/\ln t)^{(1+\delta^{-1})/2}}, \tag{4.101}$$

with

$$H = \exp\left(\frac{4\pi\delta}{g_{R_{BB}}}\left(1 - \frac{(1+\delta^{-1})g_{R_{BB}}}{g_{R_{AB}}}\right)\right) \qquad K = \left(1 + \frac{n_A}{n_B}\right)^{\frac{\delta^{-1}-1}{2}} \tag{4.102}$$

This is valid for times when $t \gg T_2$, where

$$(D_B T_2/\ln T_2) \approx \left(\frac{(H n_B)^{(1+\delta^{-1})/2}}{n_A(1+\delta^{-1})K}\right)^{\frac{2}{1-\delta^{-1}}} \tag{4.103}$$

Alternatively, if we begin with $n_B \gg n_A$, then for $\delta \neq 0$ and $(D_B t/\ln t) \gg n_B^{-1}$, we have the same results as for the second of the above cases, with $K \approx 1$. Interestingly, the logarithmic corrections we have derived in this section using the RG approach differ slightly from the Smoluchowski results given in section 4.2.

4.5 Conclusion

In this chapter we have made a comparison of two methods for treating fluctuation effects in a reaction-diffusion system. We have found that the Smoluchowski and field theory approaches are rather similar - the Smoluchowski approximation, for $d < 2$, giving the same exponents as the renormalisation group improved tree level in the field theory. In addition, we have gone on to calculate the field theoretic one loop corrections, which have yielded improved values for the exponents. The advantage of the field theory is that it provides a systematic way to calculate these corrections - a procedure which is lacking in the Smoluchowski approach. Furthermore the use of renormalisation group techniques has demonstrated universality in the asymptotic amplitudes and exponents, in that, for $d < 2$, they only depend on the diffusivities and the initial densities, and not on the reaction rates.

The theory we have developed in this chapter can easily be extended to slightly different situations. Consider first an annihilation/coagulation reaction-diffusion system, where the following reactions occur:

$$A + A \to A \qquad B + B \to B \qquad A + B \to \emptyset.$$

The Smoluchowski approach differs from before only in the absence of factors of 2 in the rate equation terms describing the same species reactions. Consequently, if we begin with $n_A \gg n_B$ then the minority species will decay as

$$b = O\left(t^{-d\left(\frac{1+\delta}{2}\right)^{d/2}}\right) \qquad (d < 2). \tag{4.104}$$

On the other hand, the field theory description lacks only the factors of 2 in the action (4.32). If this difference is followed through then the decay exponent in the RG improved tree level is seen to be the same as in the Smoluchowski approach.

However, this difference of a factor of 2 has a major effect on the response functions (where this factor appears as a power), and hence the new one loop corrections will be different from those calculated in section 4.4.2. These results should be compared with the exact solution [64, 65, 66] for the minority species decay rate $b = O(t^{-\gamma})$, where:

$$\gamma = \frac{\pi}{2\cos^{-1}(\delta/(1+\delta))}. \tag{4.105}$$

Note that in this case, although the Smoluchowski answer is qualitatively correct, it deviates considerably from the exact answer. Hence we can see that application of the Smoluchowski approach does not always lead to accurate exponents.

Another possible extension is to consider reaction-diffusion systems with more than two species of particle. For example, examining a three species system, we could have the reactions:

$$A + A \to \emptyset \qquad A + B \to \emptyset \qquad A + C \to \emptyset$$

$$B + B \to \emptyset \qquad B + C \to \emptyset \qquad C + C \to \emptyset.$$

Analysis of this situation is very similar to before, and we merely remark that in the appropriate asymptotic regimes the Smoluchowski and RG improved tree level exponents (consisting of ratios of diffusion constants) are once again identical. Hence the convergence between the Smoluchowski exponents and those obtained from the RG improved tree level is fairly robust, and is not simply confined to the two species systems we have previously been considering. A further possibility is to analyse the case where we have a continuous distribution of diffusivities, but with only a *single* reaction channel. This has been studied from the Smoluchowski point of view by Krapivsky *et al.* [31], and it would be interesting to extend our RG methods to include this situation.

Our theory could also be employed to consider clustered immobile reactants - a generalisation of the $\delta = 0$ case included in our calculations. This situation has been analysed by Ben-Naim [67] using the Smoluchowski approach, where the dimension of the cluster $d_I > 0$ was found to substantially affect the kinetics. Specifically, for codimensionality $d - d_I < 2$ (in a space of dimension d) a finite fraction of the impurities was found to survive, whereas for $d - d_I \geq 2$ the clusters decayed away indefinitely. The formalism we have presented in this chapter could be adapted to study this clustered impurity problem, where calculations could be made without reliance on the Smoluchowski approach.

4.6 Appendix A: The Mean Field Solutions

In this appendix we give more details about the solution of the mean field rate equations (4.14) and (4.15). We assume here that the reaction rates are ordered according to $2\lambda_{BB} < \lambda_{AB} < 2\lambda_{AA}$. If we define $\chi = a/b$, and let $dx = b\,dt$, then we can rewrite the rate equations in the following form:

$$\frac{d\chi}{dx} = (2\lambda_{BB} - \lambda_{AB})\chi + (\lambda_{AB} - 2\lambda_{AA})\chi^2. \tag{4.106}$$

Hence we see that χ is a decreasing function of x, meaning that at large enough times we can ignore the quadratic term in the above equation, giving:

$$\chi(x) \sim (\text{constant}) \times \exp\left(-(\lambda_{AB} - 2\lambda_{BB}) \int_0^t b(t')dt'\right). \tag{4.107}$$

If x reaches a finite limit as $t \to \infty$, then we have that $a(t) \propto b(t)$. This hypothesis is incompatible with the rate equations. Hence we reach the conclusion that $x \to \infty$ as $t \to \infty$, implying $\chi = (a/b) \to 0$ as $t \to \infty$.

Let us assume that we start the system off with initial conditions where $n_A \gg n_B$. Then we will have an early time regime where $a \gg b$, followed by a crossover to a late time regime where $b \gg a$. In the late time regime, for the B species, we may therefore neglect the effects of the $A + B \to \emptyset$ reaction and consider only the $B + B \to \emptyset$ process. This yields the density

$$b \sim (2\lambda_{BB}t)^{-1}. \tag{4.108}$$

A similar analysis on the rate equation for the A species in the late time regime suggests that we neglect the effects of the $A + A \to \emptyset$ reaction. This yields a decay $a = O(t^{-\lambda_{AB}/2\lambda_{BB}})$. However, if we are to use our field theoretic/RG methods to improve this answer we will need to know the form of the amplitude.

In order to proceed further we write

$$x = \int_0^t b(t')dt' = \frac{\ln(Et)}{2\lambda_{BB}}, \tag{4.109}$$

where E is a constant. If we integrate the rate equations from 0 to t, then we find:

$$\ln(a/n_A) = -2\lambda_{AA}\int_0^t a(t')dt' - (\lambda_{AB}/2\lambda_{BB})\ln(Et) \tag{4.110}$$

$$\ln(b/n_B) = -\ln(Et) - \lambda_{AB}\int_0^t a(t')dt'. \tag{4.111}$$

Eliminating the terms involving integrals leads to

$$\left(\frac{a}{n_A}\right)^{(1/2\lambda_{AA})}(Et)^{(\lambda_{AB}/4\lambda_{AA}\lambda_{BB})} = \left(\frac{b}{n_B}\right)^{(1/\lambda_{AB})}(Et)^{(1/\lambda_{AB})} \tag{4.112}$$

Solving equation (4.106) in the large time limit gives

$$a = \frac{b\frac{n_A}{n_B}}{1 + \frac{(\lambda_{AB}-2\lambda_{AA})}{(2\lambda_{BB}-\lambda_{AB})}\frac{n_A}{n_B}}(Et)^{\frac{-(\lambda_{AB}-2\lambda_{BB})}{2\lambda_{BB}}} \tag{4.113}$$

Substituting this into equation (4.112), we can solve for the constant E:

$$E = 2\lambda_{BB}n_B\left(1 + \frac{(\lambda_{AB} - 2\lambda_{AA})}{(2\lambda_{BB} - \lambda_{AB})}\frac{n_A}{n_B}\right)^{\frac{\lambda_{AB}}{(\lambda_{AB}-2\lambda_{AA})}} \tag{4.114}$$

This then leads us to the solution quoted in section 4.2.

4.7 Appendix B: The Smoluchowski Approximation

In this appendix we will derive the Smoluchowski form of the reaction rates quoted in section 4.2. The starting point is a statement of the diffusion equation for a density c in polar coordinates

$$\frac{\partial c}{\partial t} = D r^{1-d} \frac{\partial}{\partial r}\left(r^{d-1} \frac{\partial c}{\partial r} \right), \tag{4.115}$$

with the appropriate boundary conditions

$$c|_{r=R} = 0 \qquad\qquad c|_{r\to\infty} = c_0. \tag{4.116}$$

We now try a scaling Ansatz of the form

$$c = g\left(\frac{r}{(Dt)^{1/2}} \right). \tag{4.117}$$

Substituting into the above equation then gives:

$$g'' + \left(\frac{(d-1)}{u} + \frac{u}{2} \right) g' = 0, \tag{4.118}$$

where a prime denotes a differentiation with respect to $u = r/(Dt)^{1/2}$. Writing $h = g'$ enables this equation to be easily solved, with the result:

$$h = \frac{C e^{-\frac{u^2}{4}}}{u^{d-1}} = \frac{dg}{du}. \tag{4.119}$$

Hence the solution appropriate for our boundary conditions is

$$c = c_0 \frac{\int_{R/(Dt)^{1/2}}^{r/(Dt)^{1/2}} e^{-\frac{u^2}{4}} u^{1-d} du}{\int_{R/(Dt)^{1/2}}^{\infty} e^{-\frac{u^2}{4}} u^{1-d} du}. \tag{4.120}$$

In order to calculate the Smoluchowski reaction rates, we now need to evaluate the flux of particles across the sphere of radius R surrounding our target particle, i.e.

the quantity

$$j = DS_{d-1}R^{d-1}\frac{\partial c}{\partial r}\bigg|_{r=R}, \tag{4.121}$$

where S_{d-1} is the surface area of a unit d dimensional hypersphere. We now use the result (for $d < 2$):

$$\int_0^\infty e^{-\frac{u^2}{4}}u^{1-d}du = 2^{1-d}\Gamma\left(\frac{2-d}{2}\right). \tag{4.122}$$

Hence we see that in the large time limit the flux becomes

$$j = D^{d/2}t^{-1+d/2}\frac{2^d\pi^{d/2}c_0}{\Gamma\left(\frac{2-d}{2}\right)\Gamma\left(\frac{d}{2}\right)} \propto D^{d/2}t^{-1+d/2} \tag{4.123}$$

If we generalise to the case where both the target and background particles diffuse, we end up with the final answer quoted in section 4.2. This last step is justified by noting that if two particles are performing random walks with diffusion constants D_A and D_B, then the displacement between them also performs a random walk, but with a diffusion constant $D_A + D_B$ (see, however, Noyes [16] and Doi [22] for a critique of this and other assumptions of the Smoluchowski method).

In $d = 2$, evaluation of the integrals in equation (4.120) leads to the presence of logarithms:

$$j = \frac{2\pi Dc_0}{\ln[(Dt)^{1/2}/R]}, \tag{4.124}$$

which, in the large time limit, becomes

$$j \propto \frac{D}{\ln(Dt)}. \tag{4.125}$$

Generalising again to the case where both the target and background particles diffuse, we find the result quoted in section 4.2.

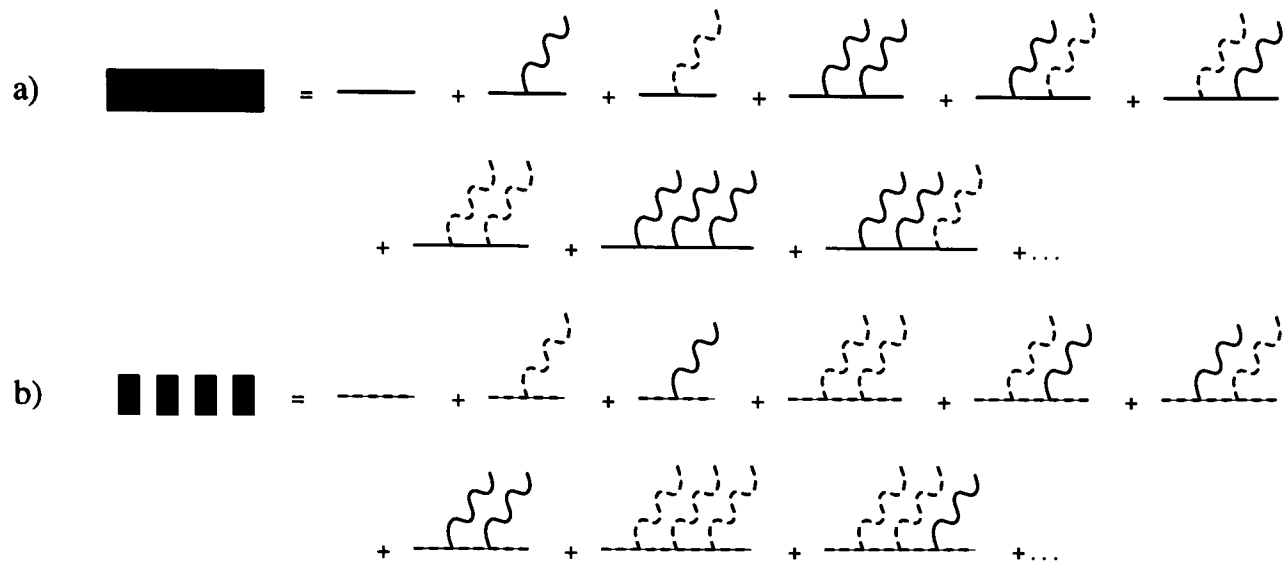

Figure 4.12: The diagrammatic equations for (a) ξ and (b) θ.

4.8 Appendix C: Response Functions

Obtaining an exact analytic expression for the response functions is, in general, very hard. Suppose we define the "trunk" to be the line of propagators onto which the density lines are attached, as shown at the bottom of figure 4.5. Difficulties arise from diagrams where the "trunk" changes from one propagator into the other, and then back again, as shown in the last of the diagrams for the L response function in figure 4.5. If diagrams of this type are initially excluded then progress can be made. Consider first the two subseries shown in figure 4.12, for the functions $\xi(k, t_2, t_1)$ and $\theta(k, t_2, t_1)$, where diagrams of the above kind have been excluded. These series can be summed exactly, using the same technique as described in [38]. First we note that the time dependence of the propagators connecting the vertices cancels to leave only a dependence on $t_2 - t_1$. The remaining pieces can then be identified as the Taylor expansion of an exponential, leading to:

$$\xi(k, t_2, t_1) = \exp\left(-k^2(t_2 - t_1)\right) \exp\left(-\int_{t_1}^{t_2} (4\lambda_{AA}a + \lambda_{AB}b)dt\right) \qquad (4.126)$$

Figure 4.13: The full diagrammatic equations satisfied by the response functions.

$$\theta(k,t_2,t_1) = \exp\left(-k^2(t_2-t_1)\delta\right)\exp\left(-\int_{t_1}^{t_2}(4\lambda_{BB}b+\lambda_{AB}a)dt\right). \tag{4.127}$$

The full response functions are now given by the diagrammatic equations shown in figure 4.13, where all possible diagrams are included. Written out explicitly these give:

$$L(k,t_2,t_1) = \xi(k,t_2,t_1) - \lambda_{AB}\int_{t_1}^{t_2}\xi(k,t_2,\tau)a(\tau)M(k,\tau,t_1)d\tau \tag{4.128}$$

$$M(k,t_2,t_1) = -\lambda_{AB}\int_{t_1}^{t_2}\theta(k,t_2,\tau)b(\tau)L(k,\tau,t_1)d\tau \tag{4.129}$$

$$N(k,t_2,t_1) = \theta(k,t_2,t_1) - \lambda_{AB}\int_{t_1}^{t_2}\theta(k,t_2,\tau)b(\tau)P(k,\tau,t_1)d\tau \tag{4.130}$$

$$P(k,t_2,t_1) = -\lambda_{AB}\int_{t_1}^{t_2}\xi(k,t_2,\tau)a(\tau)N(k,\tau,t_1)d\tau. \tag{4.131}$$

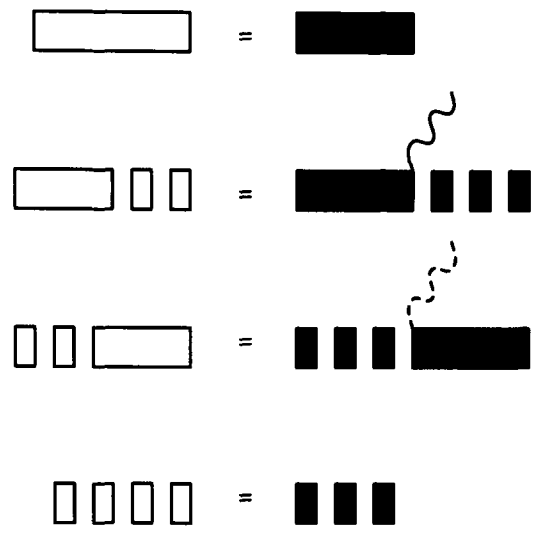

Figure 4.14: The truncated diagrammatic equations for the response functions, valid for $\langle a \rangle \gg \langle b \rangle$, or $\langle b \rangle \gg \langle a \rangle$.

In general this set of coupled integral equations is intractable - however, we can make progress in the limit where $\langle a \rangle \gg \langle b \rangle$, or $\langle b \rangle \gg \langle a \rangle$. Considering the case where $\langle a \rangle \gg \langle b \rangle$, the dominant contributions to the response functions come from diagrams with the minimum possible number of $\langle b \rangle_{cl}$ density line insertions. Accordingly, we can now truncate the full diagrammatic equations, as shown in figure 4.14. Notice that to this order L, N, and P contain no $\langle b \rangle_{cl}$ density insertions, whereas M must contain one such insertion. In this approximation we can now perform the integrals inside the ξ and θ functions, using the appropriate mean field density:

$$\int_{t_1}^{t_2} (4\lambda_{AA} a + \lambda_{AB} b) dt \approx \int_{t_1}^{t_2} \frac{4\lambda_{AA} n_A}{1 + 2\lambda_{AA} n_A t} dt = \ln \left(\frac{1 + 2\lambda_{AA} n_A t_2}{1 + 2\lambda_{AA} n_A t_1} \right)^2 \tag{4.132}$$

$$\int_{t_1}^{t_2} (4\lambda_{BB} b + \lambda_{AB} a) dt \approx \int_{t_1}^{t_2} \frac{\lambda_{AB} n_A}{1 + 2\lambda_{AA} n_A t} dt = \ln \left(\frac{1 + 2\lambda_{AA} n_A t_2}{1 + 2\lambda_{AA} n_A t_1} \right)^{\lambda_{AB}/2\lambda_{AA}}, \tag{4.133}$$

and therefore

$$\xi(k,t_2,t_1) = \left(\frac{1+2\lambda_{AA}n_A t_1}{1+2\lambda_{AA}n_A t_2}\right)^2 \exp\left(-k^2(t_2-t_1)\right) \tag{4.134}$$

$$\theta(k,t_2,t_1) = \left(\frac{1+2\lambda_{AA}n_A t_1}{1+2\lambda_{AA}n_A t_2}\right)^{\lambda_{AB}/2\lambda_{AA}} \exp\left(-k^2(t_2-t_1)\delta\right). \tag{4.135}$$

Using these expressions, it is now straightforward to derive the response functions given in equations (4.59), (4.60), (4.61), and (4.62).

4.9 Appendix D: One Loop Integrals

For the case where $\langle a\rangle \gg \langle b\rangle$ the hardest of the three diagrams of figure 4.7 to evaluate is (ii) - see equation (4.78). We shall evaluate it first in $d = 2$, and then deduce its form in $d = 2-\epsilon$. Notice that the extra integration resulting from the $\langle b\rangle_{cl}$ insertion in the loop ensures that this diagram is not divergent. Taking the asymptotic part of the t_1 and t' pieces, we find:

$$\frac{-\lambda_{AB}^2 n_B}{2\lambda_{AA}(2\lambda_{AA}n_A t)^{\lambda_{AB}/2\lambda_{AA}}} \int \frac{d^2k}{(2\pi)^2} \int_0^t dt_2 \int_0^{t_2} dt_1 \int_{t_1}^{t_2} dt' \frac{(2\lambda_{AA}n_A)^2 t_1^2}{(1+2\lambda_{AA}n_A t_2)^2\, t'^2}$$
$$\times \exp\left(-k^2(t_2(1+\delta) - 2t_1 + (1-\delta)t')\right). \tag{4.136}$$

The k and t' integrals are elementary, giving

$$\frac{-\lambda_{AB}^2 n_B}{8\pi\lambda_{AA}(2\lambda_{AA}n_A t)^{\lambda_{AB}/2\lambda_{AA}}} \int_0^t \frac{dt_2(2\lambda_{AA}n_A)^2}{(1+2\lambda_{AA}n_A t_2)^2} \int_0^{t_2} dt_1 t_1^2 \tag{4.137}$$
$$\times \left(\frac{1}{(t_2(1+\delta)-2t_1)}\left[\frac{1}{t_1}-\frac{1}{t_2}\right] + \frac{1-\delta}{(t_2(1+\delta)-2t_1)^2}\ln\left(\frac{2t_1}{(1+\delta)t_2}\right)\right).$$

Although the first part of the t_1 integral is straightforward, the second piece involving the logarithm is more difficult. However, if we make the transformation

$$v = \frac{2t_1}{(1+\delta)t_2} - 1, \tag{4.138}$$

we find:

$$\int_0^{t_2} dt_1 \frac{(1-\delta)t_1^2}{(t_2(1+\delta)-2t_1)^2} \ln\left(\frac{2t_1}{(1+\delta)t_2}\right) = \frac{1}{8}(1-\delta^2)t_2 \int_{-1}^{\frac{1-\delta}{1+\delta}} dv \frac{(1+v)^2}{v^2} \ln(1+v), \tag{4.139}$$

where all time dependency has been removed from the integral limits. The final t_2 integral is then easy to perform, and we end up with:

$$\frac{-\lambda_{AB}^2 n_B}{32\pi\lambda_{AA}(2\lambda_{AA}n_A t)^{\lambda_{AB}/2\lambda_{AA}}} \left(\delta + \frac{1}{2}(\delta^2-1)\left[\ln\left(\frac{1-\delta}{1+\delta}\right) - \int_{-1}^{\frac{1-\delta}{1+\delta}} dv \frac{(1+v)^2}{v^2}\ln(1+v)\right]\right) \ln(2\lambda_{AA}n_A t). \tag{4.140}$$

However, we now need to extend this analysis to determine the behaviour of the integral in $d = 2-\epsilon$. If we take the asymptotic part of all the pieces inside the integral, and perform power counting, we find that it should scale as $t^{-\lambda_{AB}/2\lambda_{AA}}\, t^{\epsilon/2}$. However, this procedure is not strictly valid, as in moving to the asymptotic version a false $t_2 = 0$ divergence is created. Nevertheless, the integral is dominated by contributions from late times where arguments based on power counting should be valid. Hence in $d = 2-\epsilon$ we find:

$$\frac{-\lambda_{AB}^2 n_B}{32\pi\lambda_{AA}(2\lambda_{AA}n_A t)^{\lambda_{AB}/2\lambda_{AA}}} \left(\delta + \frac{1}{2}(\delta^2-1)\left[\ln\left(\frac{1-\delta}{1+\delta}\right) - \int_{-1}^{\frac{1-\delta}{1+\delta}} dv \frac{(1+v)^2}{v^2}\ln(1+v)\right] + O(\epsilon)\right) t^{\epsilon/2} \ln(2\lambda_{AA}n_A t). \tag{4.141}$$

Further subleading corrections (in time), which we have not calculated, will lack the logarithm factor, and so will contribute to the *amplitude* for the minority species density.

We next evaluate diagram (iii) in figure 4.7. Performing the k integration yields

$$\frac{\lambda_{AB}^2 n_B n_A}{(2\lambda_{AA}n_A t)^{\lambda_{AB}/2\lambda_{AA}}} \frac{(1+\delta)^{-d/2}}{(4\pi)^{d/2}} \int_0^t dt_2 \int_0^{t_2} dt_1 \frac{(1+2\lambda_{AA}n_A t_1)}{(1+2\lambda_{AA}n_A t_2)^2} (t_2-t_1)^{-d/2}. \tag{4.142}$$

Leaving aside the prefactor in the above equation we then integrate by parts to obtain:

$$\frac{4}{\epsilon(2+\epsilon)}\int_0^t \frac{t_2^{\epsilon/2}dt_2}{(1+2\lambda_{AA}n_A t_2)} + \frac{2}{\epsilon}\left(1-\frac{2}{2+\epsilon}\right)\int_0^t \frac{t_2^{\epsilon/2}dt_2}{(1+2\lambda_{AA}n_A t_2)^2}. \tag{4.143}$$

We can now integrate by parts again to obtain the most divergent pieces of the integrals in an ϵ expansion. The first of these two integrals becomes:

$$\begin{aligned}\frac{t^{\epsilon/2}\ln(1+2\lambda_{AA}n_A t)}{\epsilon\lambda_{AA}n_A} - \frac{t^{\epsilon/2}\ln(1+2\lambda_{AA}n_A t)}{2\lambda_{AA}n_A} \\ -\frac{1}{2\lambda_{AA}n_A}\int_0^t t_2^{-1+\epsilon/2}\ln(1+2\lambda_{AA}n_A t_2)dt_2 + O(\epsilon).\end{aligned} \tag{4.144}$$

The second of the two above integrals can be rewritten:

$$\int_0^t \frac{dt_2 t_2^{\epsilon/2}}{(1+2\lambda_{AA}n_A t_2)^2} = \int_0^t \frac{dt_2 t_2^{\epsilon/2}}{(1+2\lambda_{AA}n_A t_2)^2} \tag{4.145}$$

$$\begin{aligned}-\int_0^t \frac{dt_2 t_2^{\epsilon/2}}{(1+2\lambda_{AA}n_A t_2)} + \int_0^t \frac{dt_2 t_2^{\epsilon/2}}{(1+2\lambda_{AA}n_A t_2)} \\ = -2\lambda_{AA}n_A\int_0^t \frac{t_2^{1+\epsilon/2}dt_2}{(1+2\lambda_{AA}n_A t_2)^2} + \int_0^t \frac{t_2^{\epsilon/2}dt_2}{(1+2\lambda_{AA}n_A t_2)} = \frac{t^{\epsilon/2}}{2\lambda_{AA}n_A} + O(\epsilon).\end{aligned} \tag{4.146}$$

Putting all the above terms together, ϵ expanding the prefactor, and then taking the asymptotic limit gives the result quoted in equation (4.83).

Finally, we now evaluate diagram (i) of figure 4.7. Performing the k integration yields

$$\frac{-4\lambda_{AA}^2\lambda_{AB}n_A^2 n_B}{(2\lambda_{AA}n_A t)^{\lambda_{AB}/2\lambda_{AA}}(8\pi)^{d/2}}\int_0^t dt_2\int_0^{t_2} dt_1 \frac{(t-t_2)(t_2-t_1)^{-d/2}}{(1+2\lambda_{AA}n_A t)}\frac{(1+2\lambda_{AA}n_A t_1)^2}{(1+2\lambda_{AA}n_A t_2)^3}. \tag{4.147}$$

Integrating successively by parts then gives (excluding the above prefactor):

$$\int_0^t dt_2 \frac{2(t-t_2)}{\epsilon(1+2\lambda_{AA}n_A t)}\left(t_2^{\epsilon/2} + \frac{8\lambda_{AA}n_A t_2^{1+\epsilon/2}}{(\epsilon+2)} + \frac{32\lambda_{AA}^2 n_A^2 t_2^{2+\epsilon/2}}{(2+\epsilon)(4+\epsilon)}\right)\frac{1}{(1+2\lambda_{AA}n_A t_2)^3}. \tag{4.148}$$

Expanding this expression, we end up with:

$$\int_0^t dt_2 \frac{2}{\epsilon} \frac{(t-t_2)}{(1+2\lambda_{AA}n_A t)} \frac{t_2^{\epsilon/2}}{(1+2\lambda_{AA}n_A t_2)} \tag{4.149}$$
$$- \int_0^t dt_2 4\lambda_{AA}n_A t_2^{\epsilon/2} \frac{(t-t_2)}{(1+2\lambda_{AA}n_A t)} \frac{(t_2+\frac{3}{2}\lambda_{AA}n_A t_2^2)}{(1+2\lambda_{AA}n_A t_2)^3} + O(\epsilon).$$

Integrating the first of these two pieces by parts to obtain the most divergent terms then leads to:

$$\frac{t^{\epsilon/2}}{2\lambda_{AA}^2 n_A^2 \epsilon}[\ln(1+2\lambda_{AA}n_A t) - 1] - \frac{1}{4\lambda_{AA}^2 n_A^2} \int_0^t t_2^{-1+\epsilon/2} \ln(1+2\lambda_{AA}n_A t_2) dt_2$$
$$+ \frac{t^{\epsilon/2}}{4\lambda_{AA}^2 n_A^2} + O(\epsilon). \tag{4.150}$$

A similar process can be performed on the second of the above pieces (except there are no singular contributions from that integral). Adding up all the relevant contributions yields:

$$\frac{-\lambda_{AB}n_B}{(2\lambda_{AA}n_A t)^{\lambda_{AB}/2\lambda_{AA}}(8\pi)^{d/2}} \left(\frac{2t^{\epsilon/2}[\ln(1+2\lambda_{AA}n_A t) - 1]}{\epsilon} \right. \tag{4.151}$$
$$\left. - \int_0^t t_2^{-1+\epsilon/2} \ln(1+2\lambda_{AA}n_A t_2) dt_2 - \frac{3}{2} t^{\epsilon/2} \ln(1+2\lambda_{AA}n_A t) + \frac{15}{4} t^{\epsilon/2} + O(\epsilon) \right).$$

Performing an ϵ expansion of the prefactor, and then taking the asymptotic limit, leads to the result quoted in equation (4.81).

Bibliography

[1] Wilhelmy L. 1850 *Pogg. Ann.* **81** 413, 499

[2] Harcourt A. and Esson W. 1866 *Philos. Trans.* **156** 193

[3] Benson S. 1960 *The Foundations of Chemical Kinetics* (New York: McGraw-Hill)

[4] Smoluchowski M. 1917 *Z. Phys. Chem.* **92** 215

[5] Kuzovkov V. and Kotomin E. 1988 *Rep. Prog. Phys.* **51** 1479

[6] Ovchinnikov A.A., Timashev S.F., and Belyy A.A. 1990 *Kinetics of Diffusion Controlled Chemical Processes* (New York: Nova Science Publishers)

[7] Scott S. 1994 *Oscillations, Waves and Chaos in Chemical Kinetics* (Oxford: Oxford University Press)

[8] Cross M. and Hohenberg P. 1993 *Rev. Mod. Phys.* **65** 851

[9] Turing A. 1952 *Philos. Trans. Roy. Soc. London Series B* **237** 37

[10] Castets V., Dulos E., Boissonade J., and De Kepper P. 1990 *Phys. Rev. Lett.* **64** 2953

[11] Kondo S. and Asai R. 1995 *Nature* **376** 765

[12] Kroon R., Fleurent H., and Sprik R. 1993 *Phys. Rev. E* **47** 2462

[13] Toussaint D. and Wilczek F. 1983 *J. Chem. Phys.* **78** 2642

[14] Ovchinnikov A. and Zeldovich Y. 1978 *Chem. Phys.* **28** 215

[15] Kang K. and Redner S. 1985 *Phys. Rev. A* **32** 435

[16] Noyes R. 1961 *Prog. Reac. Kin.* **1** 129

[17] Bak P., Tang C., and Wiesenfeld K. 1987 *Phys. Rev. Lett.* **59** 381

[18] Bramson M. and Lebowitz J.L. 1991 *J. Stat. Phys.* **65** 941

[19] Lee B. and Cardy J. 1995 *J. Stat. Phys.* **80** 971

[20] Alcaraz F., Droz M., Henkel M., and Rittenberg V. 1994 *Ann. Phys. (N.Y.)* **230** 250

[21] Binney J., Dowrick N.,Fisher A., and Newman M. 1992 *The Theory of Critical Phenomena* (Oxford: Oxford University Press)

[22] Doi M. 1976 *J. Phys. A: Math. Gen.* **9** 1465, 1479

[23] Peliti L. 1985 *J. Physique* **46** 1469

[24] Howard M. and Cardy J. 1995 *J. Phys. A: Math. Gen.* **28** 3599

[25] Barkema G., Howard M., and Cardy J. 1996 *Phys. Rev. E* **53** R2017

[26] Gálfi L. and Rácz Z. 1988 *Phys. Rev. A* **38** 3151

[27] Ben-Naim E. and Redner S. 1992 *J. Phys. A: Math. Gen.* **25** L575

[28] Araujo M., Larralde H., Havlin S., and Stanley H.E. 1993 *Phys. Rev. Lett.* **71** 3592 ; 1995 *Phys. Rev. Lett.* **75** 2251

[29] Cornell S. 1995 *Phys. Rev. E* **51** 4055; 1995 *Phys. Rev. Lett.* **75** 2250

[30] Howard M. 1996 *J. Phys. A: Math. Gen to appear*

[31] Krapivsky P., Ben-Naim E., and Redner S. 1994 *Phys. Rev. E* **50** 2474

[32] Derrida B., Bray A., and Godrèche C. 1994 *J. Phys. A: Math. Gen.* **27** L357

[33] Derrida B. 1995 *J. Phys. A: Math. Gen.* **28** 1481

[34] Derrida B., Hakim V., and Pasquier V. 1995 *Phys. Rev. Lett.* **75** 751

[35] Grassberger P. and Procaccia I. 1982 *J. Chem. Phys.* **77** 6281

[36] Abramowitz M. and Stegun I.A. 1965 *Handbook of Mathematical Functions* (New York: Dover)

[37] Lee B.P. 1994 *Critical Behaviour in Non-Equilibrium Systems* Ph. D. Thesis, University of California, Santa Barbara

[38] Lee B.P. 1994 *J. Phys. A: Math. Gen.* **27** 2633

[39] Janssen H. 1981 *Z. Phys. B* **42** 151

[40] Droz M. and McKane A. 1994 *J. Phys. A: Math. Gen.* **27** L467

[41] Gardiner C. 1985 *Handbook of Stochastic Methods* (Berlin: Springer-Verlag)

[42] Janssen H. 1995 *unpublished*

[43] Cornell S. 1995 *preprint*

[44] Cornell S. and Droz M. 1995 *private communication*

[45] Larralde H., Araujo M., Havlin S., and Stanley H.E. 1992 *Phys. Rev. A* **46** 855

[46] Jiang Z. and Ebner C. 1990 *Phys. Rev. A* **42** 7483

[47] Taitelbaum H., Havlin S., Kiefer J., Trus B., and Weiss G. 1991 *J. Stat. Phys.* **65** 873

[48] Chopard B. and Droz M. 1991 *Europhys. Lett.* **15** 459

[49] Cornell S., Droz M., and Chopard B. 1991 *Phys. Rev. A* **44** 4826

[50] Cornell S., Droz M., and Chopard B. 1992 *Physica* **188A** 322

[51] Taitelbaum H., Koo Y., Havlin S., Kopelman R., and Weiss G. 1992 *Phys. Rev. A* **46** 2151

[52] Koo Y., Li L., and Kopelman R. 1990 *Mol. Cryst. Liq. Cryst.* **183** 187

[53] Koo Y. and Kopelman R. 1991 *J. Stat. Phys.* **65** 893

[54] Cornell S. and Droz M. 1993 *Phys. Rev. Lett.* **70** 3824

[55] Lee B.P. and Cardy J. 1994 *Phys. Rev. E* **50** R3287

[56] Hohenberg P.C. and Halperin B.I. 1977 *Rev. Mod. Phys.* **49** 435

[57] Leyvraz F. and Redner S. 1991 *Phys. Rev. Lett.* **66** 2168; 1992 *Phys. Rev. A* **46** 3132

[58] Leyvraz F. 1992 *J. Phys. A: Math. Gen.* **25** 3205

[59] Larralde H., Araujo M., Havlin S., and Stanley H.E. 1992 *Phys. Rev. A* **46** R6121

[60] Cornell S., Koza Z., and Droz M. 1995 *Phys. Rev. E* **52** 3500

[61] Gradshteyn I.S. and Ryzhik I.M. 1994 *Table of Integrals, Series, and Products* (San Diego: Academic Press)

[62] Cardy J. 1995 *J. Phys. A: Math. Gen.* **28** L19

[63] Chandrasekhar S. 1943 *Rev. Mod. Phys.* **15** 1

[64] Fisher M.E. 1984 *J. Stat. Phys.* **34** 667

[65] Fisher M.E. and Gelfand M.P. 1988 *J. Stat. Phys.* **53** 175

[66] ben-Avraham D. 1988 *J. Chem. Phys.* **88** 941

[67] Ben-Naim E. 1996 *Phys. Rev. E* **53** 1566